

MICHAEL JOHN O'CONNELL  
Ecohydrol. of barrier island forests  
MAY, 2009  
GRADUATE ARTS AND SCIENCES

Ecohydrology of Delmarva Peninsula barrier island forests and the application of lidar to  
measure and monitor forest structure

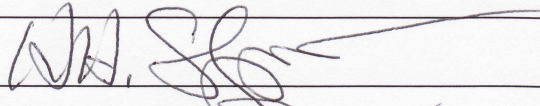
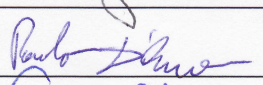
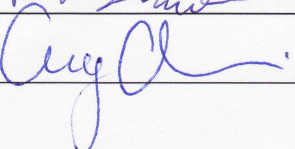
Michael John O'Connell  
Langhorne, Pennsylvania

Bachelor of Science, The Pennsylvania State University, 1996

A Dissertation presented to the Graduate Faculty  
of the University of Virginia in Candidacy for the Degree of  
Doctor of Philosophy

Department of Environmental Sciences

University of Virginia  
May, 2009

	
Stephen Hogg	
	
	

## Abstract

Mid-Atlantic barrier islands are dynamic landforms that support unique vegetation assemblages and provide protection to coastal bay and mainland ecosystems. The islands (Assateague and Parramore here) are subject to increasing destabilizing pressures from climate change. Upward vertical forcing on freshwater bodies by rising sea surface elevation is expected to significantly alter vegetation community and biophysical structure. This dissertation documents the existing spatial gradient of *Pinus taeda* L. (loblolly pine) biophysical structure, and develops a water availability proxy well correlated with forest structural metrics. This new variable, DWST, a product of depth to water table and a soil textural index, is well-suited for dynamic monitoring and modeling of vegetation change as water tables change. Dendrochronological analyses provide convincing support for the proposed average rooting zone DWST as a major constraint on forest growth.

A lidar instrument, EAARL (Experimental Advanced Airborne Research Lidar) is shown to provide accurate representations of coarse and fine forest structural metrics. EAARL canopy reflection ratio (CRR) predicts ground-based plant area index (PAI) at a forest-wide  $r^2$  of 0.73. PAI incorporates leaf area and thus can potentially track foliar adjustments due to changes in soil moisture levels at short time scales. The waveform-returning nature of the EAARL also enables very good representation of foliage density distribution. The height of peak canopy density (HPCD) is proposed as a surrogate for maximum canopy height in lidar-based studies and an indicator of hydrological gradients.

The lidar analyses and field ecohydrological system description together comprise the basis for a candidate monitoring scheme of sea level effects. With additional minimal field surveys, it is expected that this measurement system will infer changing water relations from incremental forest structural change.

## Acknowledgements

I would like to thank all the people that have made this dissertation possible. My family, Bonnie, Tom, Pat, Beth, and John for their support, love, and interest. The Rowes for the same. My friends for the laughs and respite. My colleagues for their generous natures and valuable insights. My advisor, Hank Shugart, for his guidance, his ability to teach, and his talent in conveying the big picture. My committee – Greg, Paolo, and Steve – for their help and excellent advice.

The work required the generosity of many good people in the field and lab. I wish to thank Carl Zimmerman and the Natural Resource Management staff at Assateague Island National Seashore; the VCR LTER staff; Keith Hadley and Scott Burns of Portland State University; the soil testing lab staff at Virginia Tech; Amy, Ben, Sam, Jonathan, Andrew, Natasha, Dave, and Rachel for fighting the ticks and mosquitoes while sharing the beauty of the islands.

And finally, I thank Sarah S. Rowe for her unfailing inspiration, love, and partnership throughout it all.

## Table of Contents

<b>Section</b>	<b>Page</b>
Abstract	i
Acknowledgements	iii
Table of Contents	iv
List of Figures	x
List of Tables	xvi
List of Acronyms	xix
<b>I. Introduction</b>	<b>1</b>
1.1. Background	2
1.2. Study Area	5
1.3. Study Outline	6
1.3.1. Objectives	6
1.3.2. Overview of sections	7
1.4. References	10
<b>II. Mid-Atlantic barrier island forest structural properties and site gradient expression</b>	<b>12</b>
Abstract	12
2.1. Introduction	13
2.2. Methods	17
2.2.1. General plot installation and structural measures	17
2.2.2. Crown ratio and plot canopy density distribution	19

<b>Section</b>	<b>Page</b>
2.2.3. Fine structure	20
2.2.4. Environmental measures	22
2.2.5. Parramore Island	23
2.2.6. Principal components data reductions	24
2.2.7. Dendrochronological analysis	26
2.3. Results	28
2.3.1. Plant area index	28
2.3.2. Litter	30
2.3.3. Crown ratio and HPCD	32
2.3.4. Principal components analysis: biophysical and environmental classification	36
2.3.5. Dendrochronological analyses	50
2.4. Discussion	57
2.4.1. Plant area index	57
2.4.2. Crown Ratio	58
2.4.3. Dendrochronological analyses	58
2.4.4. Climate correlations interpretation	60
2.5. Conclusions	62
2.6. References	65
III. Sea level forcing, and relationships of freshwater availability and barrier island forest biophysical structure	71
Abstract	71

<b>Section</b>	<b>Page</b>
3.1. Introduction	73
3.2. Background	75
3.2.1. General barrier island upland forest ecohydrology	75
3.2.2. Water availability and structure	77
3.2.3. Tidal forcing	78
3.2.4. Evapotranspiration	79
3.2.5. Synthesis	80
3.3. Methods	82
3.3.1. Site and biophysical stratification	82
3.3.2. Water availability and structure	84
3.3.3. Evapotranspiration	86
3.3.4. Tidal forcing	88
3.4. Results	92
3.4.1. Site and biophysical stratification	92
3.4.2. Plant area index	94
3.4.3. All biophysical structure	97
3.4.4. Shrub analysis	99
3.4.5. Soil texture index and water availability	100
3.4.6. Evapotranspiration	104
3.4.7. Developmental forces	106
3.4.8. Tidal forcing	107
3.5. Discussion	116

<b>Section</b>	<b>Page</b>
3.5.1. Plant area index	116
3.5.2. Developmental forces	117
3.5.3. New water availability index	118
3.5.4. Shrub analysis	120
3.5.5. Evapotranspiration	121
3.5.6. Tidal forcing	124
3.6. Conclusions	126
3.6.1. General conclusions	126
3.6.2. System description and factor synthesis	126
3.6.3. Predictions of effects to bio-types	128
3.7. References	130
IV. The application of the EAARL (Experimental Advanced Airborne Research Lidar) to measurement and monitoring of barrier island forest structure in an ecohydrological change scenario	137
Abstract	137
4.1. Introduction	139
4.2. Background	142
4.2.1. Lidar remote sensing	142
4.2.2. The EAARL lidar	144
4.3. Methods	146
4.3.1. General considerations	146
4.3.2. Data collections	147

<b>Section</b>	<b>Page</b>
4.3.3. EAARL data descriptions	148
4.3.4. Analyses	149
4.4. Results	152
4.4.1. Direct comparisons	152
4.4.2. Multiple regressions for stand-level metrics	157
4.4.3. PAI, and relationships of structural variables to site moisture	157
4.4.4. The EAARL correlates for moisture status monitoring	159
4.4.5. Alternative method of canopy information comparisons: principal components analysis	161
4.5. Discussion	164
4.5.1. Direct comparisons	164
4.5.2. Canopy profiles	167
4.5.3. Multiple regression models	169
4.5.4. Canopy principal components analysis	170
4.5.5. Occlusion	174
4.5.6. Ecohydrological relationships and monitoring	176
4.6. Conclusions	181
4.7. References	185
V. Summary	190
5.1. References	193
Appendix A. Canopy profiles	194

<b>Section</b>	<b>Page</b>
Appendix B. Crown lengths	199
Appendix C. PAI fluctuation	201
C.1. References	204

## List of Figures

<b>Figure</b>	<b>Page</b>
1.1. Map of Assateague and Parramore Islands of the Delmarva Peninsula	5
1.2. Conceptual model of the Mid-Atlantic barrier island sea-level and above-ground forest structure relationship, with basic monitoring cues	8
2.1. Overview map of the study area with plot locations	18
2.2. 2005 PAI readings by the sub-bio-types	29
2.3. Predicted PAI by multiple regression against field average PAI	30
2.4. The average litterfall (leaves only) through 2005	31
2.5a. Canopy presence frequency spectrums and tree stem profile charts from water-monitoring field plots of bio-type 1	33
2.5b. Canopy presence frequency spectrums and tree stem profile charts from water-monitoring field plots of bio-type 2	34
2.5c. Canopy presence frequency spectrums and tree stem profile charts from water-monitoring field plots of the outlier bio-type	34
2.5d. Canopy presence frequency spectrums and tree stem profile charts from water-monitoring field plots of PIVCR	35
2.6. PC space in the biophysical principal components analysis (PCA)	38
2.7. The dendrogram of cluster analysis results of the PC space functions developed with the plot biophysical features	39
2.8. PC space in the environmental principal components analysis (PCA)	41

<b>Figure</b>	<b>Page</b>
2.9. The dendrogram of cluster analysis results of the PC space functions developed with the plot environmental features	42
2.10. Map of the AINS biophysical (bio)-type groups	44
2.11. Map of the AINS environmental (site) type groups	45
2.12. Graphical comparisons of the sub-bio-types in magnitudes and variation of sample population statistics for biophysical metrics	46
2.13. Graphical comparisons of the site-types in magnitudes and variation of sample population statistics for environmental metrics	47
2.14a. Bio-type 1 subdivision post-dbh 20-year radial growth trends	51
2.14a. Bio-type 2 subdivision post-dbh 20-year radial growth trends	51
2.15. Site type master tree ring chronology mean sensitivity and maximum canopy height	53
2.16. Pearson correlations between yearly tree ring radial increment and the months of a 17-month climate activity cycle	55
3.1. An example of water table fluctuation data used in the White ET equation from AINS plot 29803	86
3.2. Map of Assateague and Parramore Islands of the Delmarva Peninsula	89
3.3. Pearson correlations between PAI from 2005 and coarse structural metrics collected in all plots	95
3.4. PAI values across 2005 study period for plots in the biophysical bio-types 1 and 2	95

<b>Figure</b>	<b>Page</b>
3.5. The average litterfall (leaves only) through 2005 monitoring for individual sites	97
3.6. Shrub canopy area and average height of the shrub layer in plots at AINS	100
3.7a. The STI profiles of plots in bio-type 1 with a linear best-fit trendline	102
3.7b. The STI profiles of plots in bio-type 2 with a linear best-fit trendline	103
3.7c. The STI profiles of plots in bio-type outliers with a linear best-fit trendline	103
3.8. Results of a dendrochronological analysis of radial growth rates performed on two bio-type subgroups at AINS of similar age and comparable canopy crown class positions	107
3.9a. 12-hour average tide and fresh water table levels at AINS plots in the winter dry period	109
3.9b. 24-hour average tide and fresh water table levels at PIVCR plots in the dry winter period	110
3.10. The Spearman correlation ranks of the tide and water tables for AINS and PIVCR in the winter dry period	110
3.11a. The SPECTRA procedure results for AINS plots in the dry winter period	111
3.11b. The SPECTRA procedure results for PIVCR plots in the dry winter period	112
3.12. Hourly OC Inlet tide for the winter dry period	112

<b>Figure</b>	<b>Page</b>
3.13. The best cross-correlation values between “prewhitened” tide and fresh water table levels at various lags for 7 AINS plots	113
3.14a-f. Individual AINS plot map excerpts with ARIMA results interpretations	114-115
3.15 Diagram of current water availability scale in an idealized Assateague Island soil column	120
4.1. An example of a lidar waveform returned from a 0.08ha land surface plot on AINS, August 2004	143
4.2. General EAARL survey configuration	145
4.3. Map of Assateague and Parramore Islands of the Delmarva Peninsula	147
4.4. A raw EAARL composite waveform and graphical metric descriptions	149
4.5. A comparison of an EAARL backscatter count spectrum and a field plot canopy foliage presence histogram	150
4.6. The EAARL waveform, field crown presence frequency histogram, maximum field height, and stem profile for the 10 instrumented water plots at AINS and 3 measured PIVCR plots	155-156
4.7. Regressions of the field-collected maximum canopy height, height of peak canopy density, and bare earth elevation against the respective EAARL-predicted values	157
4.8. Predictions of stand variables from multiple stepwise regressions with standard EAARL metrics MCH, CRR and HOME	158

<b>Figure</b>	<b>Page</b>
4.9. PAI values across 2005 study period for plots in the biophysical bio-types 1 and 2	159
4.10. Regressions of EAARL CRR-predicted PAI against the field-collected values	160
4.11. The PC loading locations in the canopy across all plots in the field measures of maximum foliage presence frequency and the EAARL returns of backscatter energy	162
4.12. Site type groups plotted in canopy density PCA space for field and EAARL according to their respective scores	162
4.13. New PC loading locations with HPCD as upper bounds in the field measures of maximum foliage presence frequency and the EAARL returns of backscatter energy	163
4.14 Site type groups plotted in the new HPCD-based canopy density principal component space for field and EAARL according to their respective scores	164
4.15. Correlations of HPCD and MCH with the other major structural parameters	166
4.16. Major biophysical parameters in the six environmental site types used to stratify PCA and other analyses	171
4.17. Diagram of water availability scale in an idealized Assateague Island soil column	179

<b>Figure</b>	<b>Page</b>
4.18. Conceptual model of the Mid-Atlantic barrier island sea-level and above-ground forest structure relationship, with basic monitoring cues	181
A.1. The EAARL waveform diagrams, the canopy presence frequency by height increment histograms, and the stem profiles for all plots	195-198
B.1. A comparison of the two results from separate crown length data sets for AINS plot 21901	200
C.1 The 2005 average PAI and the range in PAI of 2005 for the bio-types 1a-3	202

## List of Tables

<b>Table</b>	<b>Page</b>
2.1. Litter rates by monitoring plots and associated bio-type for the total monitoring period of 2005	32
2.2. The average crown ratios and standard deviations for the bio-types less outlier type 3	32
2.3. The variables and plot values that were used to derive principal components and group sites into biophysical and environmental types by cluster analyses of PC scores	36
2.4. Eigenvector loading values of the biophysical variables in the resultant 5 principal components	37
2.5. Scores of all plots in the first two biophysical principal components	38
2.6. Eigenvector loading values of the environmental variables in the resultant 5 principal components	40
2.7. Scores of all plots in the first two environmental principal components	41
2.8. Biophysical sub-types derived by principal components analysis of structural variables and cluster analysis of PC scores	43
2.9. Site-types derived of environmental variable principal components analysis, and the cluster analysis of PC scores by individual plots	43
2.10. The sample population statistics for HPCD, BA, SCA, PAI, and maxage by bio-type	48

<b>Table</b>	<b>Page</b>
2.11. The sample population statistics for distshore, STI, SOM, BEE, DWT, and maxage by site-type	49
2.12. ANOVA results to test indication of site-type by the major biophysical parameters	50
2.13. All bio-type ring width increment changes between ten-year averages initiated from 1-2 years after age at dbh; and departures from bio-type averages	52
2.14. List by site type of the plots contributing samples to the site type master chronologies developed for the climate correlation analyses	56
3.1. Meteorological measurement values for July 20, 2005 and annual average values for 2005 collected at AINS	88
3.2. The variables and plot values that were used to derive principal components and group sites into biophysical and environmental types by cluster analyses of PC scores	93
3.3. Site-types derived of environmental variable principal components analysis, and the cluster analysis of PC scores by individual plots	93
3.4. Biophysical sub-types derived by principal components analysis of structural variables and cluster analysis of PC scores	94
3.5. The proportional reduction of PAI in 2005 for major bio-types	96
3.6. The correlation results of change in PAI and litterfall in the biophysical types	97

<b>Table</b>	<b>Page</b>
3.7. The correlation results for the site moisture indices STI and DWT with forest structure across site and biophysical types.	98
3.8. The correlation results for DWT and PAI within biophysical types at an average two-week lag from time at DWT to time at PAI	99
3.9. The White groundwater evapotranspiration equation values for July 20, 2005	105
3.10. The Spearman correlation results of White groundwater evapotranspiration constituents and a selection of site environmental and biophysical variables	106
3.11. Summary statistics of biophysical properties of the AINS bio-types	118
4.1. The mean absolute error and standard error between directly measured field values and EAARL values in the field plots and LFPW's	153
4.2. Correlations among average PAI from 2005 and structural metrics collected in all plots	158
4.3. Numerical results of the PCA on canopy returns	162
4.4. Field plot mean maximum height of all stems (trees and shrubs) for the entire plot network	173
C.1 Total PAI fluctuation in the 2005 field collections for the bio-types varies directly with stand stature in type 1, and varies negatively in type 2	202

**List of Acronyms**

AINS	Assateague Island National Seashore
ALPS	Airborne Lidar Processing System
AMSL	Above Mean Sea Level
ANOVA	Analysis of Variance
ARIMA	AutoRegressive Integrated Moving Average
ATM	Airborne Topographic Mapper
BA	Basal Area
BEE	Bare Earth Elevation
BT	Biophysical Type
CHP	Canopy Height Profile
CRR	Canopy Reflection Ratio
CV	Coefficient of Variation
CVM	Canopy Volume Method
dbh	Diameter at Breast Height
distshore	Distance to Ocean Shoreline
DWST	Depth to Water Table • Soil Texture Index
DWT	Depth to Water Table
EAARL	Experimental Advanced Airborne Research Lidar
ET	Evapotranspiration
ET <sub>G</sub>	Evapotranspired Groundwater

GIS	Geographic Information Systems
GLM	General Linear Model
GPS	Global Positioning System
GRR	Ground Reflection Ratio
HOME	Height of Median Energy
HPCD	Height of Peak Canopy Density/Energy
IFOV	Instantaneous Field of View
IRCF	Iterative Random Consensus Filter
LAI	Leaf Area Index
LFPW	Large Footprint Waveform
lidar	Light Detection and Ranging
LTERR	Long Term Ecological Research
LTRR	Laboratory of Tree Ring Research
MAE	Mean Absolute Error
maxage	Maximum Age
MC	Master Chronology
MCH	Maximum Canopy Height
MCHOG	Myrica Cerifera Hog Island Transpiration Model
MMH	Mean Maximum Height
MSR	Multiple Stepwise Regression
NASA	National Aeronautics and Space Administration

NOAA	National Oceanic and Atmospheric Administration
NPS	National Park Service
NSF	National Science Foundation
NWS	National Weather Service
OC	Ocean City
PAI	Plant Area Index
PC	Principal Component
PCA	Principal Component Analysis
PIT	Point In Time Water Table Depth
PIVCR	Parramore Island of the Virginia Coast Reserve
PTH	Plot Average Tree Height
R	Recovery Rate (of Water Table)
RAWS	Remote Automatic Weather Station
RMSE	Root Mean Square Error
RWI	Ring Width Index
SCA	Shrub Canopy Area
SE	Standard Error
SI	Site Index
SLA	Specific Leaf Area
SLICER	Scanning Lidar Imager of Canopies by Echo Recovery
SOM	Soil Organic Matter

SPAC	Soil Plant Atmosphere Continuum
SPECTRA	Spectral Analysis
ST	Site Type
STI	Soil Texture Index
$S_Y$	Specific Yield (of Site Level Aquifer)
TNC	The Nature Conservancy
USDA	United States Department of Agriculture
USFWS	United States Fish and Wildlife Service
USGS	United States Geological Survey
USGS CCWS	USGS Center for Coastal and Watershed Studies
UTM	Universal Transverse Mercator
VCR	Virginia Coast Reserve
vol	Parabolic Volume



## **I. Introduction**

This dissertation is an effort to document baseline biophysical and environmental conditions of Mid-Atlantic barrier island forests, and determine an underlying ecohydrological mechanism that will aid in predicting effects to forest structure and development by rising sea levels. Robust biophysical and environmental classifications are pursued to clearly identify the respective gradients, and the spatial relationships between them along the barrier island “toposequence” (Brady and Weil 2008). Spatial associations of site type (based mainly on depths to water table and soil textures) and structural expression substitute for the expected temporal change in forests and their freshwater sources with sea level rise.

Upon classifying the sites, likely trajectories in development with sea level and water table rise are theorized based on the synthesis of:

- A basic understanding of geomorphologic evolution of barrier islands
- Correlating an estimate of “water availability” based on previous (Hayden *et al.* 1995) and current (this volume) theoretical work with structural metrics
- Measuring structure to a temporally fine estimate of above-ground vegetation area to assess the limits of biophysical reactivity to water availability
- Two dendroecological analyses that support the above water availability theory, help build a broad forest development paradigm

based on rooting zone dynamics, and enable a degree of temporal extrapolation forward

- Groundwater evapotranspiration estimates of the biophysical types that emphasize the interplay of structural levels (tree and shrub)

Finally, a lidar instrument is tested for mensuration reliability at the study area.

The system description emerging from the points above is proposed as a basis for a scheme to analyze and monitor above-ground biophysical structure for changing water relations with waveform-returning lidar.

### **1.1. Background**

Mid-Atlantic barrier islands are naturally fluctuating physical systems through the process of “rollover” by which sands are shifting gradually westward with dominant wind and wave forcing. Barrier islands provide critical protection to mainland shores by attenuating much of the energy of coastal storms, thereby also sheltering the highly productive marshlands and estuaries of the bay side (Ruppel et. al. 2000). Many waterbirds use these coastal bays and marshes (see Erwin 1996), and some populations of shorebirds like that of the threatened Atlantic coast piping plover (*Charadrius melodus*) depend on the barrier islands for nesting (USFWS 1996).

Resistance of the islands to storm and wave action is determined to an extent by vegetative cover. However, the loblolly (*Pinus taeda*) forests of Assateague Island National Seashore (AINS) in Maryland and to a lesser extent those of Parramore Island of

the Virginia Coast Reserve (PIVCR), lack baseline biophysical data and information describing ecological processes and functioning.

Altered storm patterns and frequencies predicted to occur with climate change could affect island geomorphology and water relations, and maritime forests may experience die-back such as occurred on Hog Island of the Virginia Coast Reserve (VCR) in the 1920's, and recently on Northern Parramore (Hayden *et al.* 1995). Salinization of groundwater due to sea level rise resulted in patterns of slash pine (*P. ellioti*) mortality on Sugarloaf Key, Florida (Ross *et al.* 1994). Shao *et al.* (1995) show that barrier island shrub water relations could be significantly affected by a change in temperature (through increased evapotranspiration).

Central to the present study is the threat posed by rising sea level to freshwater sources in simple vertical forcing of water tables and elevated saline mixing zones. Hayden *et al.* (1995) report that the VCR is undergoing a relative (land subsidence plus real sea-level rise) sea-level change of  $+3.0\text{mm yr}^{-1}$ . Freshwater reserves atop salt water should rise accordingly, changing site water tables and, theoretically, vegetation communities. The substitution of spatial scale for temporal scale in changing water levels over the island toposequence is acceptable because of the relatively simplified and observable nature of barrier geomorphology. However, important considerations are given to the interacting factor of soil texture to a simple water-table-and-sand-driven model of changing water availability.

Water availability – likely determined in large part by depth to water tables at the barrier islands (Hayden *et al.* 1995) – plays a major role in vegetation dynamics and productivity, but the governing interactions, including leaf area index (LAI) in

transpiration and photosynthesis, are not well understood (Gholz 1991). Fundamental hydrological relationships are also not well understood for AINS or PIVCR. Bolyard *et al.* (1979) applied a model developed in the Outer Banks of North Carolina to AINS, yet concluded there was insufficient information to infer a robust hydrological system description. In order to predict possible effects to the extent and distribution of vegetation communities, there must be dependable descriptions of site water conditions and sufficiently specific knowledge of forest water relations.

Potential applications and limitations of small-footprint, waveform-returning lidar (Light Detection and Ranging) systems need to be documented. Lidar monitoring of vegetation communities may provide a valuable tool in characterizing environmental effects, and in the identification of areas vulnerable to change. The NASA EAARL (Experimental Advanced Airborne Research Lidar) system appears to hold particular promise because of its ability to characterize above ground vegetation vertical density as well as bare earth topography at flexible scales. EAARL work in this dissertation involves novel techniques of data processing, analysis, and application that can inform future EAARL and general lidar-based research. Specifically, it is expected that EAARL will support the development of standardized methodologies to monitor leaf area and/or other vegetation parameters for use in modeling and interpreting forest stand processes and water relations.

## 1.2. Study Area

AINS (Fig. 1), centered at Easting 485,236m and Northing 4,224,294m (UTM Zone 18N), on the coast of Maryland is administered by the National Park Service (NPS). The unit runs 37km from the Ocean City, MD inlet to the Virginia line, is 2.5 Km at its widest, and has forested areas up to 3.5m AMSL (above mean sea level). There are 26 0.08ha (16.3m radius) plots dedicated to the full array of ground and remote measures.

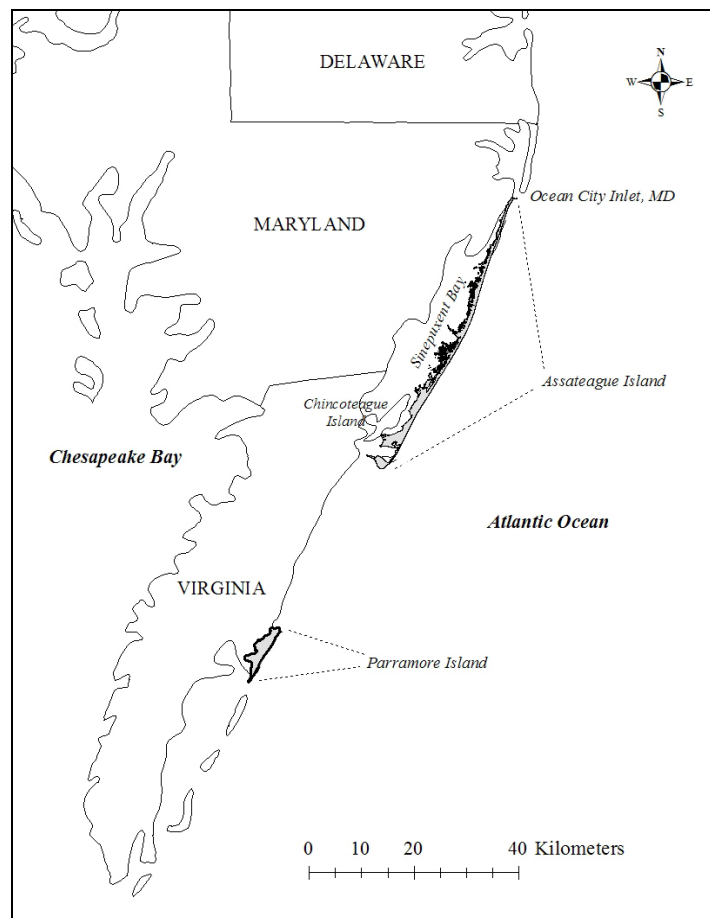


**Figure 1.1.** Assateague and Parramore Islands of the Delmarva Peninsula.

Parramore Island (Fig. 1), centered at Easting 442,933m and Northing 4,153,403m (UTM Zone 18N) is administered by The Nature Conservancy (TNC) as part of the VCR. The National Science Foundation (NSF) maintains a Long Term Ecological Research (LTER) site at the VCR. Parramore's area is approximately 13.3km long and 3km wide. Maximum forest elevation is about 7m AMSL. Of approximately 15 previously established (Richardson and Shugart 1993), loblolly-dominated forest plots (also 0.08ha) only 3 were of acceptable condition for this study. There was a massive canopy die-off from effects of a fire, bark beetle infestation, and a hurricane from September 2002 to September 2003. Canopy decline continues in impacted areas but there is extensive recruitment.

### **1.3. Study Outline**

#### **1.3.1. Objectives**

The work is designed to characterize the vulnerability of communities and structural types on Mid-Atlantic barrier islands, and predict the likely effects to these by sea-level rise and the forcing of island freshwater tables. For instance, capturing leaf area changes associated with general water availability can provide a circumstantial reference to anticipate and better model production and growth trajectories under changing water levels.

Barrier island vegetated areas are essentially geomorphologically controlled habitats with community succession dependent on the changes to island physical conditions. Woody vegetation communities on the eastern, depleting edge are generally younger, while those on the accreting western side of the advancing edge are older.

It is necessary to frame the current investigation of forest structural change as distinct from the geomorphic pre-conditioning of vegetation that is present. Because of the relatively fast geomorphic evolution of sites, and the addition of a generally spatially-constant pressure in the form of sea level, vegetation is organized along a scale of *potential* structure in this study. Such a forcing will change developmental trajectories in-situ, as geomorphic adjustment to critical ecosystem-structuring components like soil texture will not keep pace.

The project initiates investigation into describing a whole-system ecohydrological function concept of a barrier island toposequence (with a space-for-time scale substitution), representing an integrative approach to monitoring system dynamics as they change ever faster. Figure 2 is a proposed conceptual model to structure monitoring and analysis of the effects of sea level rise to barrier island forests.

### **1.3.2. Overview of sections**

Chapter 2, “Mid-Atlantic barrier island forest structural properties and site gradient expression” comprises the first comprehensive description of AINS forest structure, and the first PIVCR forest measures since 1996. Along with some extensive environmental measurements, classification groups are derived by a plot-network principal components analysis (PCA) for all succeeding analyses of gradient interactions, and predictive theory formulation. An uncommon use of standard dendrochronological data is applied to forest development questions on AINS, and common climate interactions are tested within groups with standard techniques.

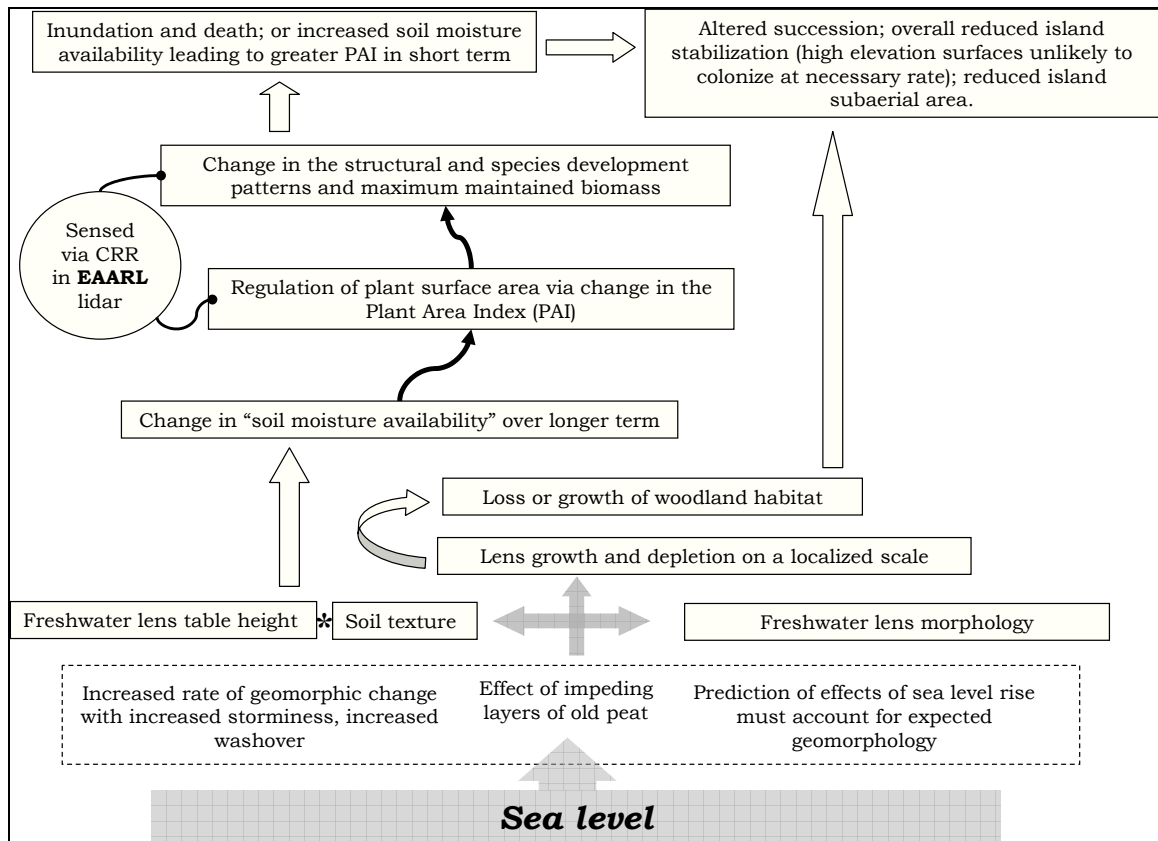


**Figure 1.2.** Conceptual model of the Mid-Atlantic barrier island sea-level and above-ground forest structure relationship. EAARL lidar would be employed at regular intervals to provide fine resolution Canopy Reflection Ratio (CRR) changes with quantified water level changes and ground-verified structural changes. Ground verification could be suspended after regression relationships of the structure-moisture interaction reach significant levels. Further remote monitoring would provide predictions of decline thresholds due to sea level rise. The figure is developed based on recommendations in Fancy *et al.* (2009) “Monitoring the Condition of Natural Resources in US National Parks.”

Chapter 3, “Sea level forcing, and relationships of freshwater availability and barrier island forest biophysical structure” develops the correlative supports for a basic theory of site water-limited growth on barriers to fashion a broad predictive relationship of rising water tables and biophysical structure adjustment. The work affirms the presence of, and coarsely characterizes, current sea-level signals in water tables to infer potential gradations in sensitivity to forcing across sites and islands.

Evapotranspirational dynamics of this habitat are studied in Chapter 3 by applying the White (1932) groundwater evapotranspiration equation to hourly water level data.

This exercise yields results that affirm well-established ecophysiological relationships. Results also help shape the main ecohydrological theory of development for barrier islands, and lend direction to future investigations into ecohydrological changes due to sea level rise.

Chapter 4 “The application of the EAARL (Experimental Advanced Airborne Research Lidar) to measurement and monitoring of barrier island forest structure in an ecohydrological change scenario” comprises a thorough ground-truthing of the EAARL instrument in the *P. taeda* forest type of the barriers. Data in the form of standard lidar metrics and new EAARL waveform-specific derivatives are further utilized for the exploratory ecological monitoring analysis here. Their predictive potentials are tested against ground parameters that are rated for their indication of general water availability. New analyses are explored to test for efficient ways of parsing lidar canopy information.

#### **1.4. References**

- Bolyard, T. H., G. M. Hornberger, R. Dolan, and B. P. Hayden. 1979. Freshwater Reserves of Mid-Atlantic Coast Barrier Islands. *Environmental Geology* **3**:1-11.
- Brady, N. C. and R. R. Weil. 2008. *The nature and properties of soils*. Fourteenth edition. Pearson Education, Upper Saddle River, N.J.
- Erwin, R. M. 1996. Dependence of waterbirds and shorebirds on shallow-water habitats in the mid-Atlantic coastal region: An ecological profile and management recommendations. *Estuaries* **19**:213-219.
- Gholz, H. L., S. A. Vogel, W. P. Cropper, K. Mckelvey, K. C. Ewel, R. O. Teskey, and P. J. Curran. 1991. Dynamics of Canopy Structure and Light Interception in *Pinus-Elliottii* Stands, North Florida. *Ecological Monographs* **61**:33-51.
- Hayden, B. P., M. C. F. V. Santos, G. F. Shao, and R. C. Kochel. 1995. Geomorphological Controls on Coastal Vegetation at the Virginia-Coast-Reserve. *Geomorphology* **13**:283-300.
- Richardson, D. L., J. H. Porter, and H. H. Shugart. 1993. Permanent Vegetation Monitoring Plots on Parramore Island: Attributes and Analysis Direction. <http://www.vcrlter.virginia.edu/davedocs/VCRASC95/richshug.html>.
- Ross, M. S., J. J. Obrien, and L. D. L. Sternberg. 1994. Sea-Level Rise and the Reduction in Pine Forests in the Florida Keys. *Ecological Applications* **4**:144-156.
- Ruppel, C., G. Schultz, and S. Kruse. 2000. Anomalous fresh water lens morphology on a strip barrier island. *Ground Water* **38**:872-881.

- Shao, G. F., H. H. Shugart, and D. R. Young. 1995. Simulation of Transpiration Sensitivity to Environmental-Changes for Shrub (*Myrica-Cerifera*) Thickets on a Virginia Barrier-Island. *Ecological Modelling* **78**:235-248.
- U.S. Fish and Wildlife Service. 1996. Piping Plover (*Charadrius melodus*), Atlantic Coast Population, Revised Recovery Plan. Hadley, Massachusetts. 258 pp.
- White, W. N. 1932. A method of estimating ground-water supplies based on discharge by plants and evaporation from soil, Washington, DC.

## **II. Mid-Atlantic barrier island forest structural properties and site gradient expression**

### **Abstract**

The inherent ephemeral nature of a barrier island accents a concern for the continued integrity of upland communities as island geomorphic evolution is increasingly forced by sea level rise. Several easily measured and mapped biophysical variables are identified here for the monitoring of changes in upland *Pinus taeda* (loblolly pine) forest subject to environmental forcing. A principal components analysis (PCA) will relate the biophysical data (and, separately, environmental variable data) to forest structure. This ecological investigation will connect forest growth and ecohydrology, initiate baselines, and characterize vulnerabilities among different classifications.

A biophysical variable, plant area index (PAI), measured with the electronic LAI-2000 (Li-Cor Biosciences, Lincoln, NE) optical instrument, can represent differences in photosynthetically active plant area across gradients as well as change within sites over monitoring periods. This latter temporal variation can be represented by the proportion of PAI range to PAI average. While promising, this resulting “fluctuation” statistic requires more verification before attributing a material equivalence. Another descriptive biophysical metric, height of peak canopy density (HPCD), is derived from merged crown ratio data in a plot and appears to be a coarse leaf-area distribution weighting. Site environmental differences, generally related to soil moisture dynamics, explain 66% of the variation in HPCD. Of the biophysical metrics measured, the most reliable site

indicator is the maximum canopy height (MCH), a finding consistent with studies in other forests. In this case, 76% of variation in MCH is explained by site conditions.

Further evidence of differential site effects on barrier island *P. taeda* growth are found using dendrochronological techniques. Growth at lower site index (SI) stands declines at a significantly faster rate than on higher SI sites. The 10-year average radial growth rate of trees declines over sampled periods of 20 years following stand initiation, and is up to 27% less in lower SI stands. This correlates with more shallow water tables in low SI sites. Root competition should be greater at these low SI sites when compared to better sites that may access more stable water tables at greater depths. It is feasible to extrapolate the average bio-type growth rates found in early stand development to predict growth and developmental reactions by biophysical groups to water table rise and greater storminess. In tree-ring chronology correlations with climate, the differences in correlation among site types can be explained by this soil profile/rooting zone and water source theory. One can reliably differentiate forest sites, on relatively small spatial scales of barrier islands, by their reactivity to shared climate.

## **2.1. Introduction**

This chapter serves to describe the methodologies and initial data relevant to the larger project investigating ecohydrological function and remote sensing of canopy structure, and to introduce and describe general developmental issues in *Pinus taeda* (loblolly pine) forest over a barrier island toposequence. The major interactions of concern in the larger project occur in the rooting zone over time with changing average

water tables as sea level rises. The direction of inquiry throughout this chapter is based on well-founded theory of water table-structured vegetation mosaics on barrier islands (Hayden *et al.* 1995; Ehrenfeld 1990), with relatively little ecohydrologic investigation into likely vegetation changes with water table rise (Ehrenfeld 1990). The broad nature of the present study requires some acceptance of circumstantial evidence of moisture relations to advance the change analysis. Depth to water table and soil texture index are utilized to characterize a site's water availability. Analyses initiated here are developed further in the succeeding chapters where predictions of effects on forest development take shape.

Principal components analysis (PCA) is used to classify sites into biophysical and environmental types. These groups act to structure all analyses and predictive theory formulations in a space-for-time scale substitution of general sea-level rise effects to island forest communities. Unlike studies that describe vegetation using detailed species presence along a continuum to derive principal components (PC's), and model an underlying environmental gradient (see Roman *et al.* 1985, and Zampella *et al.* 1992), the present study relies on PCA of general vegetation structure to predict the likely impact of changing water relations. Biophysical statistics for classes that emerge from the PCA will be assessed for general correlation with site hydrologic indicators to aid in populating a moisture/forest structure gradient. Site types derived from the environmental PCA are not dependent on biophysical types, and they provide a measurement of the direct effects of water-related abiotic variation on ecosystem properties.

Plant area index (PAI) serves as a relative index of site quality and overall forest stature among sites. It incorporates foliar area (leaf area index or LAI) and woody area.

Photosynthesis and evapotranspiration depend on leaf area (and associated stomatal density) as a surface of interaction and exchange (Gholz *et al.* 1990). Circumstantial evidence generally supports the use of LAI and PAI as indicators of site-mediated moisture availability (see Grier and Running 1977, Hennessey *et al.* 1992, Cowling and Field 2003). PAI changes intra-seasonally, and in *P. taeda*, leaf area has been found to vary temporally with moisture variables: litterfall decreases in the year following a dry year (Hennessey *et al.* 1992); and the number of foliage flushes in a year is affected by soil moisture (Spurr and Barnes 1980). However, dynamic predictive lag and transfer functions relating moisture variables and leaf area measures – thus providing for a fine-scale analytical and monitoring tool – are lacking. These effects are dealt with in Chapter 3.

Crown length measurements were collected for all trees and a unique plot-level variable – height of peak canopy density (HPCD) – that may approximate a leaf area distribution index in *P. taeda*, was developed. Crown length is important on the scale of individual trees. Nagel and O’Hara (2001) and Gillespie *et al.* (1994) find that productivity-related biomass changes occur within a crown at branch foliage distribution levels. Long and Smith (1990) argue that relative crown size indicates stemwood production efficiency, and found declining woody production per unit leaf area with increasing crown size in lodgepole pine (*P. contorta*).

The representation of foliar density distribution in HPCD is rather coarse at the scale of the plot but it distills the large amount of information found in the foliage height profiles of Aber *et al.* (1982) to a convenient index. Thus, HPCD variation is due in part to site factors that determine *P. taeda* hydraulic architecture and evapotranspirational

physiology. The raw crown data is processed in a manner analogous to the histogram source of the Ashton and Hall (1992) “stratification index”, but based on a literature search, there appears to be no metric identical to HPCD in use.

Tree ring increment growth rate serves, to an extent, to indicate variable developmental pressure by environment (along with general stand dynamics and competition effects). McClurkin (1958) found rapid radial growth response to declining site moisture variables in shortleaf pine (*P. echinata* Mill.) in N. Mississippi, though there was a non-trivial amount of unexplained variation within the time frame analyzed. Following a general recommendation (K. Hadley pers. comm.), the present method results in an alternate version of the technique employed by Nowacki and Abrams (1997) to detect release patterns in Pennsylvania oak forests where releases, measured in average growth rates, were timed with disturbances. In the present study, barrier island forest stands are compared by rates of decline over standard periods whereas the previous researchers had established proportional changes in growth as indicators for a prescribed event (Nowacki and Abrams 1997, Veblen *et al.* 1991). Using the raw ring width increment averages benefits from “discounting short-term climatic pulses and gradual ring-width changes due to tree aging, bole geometry, and long-term climate shifts” as Nowacki and Abrams (1997) note.

Differences in reactivity to previous and current-year climate can also explain radial growth variation among site types. Fritts (1976) notes that variation rates alone can indicate the degree of limitation imposed by environment on growth, with more limited sites being more sensitive. There is also opportunity to elucidate environmental control of

growth in the interpretation of specific patterns of variation and correlative directions with monthly climate.

Taken together, both dendroecological analyses allow for detailed, type-specific responses to changing water levels to be drafted and extrapolated forward for the purposes of this project.

## **2.2. Methods**

### **2.2.1. General plot installation and structural measures**

Permanent monitoring plots were installed at Assateague Island National Seashore (AINS) to represent structural gradients in the approximately 700 acres of forest on the Maryland end of Assateague Island (Fig. 1). On Parramore Island of the Virginia Coast Reserve (PIVCR) (Fig. 1) sites were chosen from an existing plot network (see *Parramore Island* section below) because they had some foliated canopy remaining after the widespread decline following a fire in 2002, subsequent beetle infestation, and Hurricane Isabel. The plots at AINS were chosen by a visual field reconnaissance. Sites included in the final array had relatively consistent canopy cover, and were judged to be generally representative of gradients of canopy and basal density, and elevation. Plot numbers were derived from the distance in kilometers south from the Ocean City Inlet, MD: E.g., 29202 is plot 2 in the 29.2km plot area.

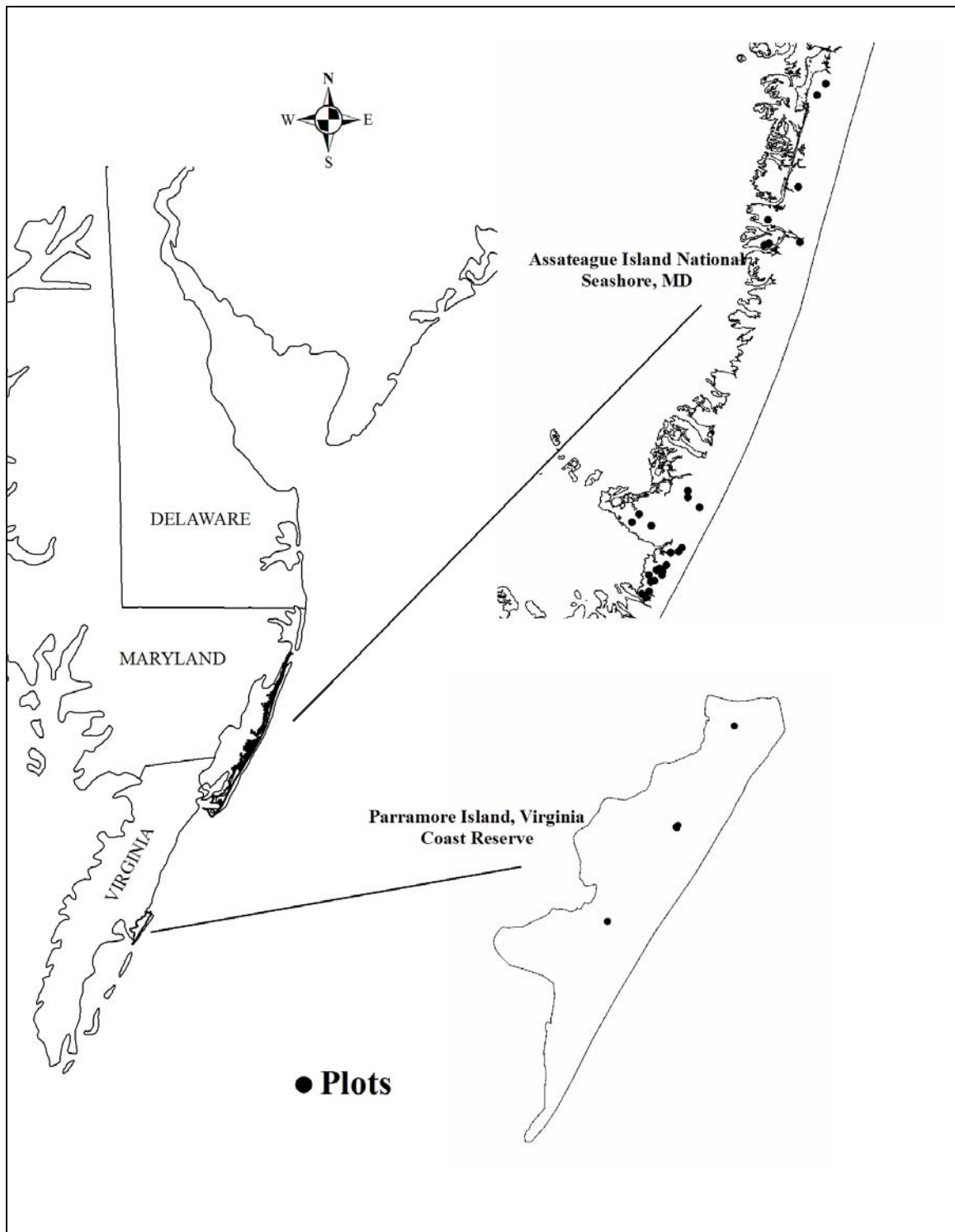


**Figure 1.** Overview of the study area including Assateague Island National Seashore, MD (AINS) to the North and Parramore Island of the Virginia Coast Reserve (PIVCR) to the South. There are 27 plots on AINS (26 of which comprise the bulk of analyses), and 3 plots on PIVCR (greatly reduced from pre-disturbance number of intact forested monitoring plots).

Plots were installed by establishing a center point, pounding a stake, and using measuring tapes or a surveyor's electronic total station to delineate a 16.3m radius circle (0.08ha area); all center points and tree trunks were mapped with the total station. Bare earth elevations were gathered with the total station and survey-grade GPS (Global Positioning System). Photo points were established at plot centers and perimeters, shot from and towards the four cardinal direction radii. Photos are catalogued from Fall 2004 and Fall 2006 in digital format.

Biophysical structure surveys of the 26 AINS plots were completed in 2005 to record (for all trees >2.5cm diameter at breast height): maximum canopy height (MCH), and crown length (length from topmost to lowermost foliated points) with a clinometer; dbh (diameter at breast height) with a fabric diameter tape; shrub stem number (>2.5cm basal diameter); and shrub canopy area (SCA) with a straight tape. Measured trees and shrubs were marked with aluminum tags and nails. Standard field measures were processed to plot-level values of basal area (BA):  $\pi*(dbh/2)^2$ , where dbh is the cumulative diameter at breast height of all plot trees, and the parabolic volume estimate (vol):  $(0.5(PTH)\pi(dbh/2)^2)$  (Whittaker *et al.* 1974) where PTH is plot average tree height. One additional plot (No. 20901) was surveyed incompletely but is included in some analyses. Maximum stand age (maxage) was determined by dendrochronological analysis as described below.

### **2.2.2. Crown ratio and plot canopy density distribution**

Crown length was converted to crown ratio by dividing by total tree height. All individual crown lengths were pooled over the plot area from the average ground level to

the maximum canopy height to create plot crown presence frequency distribution at a 10cm resolution (see histograms in Appendix A). HPCD was gathered directly from crown presence histogram data as the most frequently occupied 10cm segment (or approximate center point of multiple, adjacent peak segments). Accuracy of the frequency histograms is assumed to suffer in high-relief sites due to the averaging of ground elevation, but these sites are relatively few in number. A crown length collection accuracy issue, also relatively minor, is detailed in Appendix B.

### **2.2.3. Fine structure**

PAI was collected throughout 2004-2006 at AINS, though the 2005 growing season is best represented. The hand-held LAI-2000 derives PAI through calculation of canopy light transmittance with the Beer-Lambert Law (Pierce and Running 1988). The unit commonly underestimates biologically active leaf area, but does a good job of depicting changes across vegetation types and within sites during a season, and the PAI metric has been found to be linearly related ( $r^2=0.97$ ) to litterfall estimates of LAI (Chason *et al.* 1991). An average PAI value was calculated for all AINS plots utilizing the 2004 through 2006 measures. PAI temporal distribution in 2005 was described for only 20 of the 26 measured plots at AINS because these had adequate monitoring period lengths that could be assessed for approximate annual minima and maxima. Biophysical and environmental types were compared by average PAI and by 2005 proportional change.

As leaf area was not verified at AINS by traditional methods such as litterfall estimate, there is no accurate way to model true leaf area as a function of PAI (see

Sampson *et al.* 2003) in the present study. Appendix C details an exploratory methodology to estimate areal contribution by a foliage cohort.

The LAI-2000 is composed of five concentric light sensors capturing different ranges of zenith angles that are tuned to radiation below 490nm (blue visible light) where leaf reflectance and transmittance are minimal (Li-Cor Biosciences 1992). Following the manufacturer's recommendations (Li-Cor Biosciences 1992), "above" and below-canopy readings were collected in as close a temporal and spatial proximity as was feasible to obtain the transmittance estimate. Transmittance is used to calculate the light-blocking area within the view. Each below-canopy measurement was determined by averaging eight readings: four at each of two concentric circles within the plot footprint. "Above"-canopy calibrations were taken in open sites near study plots that allowed for unobstructed views of the sky (Li-Cor Biosciences 1992). All readings were collected in diffuse daylight at sunrise and/or dusk to prevent error associated with direct sunlight reaching the sensor (Chason *et al.* 1991).

All data processing was completed with Li-Cor FV2000 software (Li-Cor Biosciences 2004). Upon LAI-2000 manual (Li-Cor Biosciences 1992) and literature recommendations (Chason *et al.* 1991, Holst *et al.* 2004), the two outermost view rings (the flattest zenith angles) were excluded from PAI calculations. This reduced effects of light penetrating at low angles through leafless portions of trunks, and limited the inclusion of extra-plot vegetation matter (Holst *et al.* 2004). The resultant cone of view, at about a 50° zenith angle, encompasses the average stand height and circular plot size to an adequate precision.

Litterfall collections were made in the 11 plots equipped with water level monitoring wells. Hennessey *et al.* (1992) state that *P. taeda* needle fall will “represent the death of the total needle population formed in the previous year” while the timing of the fall is dependant on current seasonal climate (Hennessey *et al.* 1992). The litter weight increments were tested for correlation with PAI changes to test LAI-2000 sensitivity, and with changes in depth to water table (DWT) to test foliage sensitivity to available water. Intensive litterfall collections allowing for total leaf biomass estimates would have been excessively labor-intensive for the purposes of this study.

#### **2.2.4. Environmental measures**

Water table levels, soil texture, and precipitation were measured concurrent with the forest structure data. Weather data post-1991 are from an NPS-maintained RAWS (Remote Automatic Weather Station) at AINS, and from the National Oceanic and Atmospheric Administration (online source: NOAA National Climatic Data Center) for Snow Hill, MD prior to that time. DWT, for the purposes of initial stratification, was derived from single point-in-time (PIT) average measures to water tables during soil texture sampling in 3 soil pits per plot. 11 plots (‘water plots’) served as long-term water table monitoring sites. Here, Ecotone (Intermountain Environmental Inc.) automatic water level recorders were installed and programmed to record the water table every 30 minutes. A regression analysis shows that PIT measures can predict real average water tables in the water plots at  $r^2=0.69$ , with a root mean square error (RMSE) of 0.19m.

Soil organic matter (SOM; %organic matter) was determined by ignition (all samples were processed by The Virginia Tech University Crop and Soil Environmental

Sciences Soil Testing Lab, Blacksburg, VA) of an average sample from the top 10 cm of the 3 soil pits in a plot. Soil texture was determined in the same soil pits for 10cm increments through the soil profile to the water table. Thus, depending on a plot's topography, there are 1, 2 or 3 samples at every 10cm depth. A depth increment average sample was mixed by hand and divided by sieve shaking into the diameter (mm) classes: fines (<0.05), very fine sand (0.05-0.10), fine sand (0.10-0.15), medium fine sand (0.15-0.25) medium sand (0.25-0.50), coarse sand (0.50-1.0), and very coarse sand and gravel (>2.0). Portions were weighed on digital scales to 0.1 gram resolution.

The soil texture index (STI) variable was produced to supply a general textural variable for the principal components analysis site-typing. The fine sand:medium sand ratio was chosen for STI as they are distinct (separated by at least one other class) classes and significantly negatively correlate with the other (Spearman rank correlation  $r_s = -0.90$ ,  $p < .0001$ ). The fine sand coefficient of variation (CV) over the entire sample population is 57% and the medium sand CV is 27%. STI depicts relative fine-ness among the plot network, and hence, relative soil matric potential.

### **2.2.5. Parramore Island**

PIVCR plots were selected from the vegetation monitoring plot network established by Richardson, Porter, and Shugart (1993; VCR LTER online documentation). A field reconnaissance to find partially intact canopies in the decimated forest yielded 3 study plots. PIVCR plots 12 and 65 (Northernmost and center plots of Figure 1) tree layers were recorded in full, yet plot 91 (Southernmost, and sole intact plot) was measured only for canopy strata dominants (dominant *P. taeda*, and subcanopy

to intermediate *Persia palustris* and *Juniperas virginiana*) due to time constraints. Plots 91 and 12 were equipped with Ecotone water level recorders. Two temporary plots at PIVCR were included for maximum heights only; they were centered at water-level recorders installed transversely from the high point (plot 65-80) of a North-South ridge ('Italian Ridge') near plot 65 to a low point (plot 65-40). Sub-meter-accuracy horizontal positions of plot centers and tree stems, and average plot elevations were collected with survey-grade GPS and a total station survey instrument.

In plots 12 and 65, all attempts were made to find downed stems, and measure all standing stems according to the procedures laid out for AINS above. Downed bole lengths were measured approximately when they were fairly intact; there were 10 instances of this in plot 65, and 3 in plot 12. These were entered into the stem profile under the assumption that they may have been standing at the time of the airborne lidar (Light Detection And Ranging) survey in August of 2004 (Chapter 4). Standing snags were measured to tops, appearing in the stem profiles as "unfoliated bole" only. Of 133 original stems (as of 1996) in plot 65, 56 were located and measured. 64 of the 85 original stems were located standing in plot 12, yet only 12 had living foliage, and most of these were impacted and unhealthy; of the others standing, all were broken. 13 additional stems were found on the ground and 8 were not found.

### **2.2.6. Principal components data reductions**

To reduce the complexity of the preceding biophysical data, plot-level values of BA, maxage, PAI, HPCD, and SCA were entered into a principal components analysis (PCA; see Sneath and Sokal 1973) using the SAS "princomp" procedure (SAS Institute

2002-2003). The technique is a multivariate factor analysis that clarifies underlying linear combinations of original factors to explain much of the variation in samples (Sokal and Rohlf 1995). The results are generally two to three new orthogonal variable axes for concise spatial depiction of sample relatedness and dominant variation-alignment. MCH was not included in the biophysical PCA because of its over-riding influence as a site index (SI) determinant (tall canopies are on better sites), and because it is highly intercorrelated with the other canopy factors that are better suited to describe a biomass continuum on shorter time scales. Vol and HPCD slightly outperformed MCH in a test PCA (loading the first PC in top three descending order, respectively) providing some evidence that these are better candidates in depicting general biophysical stature at the plot level, while integrating average canopy height.

The above procedures were replicated with the abiotic environmental variables to create an environmental PC space. Bare earth elevation (BEE), distance to ocean shoreline (distshore), DWT, maxage, SOM, and STI populated this PCA. Maxage was utilized in both ordinations because it expresses biophysical and abiotic effects that would otherwise be too labor-intensive to depict in exclusive ways. Maximum stand age imparts a developmental constraint on otherwise similar heights or basal areas. Time since disturbance is also represented in maxage to an extent, and on barrier islands this will integrate many processes of soil and water environment development. Human interventions that could variably influence maxage were not analyzed.

All sites were plotted in biophysical and environmental PC space by regressing their PC2 scores against their PC1 scores in the two analyses. Cluster analysis by SAS “cluster” procedure (SAS Institute, 2002-2003) provided for the final classification into

biophysical and environmental types (“bio-types” and “site types”, respectively) based on average distance in PC space. The interoperability of the groupings was assessed by analysis of variance (with the SAS “glm” procedure, SAS Institute 2002-2003) of biophysical variables by environmental type.

### **2.2.7. Dendrochronological analysis**

One tree-ring core was drawn from at least one dominant, co-dominant, and intermediate/or subcanopy *P. taeda* tree in each plot using an increment borer. After significant drying time, the cores were mounted on grooved poplar wood blocks with wood glue. When these were dry, the cores were sanded to a smooth, glossy finish. Ring widths were measured to 0.001mm precision on a Velmex (Velmex Inc., Bloomfield, NY) measurement stage system, and the data were catalogued and dated with Medir (RL Holmes, Laboratory of Tree Ring Research - LTRR) software.

Individual series (annual ring-width increment over sampled time) dating was accomplished by using only live trees so that the dates would merely reverse from the year of coring to the pith at the center (at dbh – and therefore several years old at that height). There were generally too few total multiple-sample years per site to enable effective ‘crossdating’ (Fritts 1976) among series to thoroughly verify dates, but this is a less critical concern as ten-year spans were averaged.

To create average bio-type initiation growth trend replicates, series samples that were of approximately shared age and average canopy position, and had at least a 20-year period in common were grouped from representative plots. Having cored at tree dbh, raw trend data were drawn from at least two years after dbh age (a few very young samples

necessitated a one year + dbh buffer) to reduce further the potential influence of shading on growth. Grouping by similar age aids in reducing confounding effects of disparate stand initiation events. The final growth trend endpoints are centered at midpoints of the two ten-year periods, with the respective average ten-year ring width value.

The COFECHA (RL Holmes, LTRR) program was used to create master chronologies (MC) of ring width index (RWI) values for the site type series populations. The RWI is a transformed value derived from the standardization (Fritts 1976) of the sample series and their subsequent averaging. Standardization by COFECHA removes low-frequency trends related to common age-size relationships (Grissino-Mayer 2001) that would confound environmental signals. Site type MC's were assigned 'mean sensitivity' (Fritts 1976) values as a measure of variability in ring width useful in comparing site effects (pers. comm. K Hadley). Fritts (1976) states "the more the tree has been limited by environmental factors, the more the tree will exhibit variation in width from ring to ring."

Site type MC's were also applied in gauging a site's modulation effect on common climate during particular times of year. Each annual index value of an MC was tested for correlation with monthly temperature and precipitation of a 17-month period of interest from the previous May through the current September (Fritts 1976, Webb *et al.* 1993). The correlations were run using SAS (SAS Institute, 2002-2003) software and a program code written by Fekedulegn *et al.* (2002).

## **2.3. Results**

### **2.3.1. Plant area index**

In the 2005 field season PAI increased from Spring (there was generally a mid-April start of measure) through late Summer for most sites, with maximum values recorded from September 13 to October 19. Note that measurements are paced somewhat widely and may not represent actual extrema (Figure 2; vertices in graphs mark measurements). Several plots are not trending down as of the last Fall-measured PAI, and if they continued to rise this would result in the underestimation of the calculated annual range and average (see 21902 in bio-type 1a for example; Fig. 2). It seems however, that readings must decline soon after because, for example, *P. taeda* LAI peaks in September in the “sandhills” of North Carolina (Sampson *et al.* 2003), about 580km to the southwest of AINS.

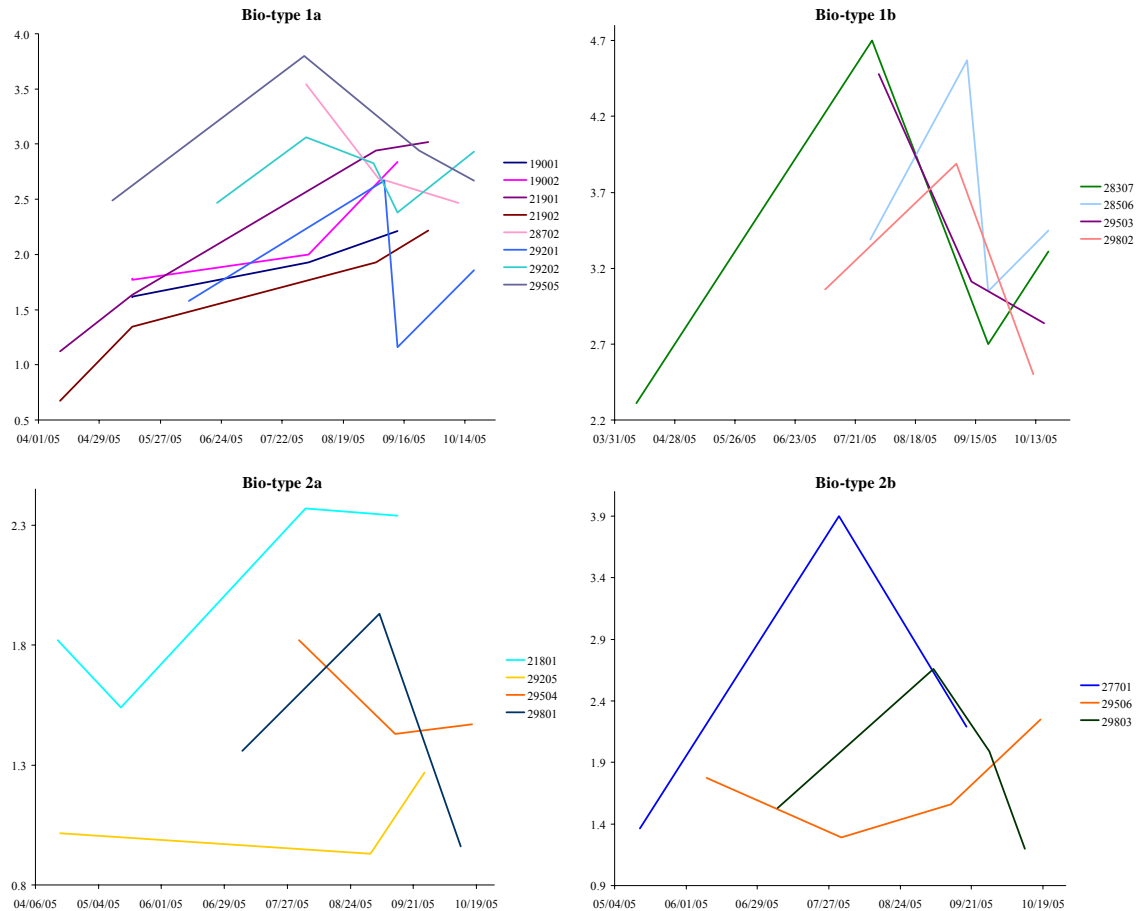


**Figure 2.** 2005 PAI readings by the sub-bio-types (less outlier type). Vertex positions denote times of measurement.

The spikes recorded around October 18-19 after troughs for plots 29202, 29201 (bio-type 1a), and 28307, 28506 (bio-type 1b) appear to correspond with a slowing rate of decline in other plots (Fig. 2). It is feasible that an anomalous sky condition occurred around these two days such that the difference between above-canopy and below-canopy as determined by the LAI-2000 is less than the preceding measure. This may occur if there is discontinuous cloud cover.

To evaluate the interrelatedness at plot level of projected plant area and the common forest metrics, the biophysical variables: plot average tree height (PTH), MCH,

HPCD, BA, and vol are tested in their predictive power for PAI (average 2005) in a multiple regression exercise (Figure 3). Somewhat surprisingly, only MCH is retained at a significant level ( $p=0.06$ ) with the resultant equation:

$$\text{Average 2005 PAI} = 0.8415 + 0.1037 (\text{MCH}) \quad (1)$$

where  $R^2=0.40$  and  $\text{RMSE}=0.70$ . The PAI fluctuation value (PAI range:PAI average; see Appendix C) is poorly modeled at  $R^2=0.18$  with only MCH retained in a multiple regression with the same biophysical metrics as above.

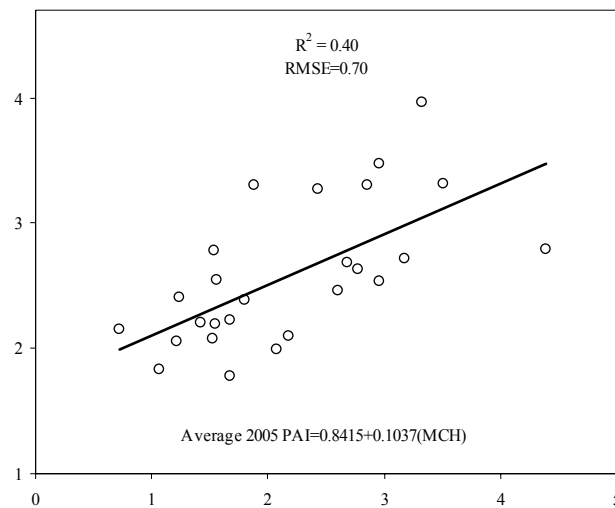


**Figure 3.** Predicted PAI by multiple regression (max canopy height is retained) against field average PAI (2005).

### 2.3.2. Litter

Patterns of litterfall are discernable (Figure 4) yet they are too coarse to allow for material loss calculations with change in soil moisture and other environmental indices. There are rough negative correlations in PAI and litterfall as would be expected. The resulting pattern does follow a similar one outlined by Gresham (1982) for *P. taeda* on the North Carolina coastal plain (for two out of three years in his study): a peak occurred

in early September, then a trough, and finally a large peak in the late fall. Comparing this to the PAI information in Figure 2, it is noted that a number of plots reach maximum PAI from mid-July to mid-August, during the first drop in litterfall rates and the slight rise towards September 1. The other discernable PAI peaks then occur in early September around the falling rates of litterfall after small peaks. Finally, the average litterfall rate for 2005 does trend with broad bio-types (Table 1), i.e. the larger bio-type 1 has greater litterfall rates than the smaller bio-type 2, though it does not correlate to a high degree with plot volume as there may be an underlying abiotic influence. At the current resolution, however, there are no significant correlations between litterfall and DWT (not shown) for all bio-types and times.

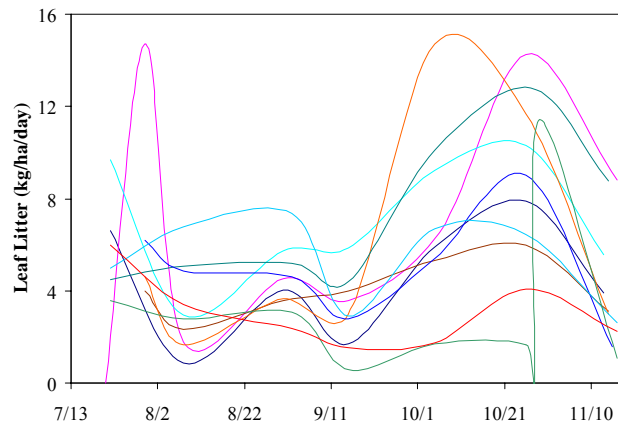


**Figure 4.** The average litterfall (leaves only) through 2005 monitoring, in  $\text{kg ha}^{-1}\text{day}^{-1}$  for individual sites ( $n=10$ ). Plot 21903 is not represented here as it skews the chart by a very large needle drop late in the year.

Bio-type	Plot	2005 Litter Rate (kg ha <sup>-1</sup> day <sup>-1</sup> )	Volume (m <sup>3</sup> )
Outlier	21903	0.62	199.76
1b	28307	0.44	368.07
1a	21901	0.43	241.51
1a	27703	0.40	198.88
1a	29202	0.32	292.56
2b	28703	0.32	144.91
2a	21801	0.26	57.62
2a	29205	0.22	82.06
2b	29803	0.18	113.53

**Table 1.** Litter rates by monitoring plots (n=9) and associated bio-type for the total monitoring period (about 114 days) of 2005, with total plot parabolic volume noted. Data are listed in order of descending litter rate.

### 2.3.3. Crown ratio and HPCD

The crown ratios (foliated crown:total tree height) at AINS are very similar among bio-types (about 45%), with bio-type 2a anomalous at 53% (Table 2; see Figure 5a-5c and Appendix A for graphical data; note that the stem profile examples in Figure 5a-5c are from the water plots). Alternatively, HPCD in plots is quite characteristic of bio-types as seen in Table 4 where HPCD loads the first principal component more than the other metrics. HPCD values can be assessed directly from the frequency histograms of Figures 5a-5c and Appendix A.

Bio-type	Average Crown Ratio (%)	Standard Deviation
1a (n=8)	46	10
1b (n=4)	45	8
2a (n=4)	53	5
2b (n=3)	45	5

**Table 2.** The average crown ratios (crown length:tree height) and standard deviations for the bio-types less outlier type 3.

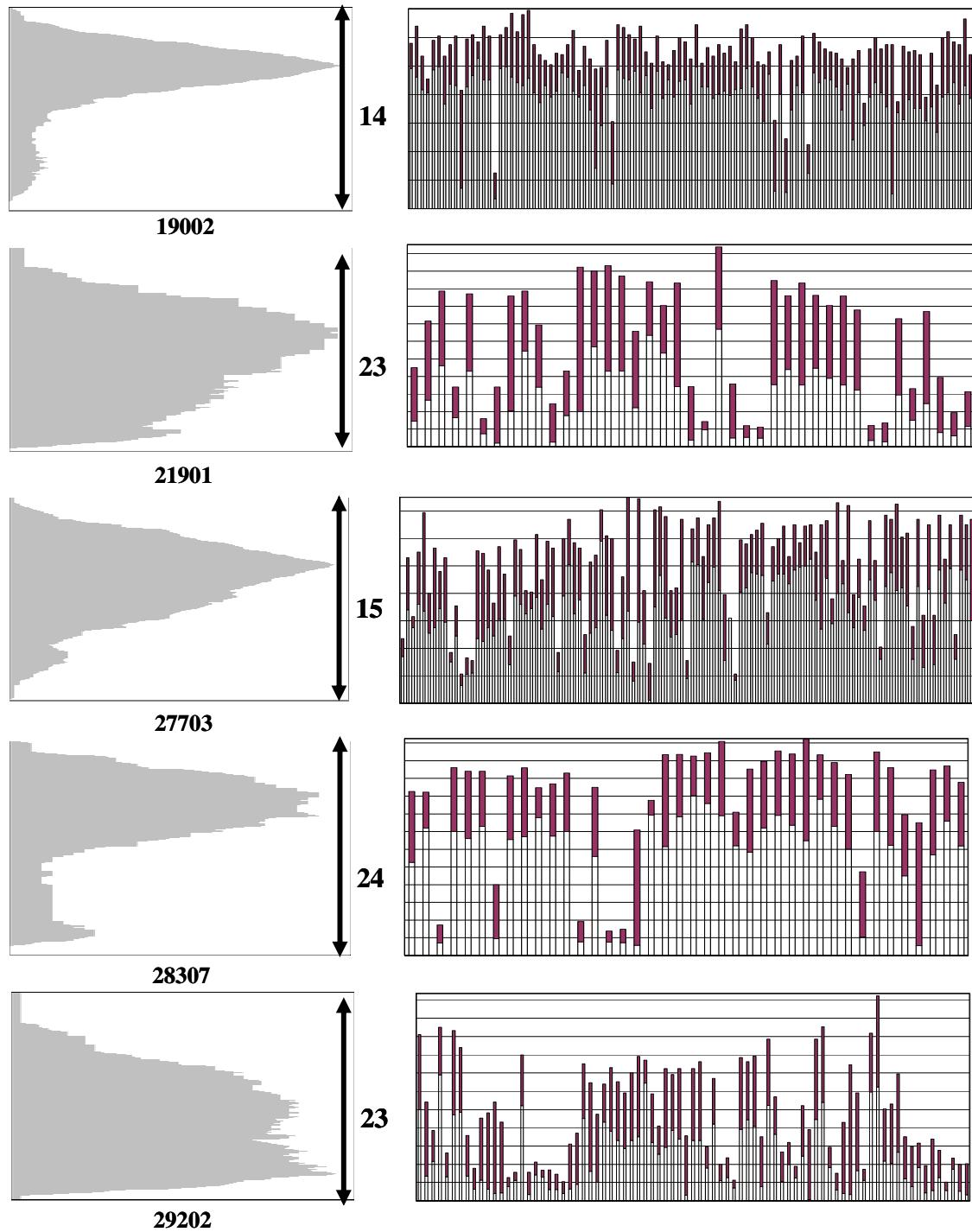


**Figure 5a.** Example canopy presence frequency spectrums (left) and tree stem profile charts (right) from water-monitoring field plots of bio-type 1. Foliated crown lengths in profiles are shaded (■); unfoliated bole lengths are open (□). Arrows indicate the maximum canopy height (m) listed in center of figure.

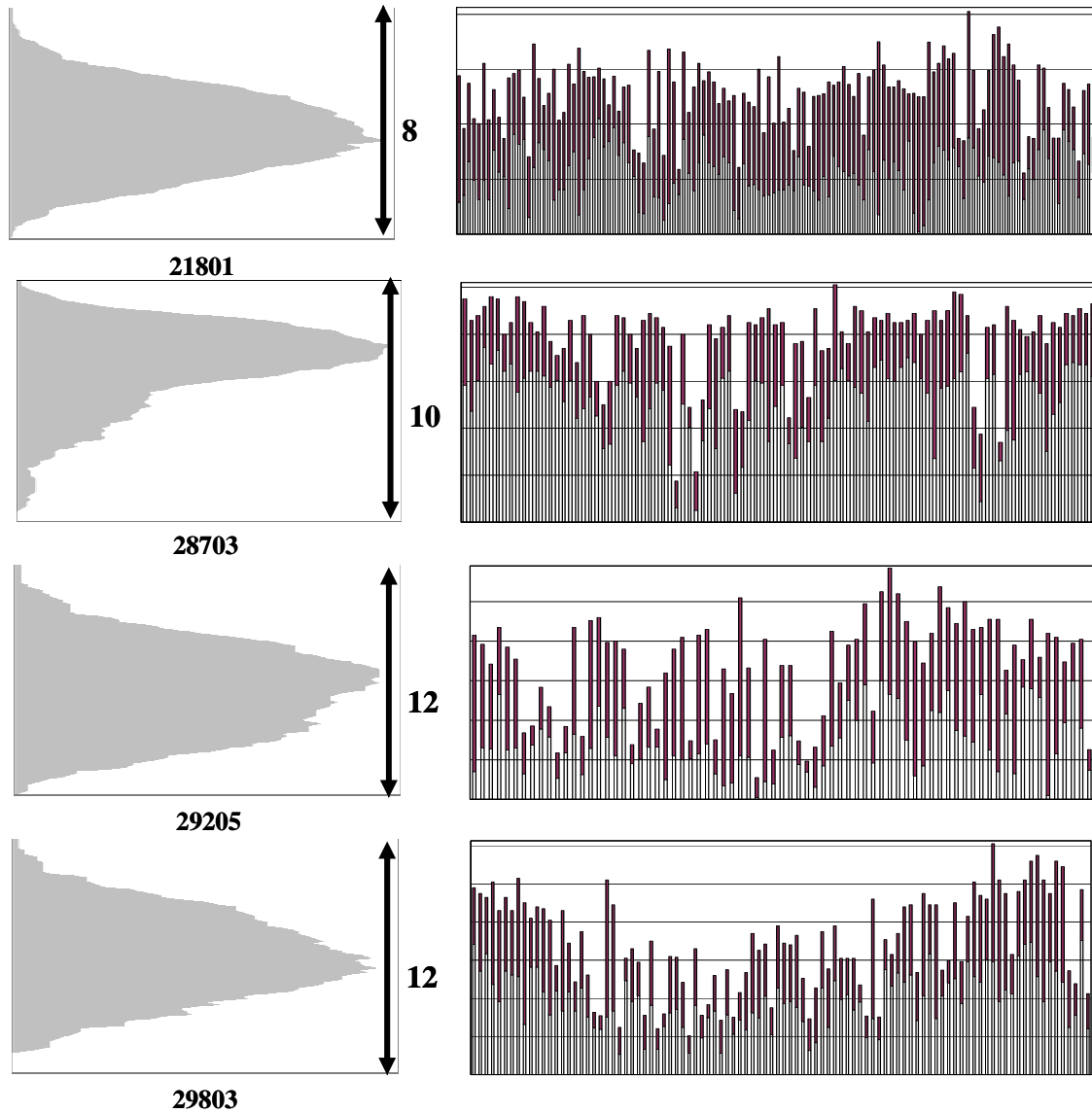


**Figure 5b.** Example canopy presence frequency spectrums (left) and tree stem profile charts (right) from water-monitoring field plots of bio-type 2. Foliated crown lengths in profiles are shaded (■); unfoliated bole lengths are open (□). Arrows indicate the maximum canopy height (m) listed in center of figure.

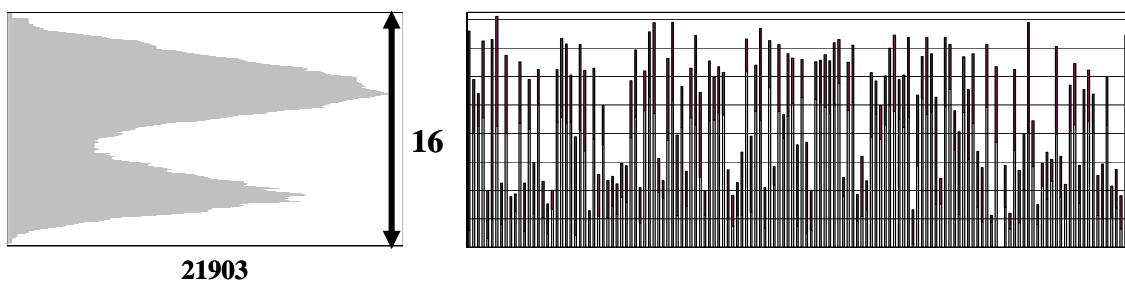


**Figure 5c.** Example canopy presence frequency spectrums (left) and tree stem profile charts (right) from the water-monitoring field plot of the outlier bio-type. Foliated crown lengths in profiles are shaded (■); unfoliated bole lengths are open (□). Arrows indicate the maximum canopy height (m) listed in center of figure.

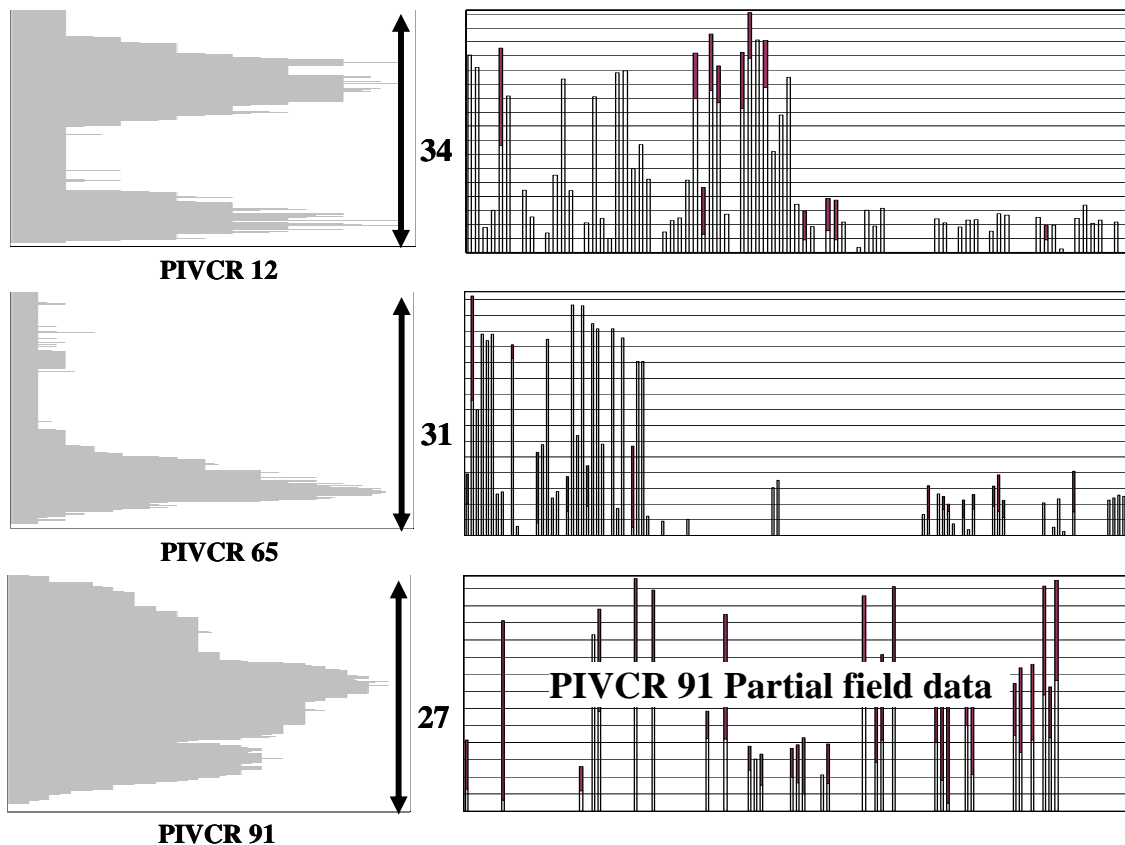


**Figure 5d.** Example canopy presence frequency spectrums (left) and tree stem profile charts (right) from the PIVCR field plots of the original monitoring network. Foliated crown lengths in profiles are shaded (■); unfoliated bole lengths are open (□). Arrows indicate the maximum canopy height (m) listed in center of figure. Missing and dead trees are represented by gaps in the stem profile. PIVCR 91 data are from an incomplete sample.

PIVCR stem profile charts in Figure 5d exhibit the loss of the majority of biomass since 1996 (date of last measurements). Gaps in the stem profile chart represent fallen stems (except in plot 91 where data are incomplete; this plot was unaffected by the disturbances). Using Richardson, Porter, and Shugart (1996) data (available from VCR-LTER website data archive) as initial condition, woody canopy volume reduction is at least 75% at plots 12 and 65 since the 2002 disturbances. This likely underestimates island-wide change as the plots surveyed are those that appeared least affected by the disturbances.

### 2.3.4. Principal components analysis: biophysical and environmental classification

The raw data for the AINS PCA are in Table 3. Table 4 lists the 5 new principal component variables (PC1-PC5) and the constituent original variables of the biophysical analysis. Note that the original metrics are listed in descending order of eigenvector loading of PC1. HPCD variation loads PC1 at the highest rate (0.58), with BA and Maxage the next nearest at similar rates (0.55 and 0.53, respectively). PC2 is comprised of SCA to a great extent (0.74), and then PAI (0.66).

Plot	BIOPHYSICAL							ENVIRONMENTAL				
	PAI	Vol	MCH	HPCD	SCA	BA	Maxage	DWT	SOM	STI	Distshore	BEE
19001	1.8	258.5	17.7	12.0	13.1	34.4	65	0.43	0.95	0.09	806	0.57
19002	2.1	230.3	13.9	9.9	179.9	40.0	58	0.18	1.01	0.13	705	0.42
20901	3.3	---	---	---	---	---	24	0.21	1.08	0.08	679	0.36
21801	1.7	57.6	8.1	3.4	175.0	19.0	21	0.33	1.31	0.06	346	0.34
21901	2.1	241.5	22.8	13.5	5.9	29.7	63	0.71	1.58	0.16	1013	1.34
21902	1.4	191.0	14.1	9.3	40.0	34.1	61	0.21	2.13	0.13	932	0.40
21903	3.2	199.8	16.3	10.8	847.4	29.9	64	0.29	1.18	0.12	1079	0.18
27701	2.7	118.2	11.2	6.0	57.1	28.3	23	0.33	1.25	0.10	329	1.18
27703	2.7	198.9	15.4	10.5	1.8	32.9	40	0.55	0.87	0.10	631	1.03
27704	3.0	406.7	22.9	15.5	149.3	41.9	42	0.32	1.01	0.13	691	0.77
28304	4.7	134.8	17.9	4.5	836.3	20.8	11	0.36	3.59	1.00	1389	0.41
28307	3.0	368.1	24.4	18.0	18.5	35.2	54	0.57	7.62	1.13	1327	0.53
28506	3.3	469.6	29.2	18.8	326.0	38.2	90	0.37	22.09	0.72	1015	0.46
28702	2.7	188.2	14.6	9.0	0.0	31.1	56	0.54	2.82	0.09	421	0.51
28703	2.2	144.9	10.1	7.3	106.2	33.8	29	0.39	4.43	0.10	294	0.92
28704	1.9	92.2	12.4	4.8	62.7	28.2	13	0.22	1.30	0.10	268	0.91
29201	1.9	150.0	10.9	7.2	41.6	33.9	44	0.23	3.70	0.14	390	0.73
29202	2.6	292.6	22.5	10.5	0.0	39.5	67	1.20	2.29	0.17	509	1.36
29203	1.8	181.3	15.5	8.7	0.0	31.6	54	0.45	0.97	0.16	475	0.75
29205	1.1	82.1	11.7	6.3	0.0	20.3	34	0.51	1.50	0.13	383	0.86
29503	3.5	280.0	17.1	13.6	24.2	39.1	51	0.23	4.27	0.54	502	0.27
29504	1.5	89.7	10.7	5.1	67.8	21.8	33	0.41	1.74	0.11	448	0.22
29505	3.0	220.2	16.8	6.8	198.8	34.7	44	0.53	2.72	0.22	598	0.51
29506	1.7	108.3	12.2	6.3	246.1	27.3	26	0.29	1.63	0.12	369	0.52
29801	1.3	69.2	8.6	5.0	206.4	20.2	28	0.25	1.01	0.09	444	0.04
29802	3.1	373.4	22.8	16.5	18.0	39.5	64	0.45	13.22	0.14	548	0.14
29803	1.8	113.5	12.1	5.5	238.6	25.0	29	0.33	0.59	0.08	437	0.15

**Table 3.** The variables and plot values (n=27; plot 20901 was not measured for most biophysical traits) that were used to derive principal components (PC) and group sites into biophysical and environmental types by cluster analyses of PC scores. PAI is study period (2004-2006) average plant area index in  $m^2/m^2$ ; Vol is parabolic volume ( $m^3$ ); MCH is the maximum canopy height (m); HPCD is the height (m) of the peak canopy density; SCA is area ( $m^2$ ) of shrub canopy dripline; BA is basal area ( $m^2$ ); Maxage is the maximum age of trees in years; DWT is depth to water table (m; point-in-time); SOM is soil organic matter (%) from the top 10 cm of soil; STI is the soil texture index (fine sand:medium sand); Distshore is distance (m) from the ocean shoreline; BEE is bare earth elevation (m).

	PC1	PC2	PC3	PC4	PC5
HPCD	0.58	0.00	0.07	-0.58	0.57
BA	0.55	-0.09	-0.36	0.72	0.22
Maxage	0.53	-0.12	0.64	0.07	-0.54
PAI	0.28	0.66	-0.48	-0.23	-0.46
SCA	-0.10	0.74	0.48	0.30	0.34

**Table 4.** Eigenvector loading values of the biophysical variables in the resultant 5 principal components.

Applying the Kaiser (1960) rule, only PC1 and PC2 are accepted for further analysis because their eigenvalues of the PC correlation matrix are greater than 1 (not shown). Biophysical PC1 and PC2 explain 83% of total variation of the new factor data set. The ‘scores’ of all plots for PC1 and PC2 are listed in Table 5. These are the raw plotting data for Figure 6 (PC2 on PC1) from which the cluster analysis determines relatedness (average distance) producing the dendrogram of Figure 7. Subsequent classifications into types is based on visual inspection of the dendrogram.

Plot	PC1	PC2
19001	1.03	-1.04
19002	1.03	-0.30
21801	-2.66	-0.16
21901	0.88	-0.78
21902	0.38	-1.28
21903	0.56	2.85
27701	-1.13	0.10
27703	0.33	-0.21
27704	1.81	0.40
28304	-1.93	4.43
28307	1.98	-0.03
28506	3.26	0.96
28702	0.42	-0.31
28703	-0.54	-0.20
28704	-1.84	-0.42
29201	-0.19	-0.73
29202	1.56	-0.55
29203	0.06	-1.02
29205	-1.95	-1.33
29503	1.79	0.33
29504	-1.89	-0.76
29505	0.10	0.60
29506	-1.51	-0.06
29801	-2.31	-0.41
29802	2.42	-0.08
29803	-1.68	0.01

**Table 5.** Scores of all plots in the first two biophysical principal components.

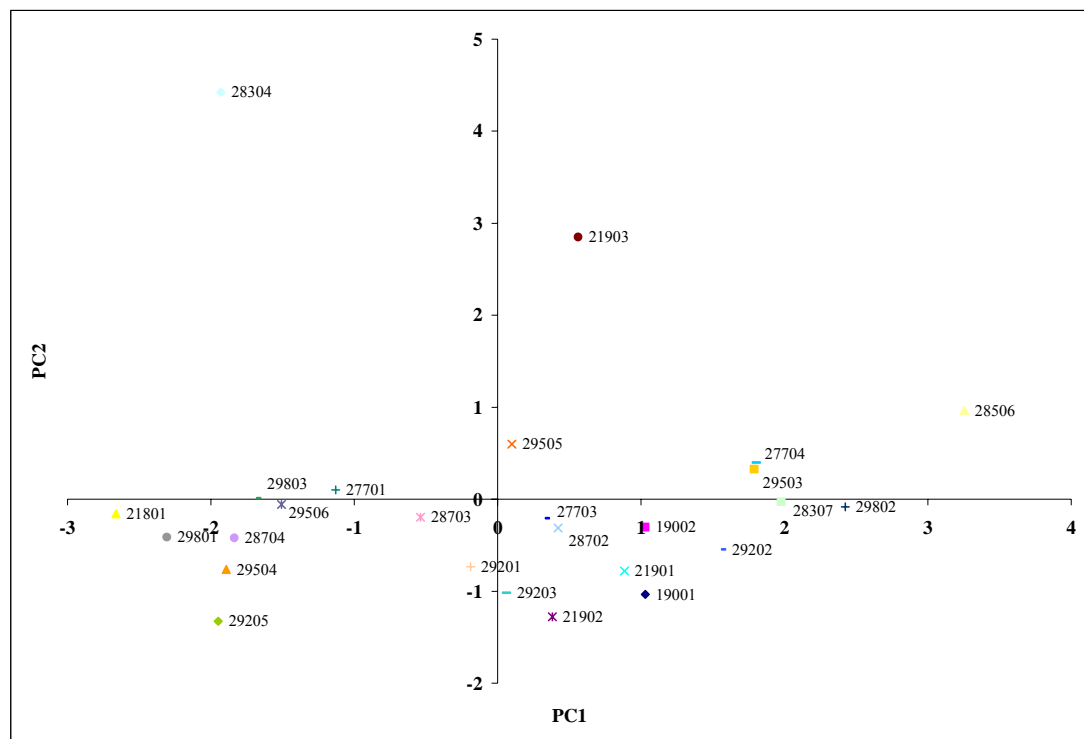


**Figure 6.** PC space in the biophysical principal components analysis (PCA). Scores by plot for PC2 are plotted against scores for PC1.

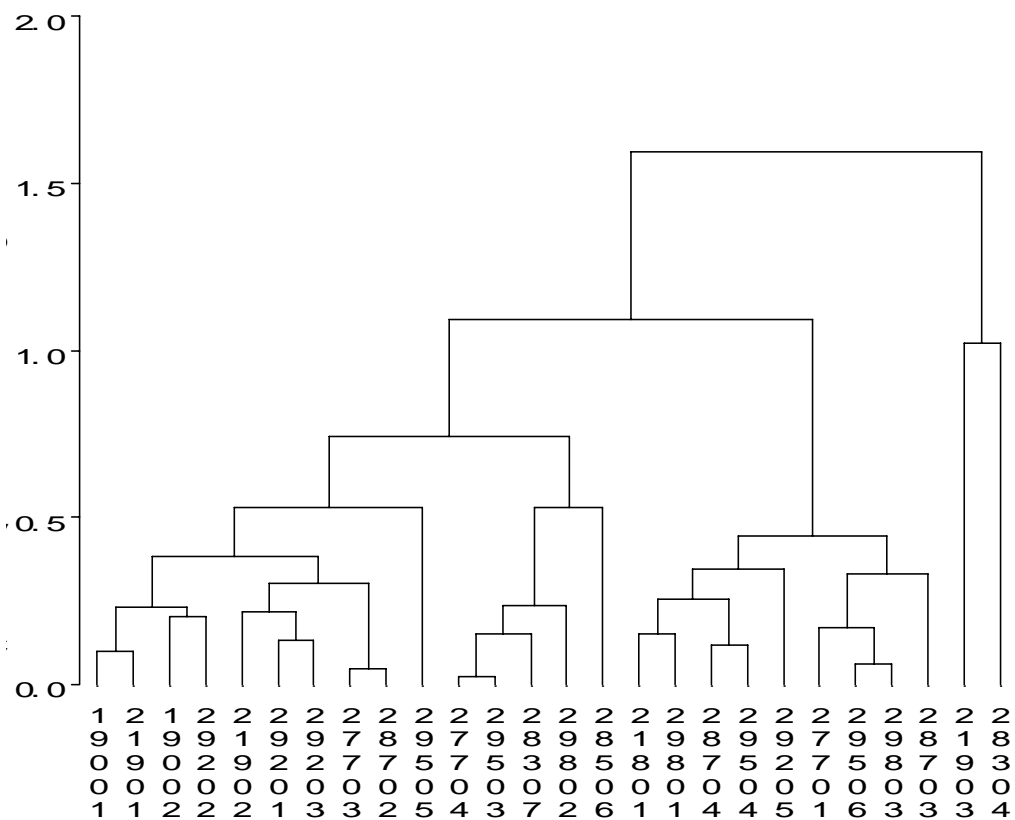


**Figure 7.** The dendrogram of cluster analysis results of the PC space functions developed with the plot biophysical features. Average distance in PC space between plots is on the y-axis. Plots are listed individually at terminating branches. SAS (SAS Institute 2002-2003) graphical output.

Table 6 lists the 6 principal component variables (PC1-PC6) and the original variables of the environmental analysis. PC1 is loaded equally by distshore and STI at 0.52. SOM also comprises a fair amount of the variation for PC1 at 0.49. PC2 is loaded by DWT at 0.68, then BEE at 0.66.

	PC1	PC2	PC3	PC4	PC5	PC6
Distshore	0.52	-0.08	0.41	-0.51	0.21	0.50
STI	0.52	-0.14	0.50	0.32	-0.12	-0.59
SOM	0.49	-0.07	-0.42	0.63	0.08	0.42
Maxage	0.43	0.26	-0.58	-0.43	0.18	-0.44
DWT	0.15	0.68	0.08	-0.01	-0.69	0.17
BEE	-0.09	0.66	0.26	0.25	0.65	-0.02

**Table 6.** Eigenvector loading values of the environmental variables in the resultant 5 principal components.

As the PC1 and PC2 variables explain just 67% of the total variation of the new factor data (though theirs are the only eigenvalues greater than 1), PC3 (loaded by negative association with maxage) is included in a test cluster analysis. In another test, maxage is eliminated from the PCA. Both exercises led to less intuitive classifications (not shown) based on site knowledge. The lower explained variation in the first two PC variables is due to the lower correlation among the original environmental variables compared to that in the biophysical PCA. Note that plot 20901 is included in the environmental PCA, but not in the biophysical analysis due to lack of data (Table 3). The plot environmental PC scores are in Table 7, the PC space regression in Figure 8, and the resulting dendrogram of cluster analysis in Figure 9.

Plot	PC1	PC2
19001	0.28	0.39
19002	-0.11	-0.79
20901	-0.95	-1.22
21801	-1.49	-0.81
21901	0.79	2.59
21902	0.49	-0.77
21903	0.79	-0.89
27701	-1.62	0.74
27703	-0.59	1.34
27704	-0.47	0.10
28304	2.03	-1.50
28307	3.67	-0.13
28506	4.61	-0.38
28702	-0.27	0.59
28703	-1.10	0.50
28704	-1.95	-0.23
29201	-0.68	-0.21
29202	0.47	4.40
29203	-0.42	0.69
29205	-1.00	0.86
29503	0.58	-1.19
29504	-0.83	-0.67
29505	-0.01	0.29
29506	-1.27	-0.59
29801	-1.13	-1.56
29802	1.36	-0.49
29803	-1.16	-1.07

**Table 7.** Scores of all plots in the first two environmental principal components.

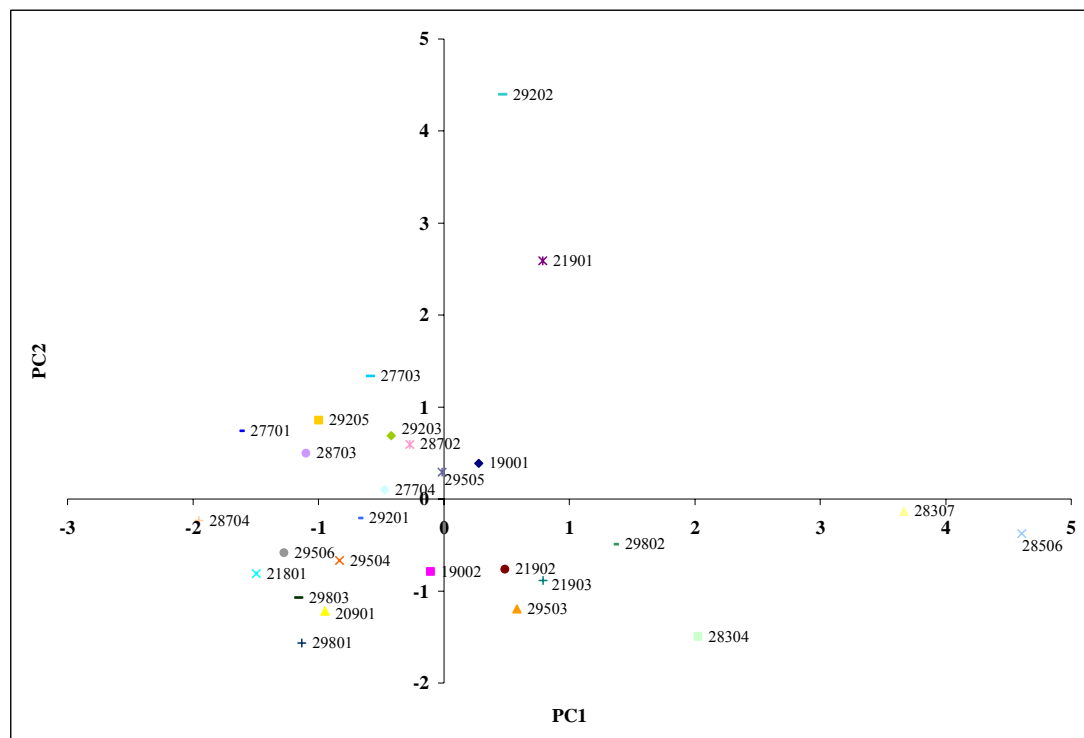


**Figure 8.** PC space in the environmental principal components analysis (PCA). Scores by plot for PC2 are plotted against scores for PC1.



		Biophysical Types				
		1A	1B	2A	2B	Outliers
Plots		19001	27704	21801	27701	21903
		19002	28307	28704	28703	28304
		21901	29503	29504	29506	
		29202	29802	29801	29803	
		21902	28506	29205		
		29201		20901*		
		29203				
		27703				
		28702				
		29505				

**Table 8.** Biophysical sub-types derived by principal components analysis of structural variables and cluster analysis of PC scores. The Outlier group is excluded from most analyses. \*This plot is included in 2A based on visual estimation only.

		Environment Site-Types					
		1A	1B	2	3	4	5
Plots		19001	27701	21801	19002	21901	28307
		27704	27703	28704	21902	29202	28506
		28702	28703	29504	21903		
		29201	29205	29506	28304		
		29203		29801	29503		
		29505		29803	29802		

**Table 9.** Site-types derived of environmental variable principal components analysis, and the cluster analysis of PC scores by individual plots.

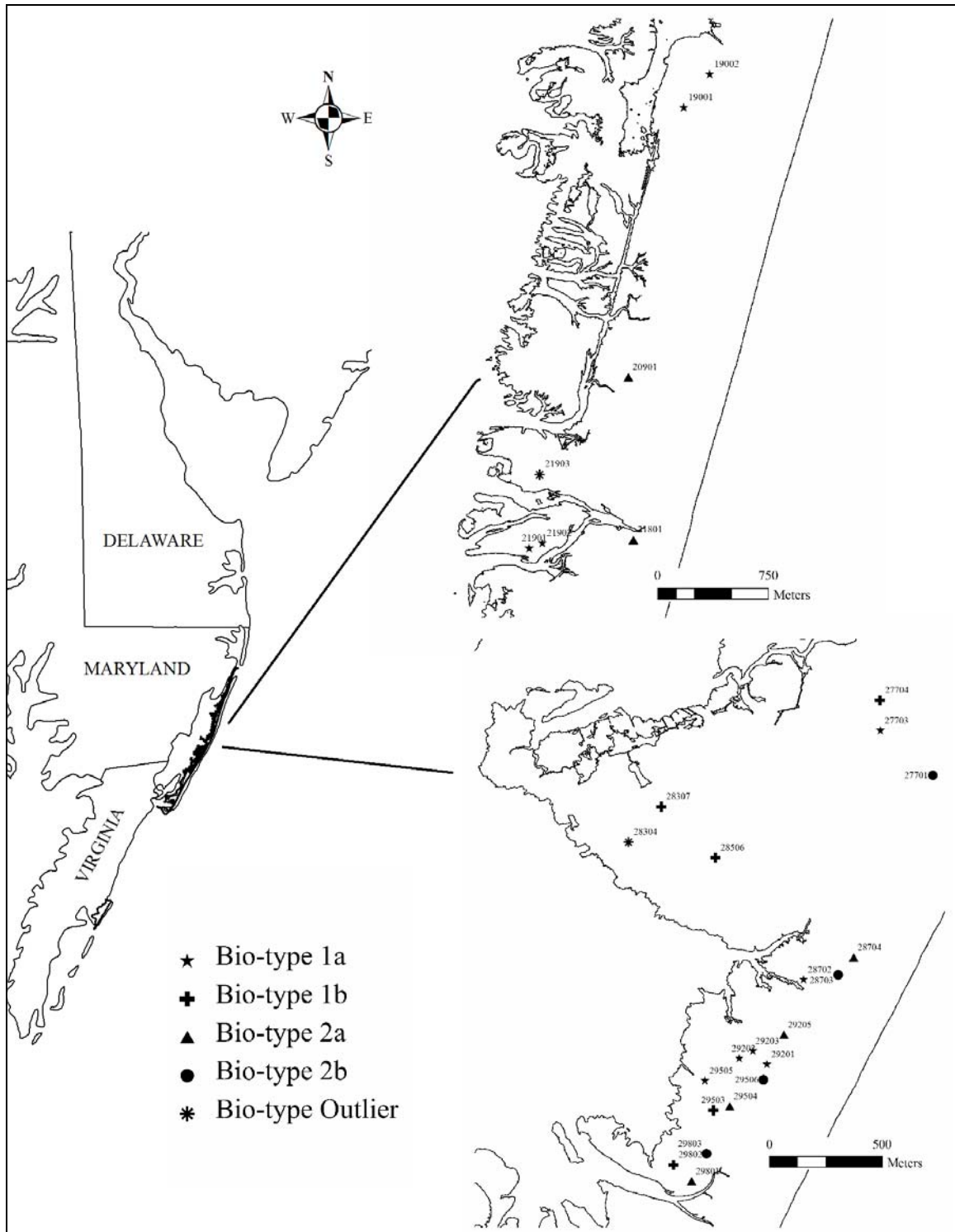


**Figure 10.** Map of the AINS biophysical (bio)-type groups divided into Northern and Southern regions.

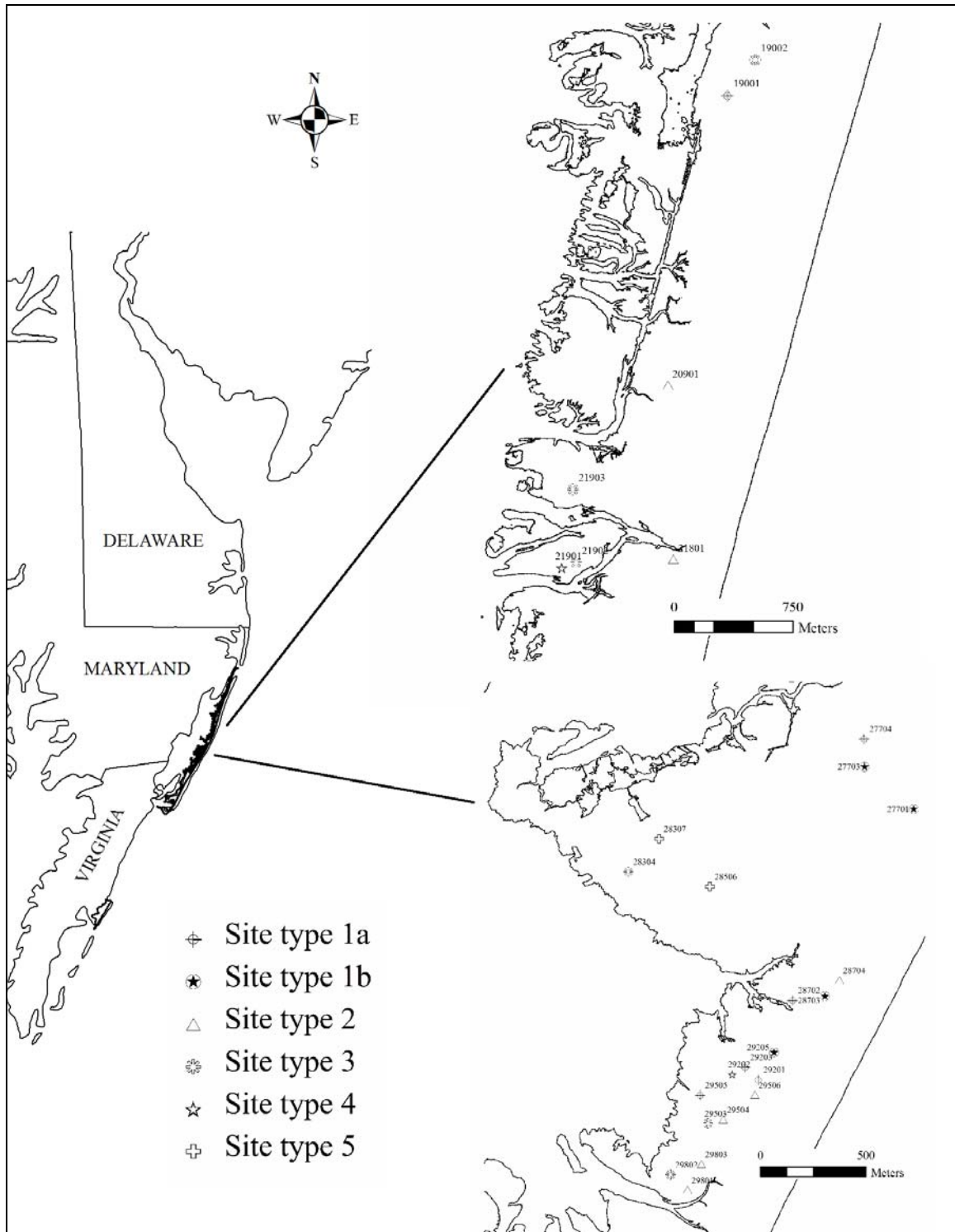


**Figure 11.** Map of the AINS environmental (site) type groups divided into Northern and Southern regions.

The patterns of magnitude and variation in original metrics by new organizational type are graphed in Figure 12 (biophysical values of the 5 bio-types) and Figure 13 (environmental values of the 6 site types). The tabular counterparts of these figures are Tables 10 (bio-type values) and 11 (site type values).

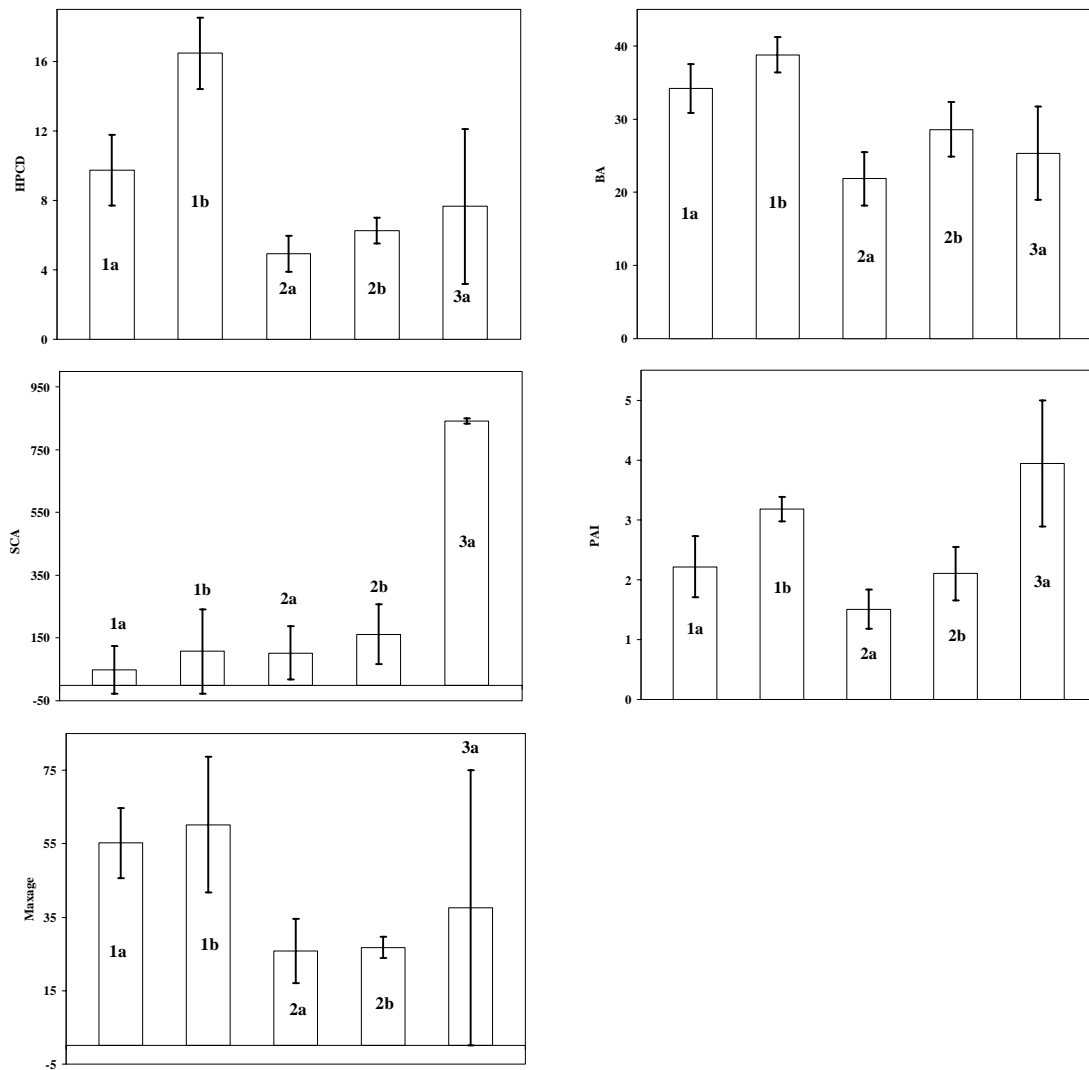


**Figure 12.** Graphical comparisons of the sub-bio-types in magnitudes and variation of sample population statistics for HPCD (height of peak canopy density, m), BA (basal area,  $m^2 ha^{-1}$ ), SCA (shrub canopy dripline area,  $m^2 plot^{-1}$ ), PAI (plant area index,  $m^2 m^{-2}$ ), and maxage (maximum tree age, years) where '3a' is the outlier type. The bars represent one +/- standard deviation (s).

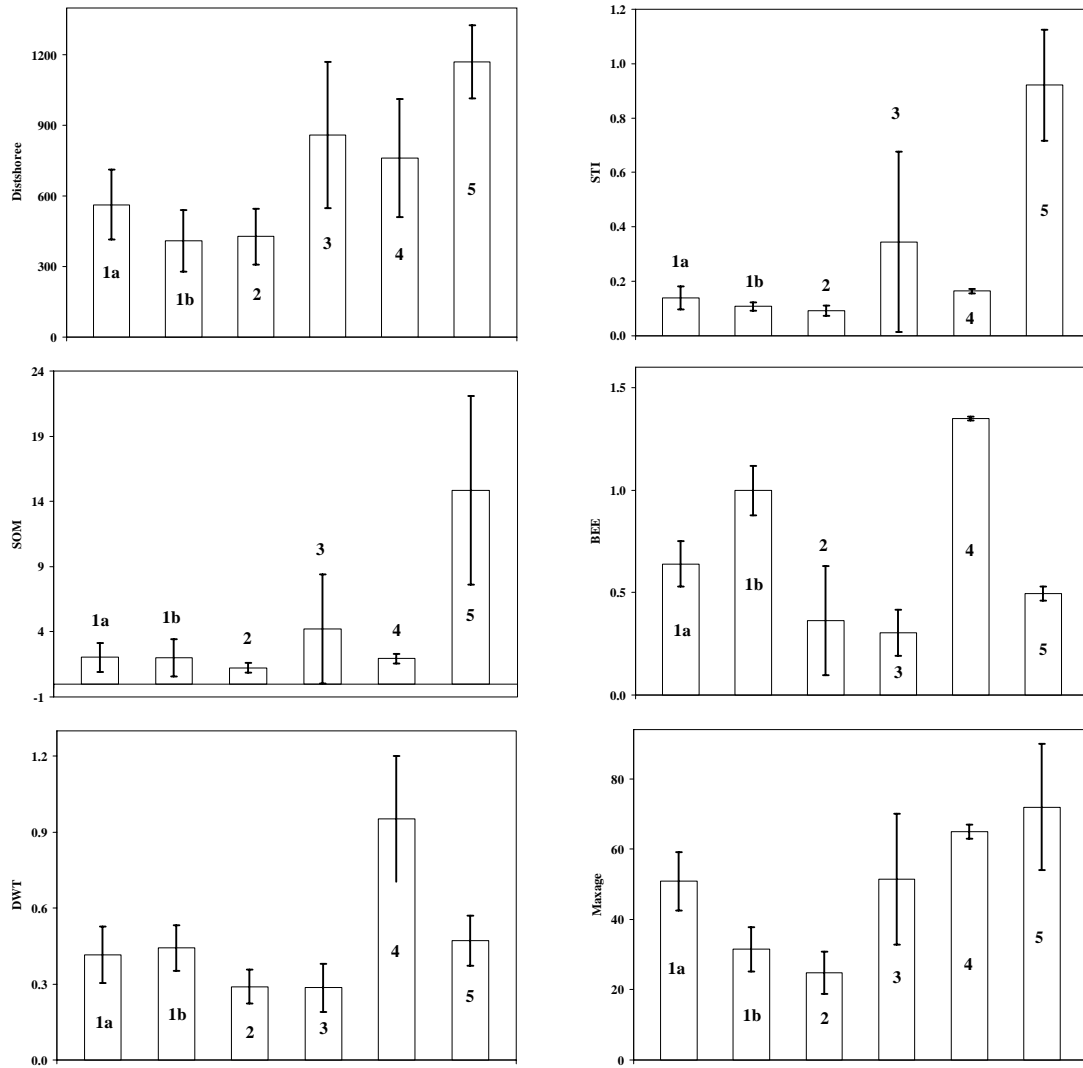


**Figure 13.** Graphical comparisons of all environmental site-types in magnitudes and variation of sample population statistics for distshore (distance from ocean shoreline, m), STI (soil texture index, fine sand:medium sand), SOM (soil organic matter, %, top 10cm), BEE (bare earth elevation, m), DWT (depth to water table, m), and maxage (estimated time since tree colonization at site, years). The bars represent one +/- standard deviation (s).

		Bio-types				
		<b>1a</b>	<b>1b</b>	<b>2a</b>	<b>2b</b>	<b>3</b>
<i>n</i>		10	5	5	4	2
<b>HPCD</b>	Avg.	9.74	16.47	4.92	6.25	7.65
	s	2.04	2.04	1.04	0.74	4.45
	CV	21	12	21	12	58
<b>BA</b>	Avg.	34.19	38.77	21.87	28.59	25.36
	s	3.34	2.42	3.65	3.72	6.39
	CV	10	6	17	13	25
<b>SCA</b>	Avg.	48.11	107.21	102.37	162.02	841.82
	s	76.20	134.50	85.65	94.96	7.86
	CV	158	125	84	59	1
<b>PAI</b>	Avg.	2.22	3.18	1.51	2.10	3.95
	s	0.51	0.21	0.33	0.45	1.05
	CV	23	6	22	21	27
<b>Maxage</b>	Avg.	55.20	60.20	25.80	26.75	37.50
	s	9.55	18.42	8.81	2.87	37.48
	CV	17	31	34	11	100

**Table 10.** The sample population statistics (average, standard deviation, and coefficient of variation) for the PCA variables: HPCD (height of peak canopy density, m), BA (basal area, m<sup>2</sup> ha<sup>-1</sup>), SCA (shrub canopy dripline area, m<sup>2</sup> plot<sup>-1</sup>), PAI (plant area index, m<sup>2</sup> m<sup>-2</sup>), and maxage (maximum tree age, years). Note bio-type '3' is the outlier group. CV is in %.

	<i>n</i>	Site-types					
		<b>1a</b>	<b>1b</b>	<b>2</b>	<b>3</b>	<b>4</b>	<b>5</b>
		6	4	6	6	2	2
<b>Distshore</b>	Avg.	563.31	409.27	427.33	858.86	761.12	1170.69
	s	149.85	131.83	119.36	311.53	252.01	156.17
	CV	27	32	28	36	33	13
<b>STI</b>	Avg.	0.14	0.11	0.09	0.34	0.16	0.92
	s	0.04	0.01	0.02	0.33	0.01	0.20
	CV	31	13	20	96	5	22
<b>SOM</b>	Avg.	2.03	2.01	1.24	4.23	1.93	14.86
	s	1.10	1.41	0.36	4.19	0.35	7.24
	CV	54	70	29	99	18	49
<b>BEE</b>	Avg.	0.64	1.00	0.36	0.30	1.35	0.50
	s	0.11	0.12	0.27	0.11	0.01	0.04
	CV	18	12	73	37	1	7
<b>DWT</b>	Avg.	0.42	0.44	0.29	0.29	0.95	0.47
	s	0.11	0.09	0.07	0.09	0.25	0.10
	CV	27	20	23	33	26	21
<b>Maxage</b>	Avg.	50.83	31.50	24.86	51.50	65.00	72.00
	s	8.25	6.26	5.99	18.64	2.00	18.00
	CV	16	20	24	36	3	25

**Table 11.** The sample population statistics (average, standard deviation, and coefficient of variation) for the PCA variables: distshore (distance from ocean shoreline, m), STI (soil texture index, fine sand:medium sand), SOM (soil organic matter, %, top 10cm), BEE (bare earth elevation, m), DWT (depth to water table, m), and maxage (estimated time since tree colonization at site, years). CV is in %.

In order to demonstrate the predictive power of the clusters, an analysis of variance (ANOVA) with the SAS glm (general linear model) procedure (SAS Institute 2002-2003) is performed on the major biophysical metrics as expressed by site types. Among the six variables tested, site explains 76% of the variation in MCH, 69% in volume, and 66% in HPCD (Table 12). BA and PAI are more invariant at 49% and 39%, respectively. All coefficients of determination are significant at  $p < 0.01$  except PAI ( $p = 0.06$ ).

<b>Metric</b>	<b>Coefficient of Determination, <math>r^2</math></b>
MCH	0.76
Vol	0.69
HPCD	0.66
Maxage	0.62
BA	0.49
PAI	0.39

**Table 12.** ANOVA results to test indication of site-type by the major biophysical parameters. Results are interpreted as the fraction of variation explained by site groupings in each biophysical variable.

### 2.3.5. Dendrochronological analyses

Figures 14a and 14b display the initiation growth trendlines, and Table 13 the processed trend data for the six bio-type/age group divisions. All bio-type (BT) 1 configurations (sub-type/stand age) decline in growth more slowly than bio-type (BT) 2 configurations (not including BT1b 2-3 decade; but these are not representative samples as they comprise only two plots for a total of two composites). Note that bio-type 2 is limited to 2-3 decade samples. The 4-5 decade samples and 2-3 decade samples in bio-type 1a are very similar in trajectory. This may indicate the effectiveness of site grouping here with similarity in growth of distinct cohorts likely due to site effects; the difference in growth seen across bio-types may therefore be reasonably attributed to site. The rare inclining trends seem to signify even-agedness, E.g., BT1a-7 (includes plots 28702 and 21902); as does a very slowly decreasing rate, E.g., BT1a-2 (plots 19001, 19002). Comparing the average growth rate from raw endpoint data (not shown) on which Figures 14a-14b and Table 13 are based, results in bio-type 1a 2-3 decade chronologies (-42%) declining about 27% slower than bio-type 2b chronologies (-69%).

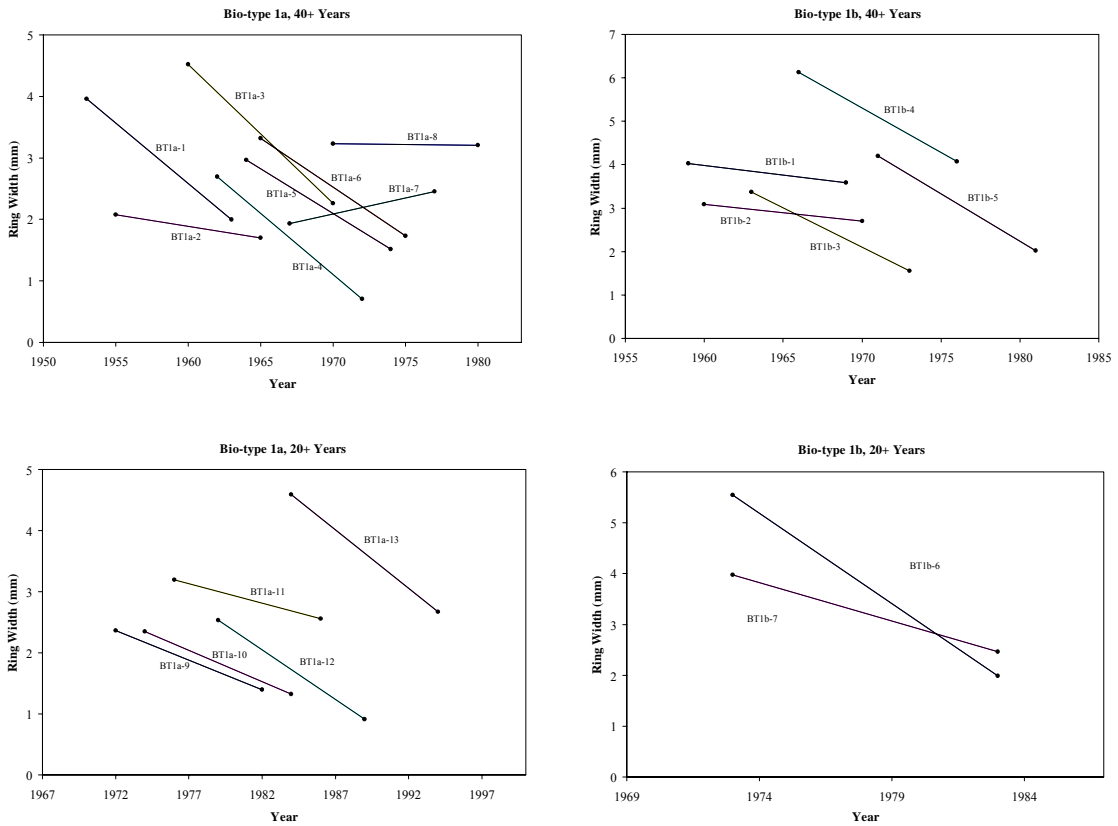


**Figure 14a.** Bio-type 1 subdivision post-dbh 20-year growth trends (data averaged from 5 years beyond either endpoint) for 40 year old+ stands (top) and 20 year old+ stands (bottom).

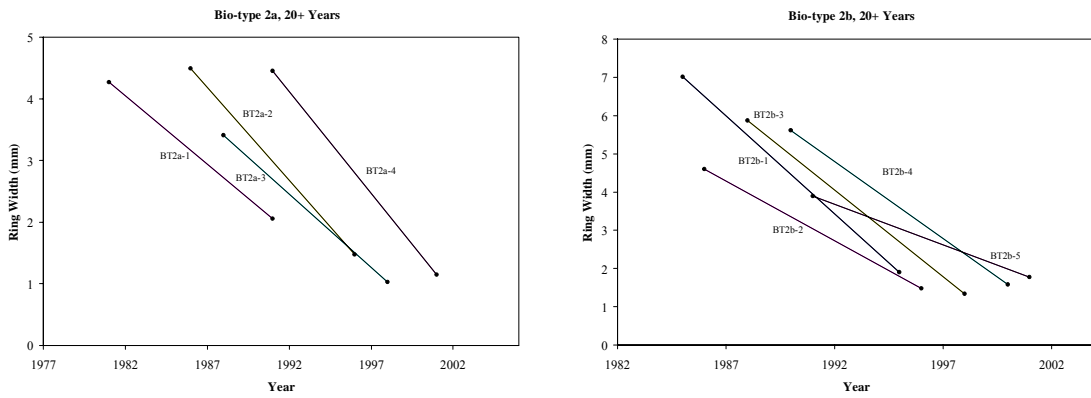


**Figure 14b.** Bio-type 2 subdivision post-dbh 20-year growth trends (data averaged from 5 years beyond either endpoint) for the 20 year old+ stands.

Trend chronology ID	10 year change in average ring width (mm)	Departure from average (in standard deviations)	Plots included in trend chronology; canopy position of sample tree			
<b>Bio-type 1a, 4-5 decade samples</b>						
BT1a-1	-1.97	0.69	21901	codom	21901	dom
BT1a-2	-0.38	-1.17	19001	dom	19002	dom
BT1a-3	-2.25	1.02	29202	dom	29203	codom
BT1a-4	-1.99	0.71	19002	codom		
BT1a-5	-1.45	0.08	29203	dom	19001	intermed
BT1a-6	-1.59	0.24	29203	intermed	29202	subcan
BT1a-7	0.52	-2.22	28702	dom	28702	codom
BT1a-8*	-0.02	-1.59	29201	codom	29505	subcan
			21902	codom	21902	intermed
<b>Average (Alt.)</b>	-1.38 (-1.60)					
<b>s</b>	0.85					
<b>Bio-type 1a, 2-3 decade samples</b>						
BT1a-9	-0.96	-0.51	29201	intermed	29201	dom
BT1a-10	-1.03	-0.39	27703	codom	27703	intermed
BT1a-11	-0.63	-1.15	27703	dom	29505	dom
BT1a-12	-1.62	0.74	19002	intermed		
BT1a-13	-1.92	1.31	29505	intermed		
<b>Average</b>	-1.23					
<b>s</b>	0.52					
<b>Bio-type 1b, 4-5 decade samples</b>						
BT1b-1	-0.44	-1.05	28702	intermed	28307	dom
BT1b-2	-0.39	-1.11	28506	intermed	28506	codom
BT1b-3	-1.82	0.49	29503	subcan	28902	codom
BT1b-4	-2.05	0.76	29503	dom	29802	codom
BT1b-5	-2.19	0.91	27704	intermed	29503	dom
<b>Average</b>	-1.38					
<b>s</b>	0.89					
<b>Bio-type 1b, 2-3 decade samples</b>						
BT1b-6	-3.56	0.71	27704	dom	27704	codom
BT1b-7	-1.52	-0.71	28307	codom	28307	intermed
<b>Average</b>	-2.54					
<b>s</b>	1.44					
<b>Bio-type 2a, 2-3 decade samples</b>						
BT2a-1	-2.21	-1.01	29205	dom	29504	dom
BT2a-2	-3.02	0.56	29205	codom	29801	codom
BT2a-3	-2.39	-0.66	29504	codom	29205	intermed
BT2a-4*	-3.31	1.11	29504	subcan	29801	dom
29801						dom
<b>Average (Alt.)</b>	-2.73 (-2.54)					
<b>s</b>	0.52					
<b>Bio-type 2b, 2-3 decade samples</b>						
BT2b-1	-5.11	1.13	28703	codom	29803	dom
BT2b-2*	-3.13	-0.56	29803	subcan	28703	dom
BT2b-3	-4.53	0.63	28703	intermed	29506	dom
BT2b-4	-4.03	0.21	29506	codom	27701	dom
BT2b-5	-2.13	-1.41	29803	codom	27701	codom
20901						dom
<b>Average (Alt.)</b>	-3.78 (-3.95)					
<b>s</b>	1.18					

**Table 13.** All bio-type ring width increment changes between ten-year averages initiated from 1-2 years after age at dbh. Departures from bio-type averages are assessed for each composite chronology, and the component plots and the sample stand positions (subcan=subcanopy; intermed=intermediate; codom=codominant; dom=dominant) are listed for each composite. Type average rates in parentheses () are values determined by excluding samples of cross-cohort (E.g., subcan and dom) origination denoted by \*.

Some general conclusions about bio-type environments can be made. The overriding effect on growth rates may be DWT. Bio-type 1 (a and b) long-term average DWT is 0.80m (n=5), and bio-type 2 (a and b) average is 0.44m (n=5). These conditions interact with the beneficial effects of higher elevation at island interiors of increased protection from storm surge effects to water source, and physical effects of salt spray and wind. Protection allows for water table accession by more slowly establishing, stable stands. A rooting habit and water table access theory of structural determination is thoroughly covered in Chapter 3.

In testing the general site effect on growth, the mean ring width chronology sensitivity does correlate strongly negatively ( $r_s=-0.99$ ,  $p=0.0003$ ) with site index (SI) as traditionally represented by MCH (Figure 15). The mean sensitivity values are: Site type (ST)-5, 0.221; ST-4, 0.239; ST-3, 0.290; ST-2, 0.308; ST-1b, 0.308; and ST-1a, 0.293.

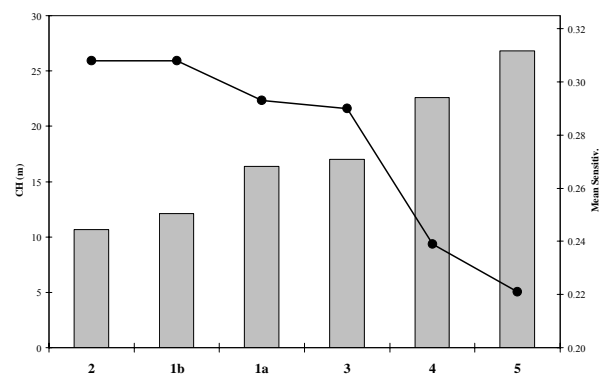


**Figure 15.** Site type master tree ring chronology mean sensitivity (●) and maximum canopy height (■).

Climate correlations are in Figure 16. These support the sensitivity interpretation. The number of significant correlations is greater in the site types with lower SI (ST-2, 1b and 1a) than those with greater SI (ST-3, 4, and 5). Broadly comparing sites between the

SI levels, temperature plays a more important role in the smaller stature sites. Across all sites, fewer significant interactions occur with precipitation. A section of the “Discussion” is devoted to the interpretation of individual results as related to site ecohydrology and attendant development.

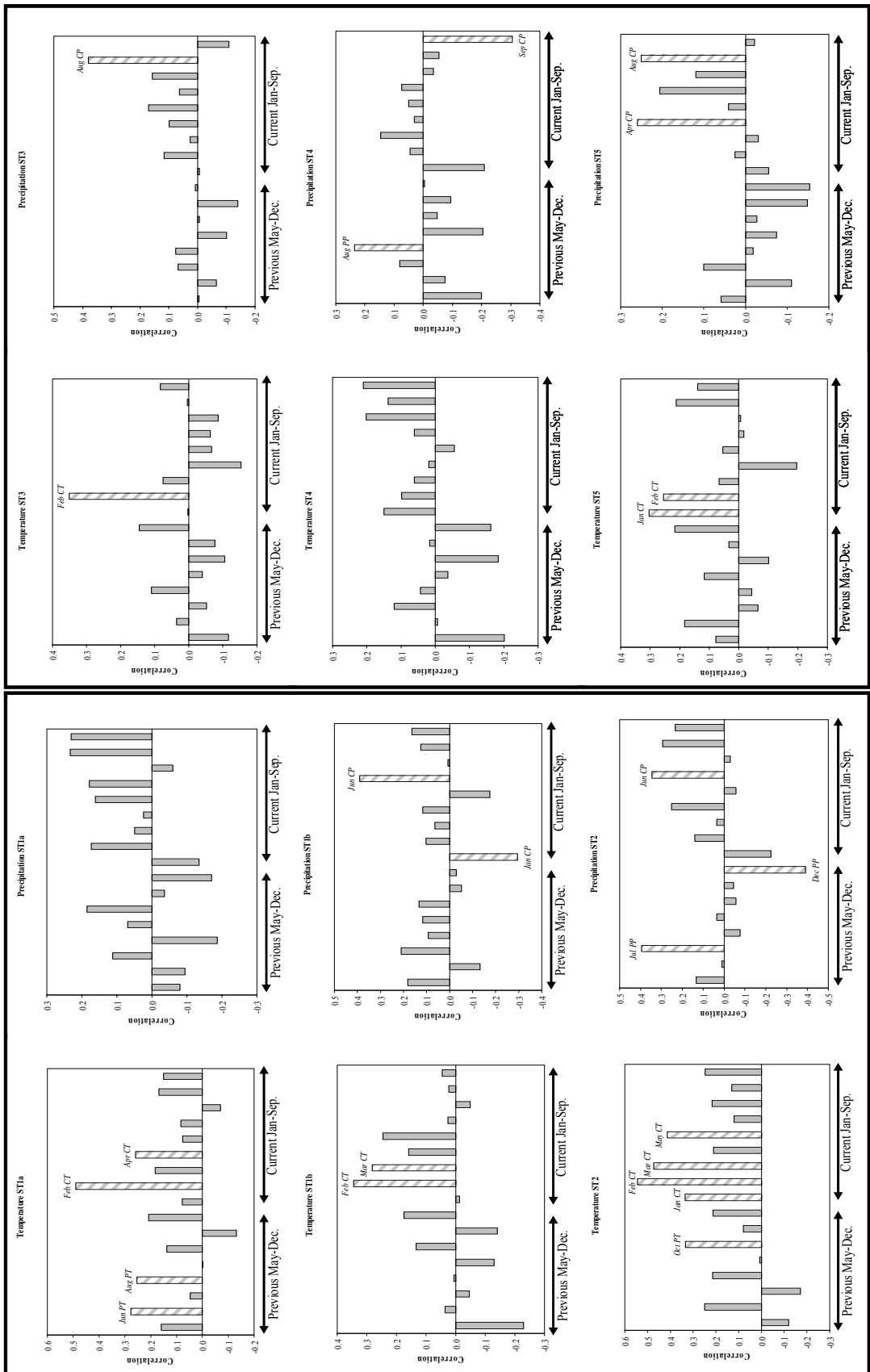


**Figure 16 (previous page).** Pearson (r) correlations between yearly tree ring radial increment and the months of a 17-month climate activity cycle (previous May – current September). The banded columns are months that are significant to at least  $p=0.1$  (and generally more so).

The component series of the site type MC's used in the climate correlations are listed in Table 14 with their canopy strata position. The inclusion of subcanopy and dominant mixtures in ST-1a and ST-2 should be noted as this could contribute erroneously to some of the significance. This possibility is minimized as the raw series' (used to create the MC) intercorrelation is above the COFECHA (RL Holmes, TRRL) critical level (at  $p=0.01$ ) in ST-2 ( $r=0.538$  for critical level 0.516), and close in ST-1a ( $r=0.446$  for critical level 0.453).

Site type	Sampled plots/canopy positions									
<b>1a</b>	28702	28702	29203	27704	29505*					
	codom	dom	dom	dom	subcan					
<b>1b</b>	29205	29205	29205	28703	28703	27703				
	interm	dom	codom	dom	codom	dom				
<b>2</b>	29803	29803	29803	29801	29801	29801	29504	29504	29506	
	codom	dom	subcan	codom	dom	dom	codom	subcan	dom	
<b>3</b>	29802	29503	21903	29202	19002					
	codom	dom	codom	dom	dom					
<b>4</b>	21901	29202								
	codom	dom								
<b>5</b>	28307	28506	28506							
	interm	interm	codom							

**Table 14.** List by site type of the plots contributing samples to the site type master chronologies developed for the climate correlation analyses. Canopy position is denoted for each sample.

*\*Though it is in the subcanopy strata of this plot, the sample from 29505 is an older open-grown individual with relatively large basal area.*

## **2.4. Discussion**

### **2.4.1. Plant area index**

Statistically significant differences in PAI are measured among the AINS bio-types as 73% of variation in average PAI is explained by bio-type (SAS Proc GLM analysis, not shown). The LAI-2000 instrument is also sensitive enough to be used at AINS for intra-seasonal leaf area change (see Figure 2) within plots.

The annual PAI fluctuation statistic (Appendix C) is a rough estimate of a foliage cohort contribution to light-blocking area. As there are no clear start and end points in our field data, a pure areal increase from a minimum is unwarranted. Definitive statements about leaf area change through our fluctuation proxy will wait for more comprehensive study. Based on the sensitivity of PAI within AINS plots there is clear potential for an ecosystem-specific PAI to LAI predictive linear relationship to be developed along the lines of Gower and Norman (1991), and Stenberg *et al.* (1994) with verification by a field estimate of LAI (E.g., by needlefall estimate). Also, Sampson *et al.* (2003) detail a dynamic non-linear leaf area growth and abscission relationship with LAI-2000 PAI temporal change (also see Sampson and Allen 1995) that could provide a model for future analyses.

The lack of a highly predictive relationship between PAI and “coarse” stand metrics (Figure 4) could be a matter of lacking a true annual average PAI for all plots. Alternately, perhaps parsing the stand metrics to distributional statistics from all stem diameters (Van Laar and Acka 2007), for example, could improve agreement as the LAI-2000 is dependent on the arrangement of light-blocking elements (Smolander and

Stenberg 1996; Sampson and Allen 1995) in addition to pure size. Long and Smith (1990) note that LAI can be rather invariant across some broad structural divisions.

#### **2.4.2. Crown Ratio**

Though, as Nagel and O'Hara propose, “greater crown length [in multi-aged compared to even-aged stands] result[s] in different light regimes that may influence ecophysiological leaf traits” such as gas exchange, leaf Nitrogen, and specific leaf area, crown ratio alone is not a good stand structural indicator (Table 2) at the scale (bio-type) at which monitoring should be done. HPCD, however, is a site-variant crown distribution index similar in theory to the Weibull distribution parameters used by Xu and Harrington (1998). HPCD distills canopy structure distribution as it relates to site energy and material fluxes, especially evapotranspirational feedbacks (see Chapter 3), in a very simplified manner. The crown presence frequency histograms (Figs 5a-5d, App. A) roughly approximate the stand-level “foliage-height profiles” Aber *et al.* (1982) developed to differentiate structural expression along a moisture gradient in New England. The histograms are used further in Chapter 4 to compare canopy distribution principal components to lidar return principal components.

#### **2.4.3. Dendrochronological analyses**

The 20-year growth trends decline faster in bio-type 2 than in bio-type 1. *P. taeda* is shade-intolerant, and even if individuals are shade-established, Shelton and Cain (2000) note that shade tolerance decreases with age in shade-grown seedlings. Within a few years after attaining dbh, rather common long-term growth patterns could then be

expected among individuals that have attained the present canopy. It is then feasible to attribute growth differences between classes to site effects. As shade-suppressed survival is limited to a few years, tree aging results are determined to be reliable. Separating the chronologies into age groups further controls growth effects related to stand developmental issues, allowing for testing of environmental effects.

Johnson and Young (1992) posit that more stationary chronologies are indicative of an overall more stable habitat on PIVCR compared to Hog Island of the VCR. Studies in the Florida barriers point to water availability as a general vegetation stabilizer from evidence in swale communities along a geomorphic gradient (Snyder and Boss 2002). It seems likely, after accounting for the over-riding influence of island position as it relates to storm and surge vulnerability, that variance remaining in growth at AINS is due to average DWT and root competition for the respective water sources: vadose precipitation in shallow soils of bio-type 2, and groundwater table in deeper soils of bio-type 1 (also see Chapter 3).

In shallow soils, it appears that vegetation utilizes water preferentially from the profile and not the water table as a waterlogging/flooding avoidance response or for general competitive advantage. Pezeshki (1992) shows that increases in waterlogging and salinity result in significant reductions in stomatal conductance and carbon assimilation in *P. taeda*. Established canopy trees in bio-type 1 may have a less volatile water source in having root access to deeper water tables and larger water lenses. As access to shallower water tables in bio-type 2 does not confer a competitive advantage (because this is easily achieved), trees are competing with shrubs much of the time for the fleeting vadose zone precipitation.

The broad inferences of past radial growth here can not be thoroughly verified as currently structured, and are intended as secondary to the main purposes of the succeeding chapters. Initial results, however, indicate there is significant potential in expanded study of this nature. Developmental trajectories in all AINS types are under pressure with increasing vertical water table forcing. Researchers will be better able to model effects to growth with knowledge of inherent growth probabilities imposed by edaphic features.

#### **2.4.4. Climate correlations interpretation**

ST-2 (small stature/most recently colonized; see Fig. 11 map) significant correlations of RWI and temperature are from October previous, and January, February, March and May of the concurrent increment (Fig. 16). ST-1a and 1b have fewer significant months, and the 1a MC alone correlates with June and August previous (though less than 0.30).

Employing ST-2 to exemplify the far end of the sensitivity scale (Fig. 15), it is noted that these are low elevation, shallow water table sites (Figure 13) perhaps more vulnerable to inundation and associated reduced water absorption (Spurr and Barnes 1980) if drainage/uptake is not rapid. Higher temperatures can act to increase evaporative demand and reduce threats from inundation; it is necessary to note that *P. taeda* will also transpire in winter on sunny days (Martin 2000). Perhaps the ubiquity of February current temperature as a relatively strong positive correlate (see also ST-3, Fig. 16) is related to the fact that average current February precipitation since 1957 (ST-1a inception) is not notable at 8.3cm (NWS, Ocean City, MD) with a CV of 45%, but the average

temperature of this analytical month has a 2.1°C standard deviation (with a 3.3°C average and CV of 64%). As days get longer, a warm period could be expected to increase evapotranspiration and attendant photosynthesis. Also, the February effect may come from a (presumed) negative relationship between average Nor'easter storm activity and temperature. Davis et al (1993) found that February had the greatest number (slightly more than January and March) of Atlantic coast Nor'easter storms over a 41-year period (1943-1984).

Positively correlated current precipitation months seen at both SI levels is a straightforward growth relationship (June in ST-1b and ST-2; April and August in ST-5 and August in ST-3). In ST-2, negatively-related precipitation of December previous perhaps indicates inundation at this time that does not allow for proper cold-season transpiration. Precipitation is a positive factor from July previous: if precipitation is too low, heat at this time of year may cause an interruption of growth by increasing wilting. This could lead to lower growth as stated earlier, where the number of foliage flushes has been found to depend on soil moisture (Hennessey *et al.* 1992). Benefits of a late summer flush may be delayed to the next year's growth as photosynthate is routed to storage as current cambial growth is slowing (Fritts 1976).

ST-1a has no significant correlations with precipitation. Of the lower SI site types, ST-1a sites are mid-range in BEE and DWT, slightly higher in STI (signifying greater water-holding capacity) and are more established (higher maxage), so there is perhaps less competition for vadose-zone rain water.

ST-4 expresses no significant temperature correlations, though interestingly, it peaks in July (previous and current) positively. These are the deepest sites (Fig. 13) and

are likely preferentially accessing the water table such that they are less vulnerable to drought in summer. The ST-4 positive relationship between growth and August previous precipitation is explained by the ST-2 July previous reasoning above. A negative relationship with September current precipitation in ST-4 may indicate benefits from lack of hurricanes and other coastal storms, though one would expect to see this repeated in the more exposed sites.

## **2.5. Conclusions**

PCA has aided greatly in focusing site and biophysical analyses and has become indispensable in crafting predictive theories of structural change, and extrapolating from past growth and site relationships to current interactions. The following chapter utilizes the data and classifications presented here to focus the search for a key ecohydrological mechanism in barrier forest development, and produces a testable theory of changing growth with rising water tables. Going forward, it would be optimal to perform a field verification of the biophysical structural groups and environmental site types in new areas. Also, a human intervention factor to scale maxage may aid in explaining more variation among types.

The LAI-2000 is successful in capturing seasonal changes and perhaps finer scale incremental changes with litterfall. PAI as measured is not reliable for depicting underlying environmental gradients (39% variation in average PAI is explained by site type). In Chapter 3 the available plant areal change data is utilized, however, to draw fairly reliable conclusions across bio-types regarding site moisture relations. With

continued study, perhaps in temporally-concentrated field collections of PAI, litter, and soil moisture, a material equivalency for leaf area as measured by the LAI-2000 can be derived. This would enable fine-scale time-series modeling to predict growth and community development with rising water tables that could be verified in a monitoring time frame.

The derivation of a plot level crown density frequency histogram from crown ratios is helpful in differentiating sites by providing the integrative canopy distribution metric, HPCD. HPCD could improve on maximum canopy height as an indicator if shrubs are included in a final foliated presence frequency. Related work in Chapter 3 shows that the SCA component, more than the other major biophysical metrics tested, correlates to water table depth ( $r_s = -0.80$ ,  $p = 0.009$ ). In fact, HPCD currently outperforms MCH in the correlation to DWT. DWT is a major environmental variable of interest as it is directly related to sea level (Chapter 3). HPCD is also better modeled by lidar returns than MCH (Chapter 4). As PAI interpretability improves, plot level values of HPCD can be used to estimate leaf area distribution – which can greatly affect production in sites with similar average LAI (Long and Smith 1990). This is important to the monitoring of vegetation biophysical and community structure, and associated production and water use with increasingly common remote sensing techniques (see Chapter 4).

Through analysis of radial growth trends and climate-growth correlations using dendrochronological techniques, environmental modulation of growth is described for AINS trees. It appears that stability can increase with DWT assuming preferential water table access. Typical severe climate pressures aside, trees at shallow groundwater sites appear to contend with greater rooting competition. These findings are crucial in

predicting the bio-type-specific changes with sea level rise drafted in Chapter 3. Growth rate and DWT relationships may be strengthened by more water table sampling and perhaps the expansion of monitoring into intra-seasonal radial growth with dendrometers.

That the lower site index stands have a greater number of significantly correlating climate months at greater rates than the ‘better sites’ is yet more evidence that site is affecting growth by modulating inputs. The significant finding here is of greater overall dependence of generally more shallow, more recently colonized sites on climate patterns (generally temperature as it relates to evapotranspiration and photosynthesis). With greater sampling rates over the physical gradients of interest, reliable functional relationships of climate and DWT and growth should emerge to aid in the modeling of effects of rising water tables to barrier island forests.

PIVCR forest regeneration should be monitored, and experimentation should commence on rooting zone interactions and related above-ground growth. Work here could provide an extraordinary resource to forest ecologists and ecohydrologists interested in documenting structural development as depends on barrier island freshwater lens dynamics.

## 2.6. References

- Aber, J. D., J. Pastor, and J. M. Melillo. 1982. Changes in Forest Canopy Structure Along a Site Quality Gradient in Southern Wisconsin. *American Midland Naturalist* **108**:256-265.
- Ashton, P. S. and P. Hall. 1992. Comparisons of Structure among Mixed Dipterocarp Forests of North-Western Borneo. *Journal of Ecology* **80**:459-481.
- Chason, J. W., D. D. Baldocchi, and M. A. Huston. 1991. A Comparison of Direct and Indirect Methods for Estimating Forest Canopy Leaf-Area. *Agricultural and Forest Meteorology* **57**:107-128.
- Cowling, S. A. and C. B. Field. 2003. Environmental control of leaf area production: Implications for vegetation and land-surface modeling. *Global Biogeochemical Cycles* **17**::-.
- Davis, R. E., R. Dolan, and G. Demme. 1993. Synoptic Climatology of Atlantic Coast North-Easterns. *International Journal of Climatology* **13**:171-189.
- Fekedulegn, B.D., Colbert, J.J., Hicks Jr., R.R., Schuckers, M.E. 2002. Coping with multicollinearity: An example on application of principal components regression in dendroecology. Research Paper NE-721, USDA Forest Service, Northeastern Research Station, Newton Square, PA.
- Fritts, H. C. 1976. *Tree rings and climate*. Academic Press, London; New York.
- Gholz, H. L., K. C. Ewel, and R. O. Teskey. 1990. Water and Forest Productivity. *Forest Ecology and Management* **30**:1-18.

- Gillespie, A. R., H. L. Allen, and J. M. Vose. 1994. Amount and Vertical-Distribution of Foliage of Young Loblolly-Pine Trees as Affected by Canopy Position and Silvicultural Treatment. *Canadian Journal of Forest Research-Revue Canadienne De Recherche Forestiere* **24**:1337-1344.
- Gower, S. T. and J. M. Norman. 1991. Rapid Estimation of Leaf-Area Index in Conifer and Broad-Leaf Plantations. *Ecology* **72**:1896-1900.
- Gresham, C. A. 1982. Litterfall Patterns in Mature Loblolly and Longleaf Pine Stands in Coastal South-Carolina. *Forest Science* **28**:223-231.
- Grier, C. C. and S. W. Running. 1977. Leaf Area of Mature Northwestern Coniferous Forests - Relation to Site Water-Balance. *Ecology* **58**:893-899.
- Grissino-Mayer, H. D. 2001. Evaluating crossdating accuracy: A manual and tutorial for the computer program COFECHA. *Tree-Ring Research* **57**: 205-221.
- Hennessey, T. C., P. M. Dougherty, B. M. Cregg, and R. F. Wittwer. 1992. Annual Variation in Needle Fall of a Loblolly-Pine Stand in Relation to Climate and Stand Density. *Forest Ecology and Management* **51**:329-338.
- Holmes, R.L. 1983. Computer-assisted quality control in tree-ring dating and measurement. *Tree-Ring Bulletin* **43**: 69-78.
- Holmes, R. L. 1994. MEDIR Measuring Software. Tucson Laboratory of Tree-Ring Research, The University of Arizona.
- Holst, T., S. Hauser, A. Kirchgassner, A. Matzarakis, H. Mayer, and D. Schindler. 2004. Measuring and modelling plant area index in beech stands. *International Journal of Biometeorology* **48**:192-201.

- Johnson, S. R. and D. R. Young. 1992. Variation in Tree-Ring Width in Relation to Storm Activity for Mid-Atlantic Barrier-Island Populations of *Pinus-Taeda*. *Journal of Coastal Research* **8**:99-104.
- Kaiser, H. F. 1960. The Application of Electronic Computers to Factor Analysis. *Educational and Psychological Measurement* **20**:141-151.
- Li-Cor Bio-Sciences. 1992. LAI-2000 Plant Canopy Analyzer Operating Manual. Lincoln, NE 68504.
- Li-Cor Bio-Sciences. 2004. FV2000 LAI-2000 File Viewer Software Version 1.01. Lincoln, NE 68504.
- Long, J. N. and F. W. Smith. 1990. Determinants of Stemwood Production in *Pinus-Contorta* Var *Latifolia* Forests - the Influence of Site Quality and Stand Structure. *Journal of Applied Ecology* **27**:847-856.
- Martin, T. 2000. Winter Season Tree Sap Flow and Stand Transpiration in an Intensively-Managed Loblolly and Slash Pine Plantation. *Journal of Sustainable Forestry* **10**:155-163.
- McClurkin, D.C. 1958. Soil moisture content and shortleaf pine radial growth in north Mississippi. *Forest Science* **4**: 232-238.
- Nagel, L. M. and K. L. O'Hara. 2001. The influence of stand structure on ecophysiological leaf characteristics of *Pinus ponderosa* in western Montana. *Canadian Journal of Forest Research-Revue Canadienne De Recherche Forestiere* **31**:2173-2182.
- National Oceanic and Atmospheric Administration (NOAA), National Climatic Data Center. 2009 Archive Data. <http://www.ncdc.noaa.gov/oa/ncdc.html>.

- Nowacki, G. J. and M. D. Abrams. 1997. Radial-growth averaging criteria for reconstructing disturbance histories from presettlement-origin oaks. *Ecological Monographs* **67**:225-249.
- Pezeshki, S. R. 1992. Response of *Pinus-Taeda* L to Soil Flooding and Salinity. *Annales Des Sciences Forestieres* **49**:149-159.
- Pierce, L. L. and S. W. Running. 1988. Rapid Estimation of Coniferous Forest Leaf-Area Index Using a Portable Integrating Radiometer. *Ecology* **69**:1762-1767.
- Roman, C. T., R. A. Zampella, and A. Z. Jaworski. 1985. Wetland Boundaries in the New-Jersey Pinelands - Ecological Relationships and Delineation. *Water Resources Bulletin* **21**:1005-1012.
- Richardson, D. L., J. H. Porter, and H. H. Shugart. 1993. Permanent Vegetation Monitoring Plots on Parramore Island: Attributes and Analysis Direction. <http://www.vcrlter.virginia.edu/davedocs/VCRASC95/richshug.html>.
- Richardson, D. L., J. H. Porter, and H. H. Shugart. 1996. 1996 Parramore Permanent Plot Resurvey. [http://www.vcrlter.virginia.edu/cgi-bin/w3-msql2/data/query/projects/show\\_proj.html?QPROJ\\_ID=VCR05086](http://www.vcrlter.virginia.edu/cgi-bin/w3-msql2/data/query/projects/show_proj.html?QPROJ_ID=VCR05086).
- Sampson, D. A., T. J. Albaugh, K. H. Johnsen, H. L. Allen, and S. J. Zarnoch. 2003. Monthly leaf area index estimates from point-in-time measurements and needle phenology for *Pinus taeda*. *Canadian Journal of Forest Research-Revue Canadienne De Recherche Forestiere* **33**:2477-2490.
- Sampson, D. A. and H. L. Allen. 1995. Direct and Indirect Estimates of Leaf-Area Index (Lai) for Lodgepole and Loblolly-Pine Stands. *Trees-Structure and Function* **9**:119-122.

- SAS Institute Inc. 2002-2003. Statistical Analytical Software Version 9.1 for Windows. Cary, NC.
- Shelton, M. G. and M. D. Cain. 2000. Regenerating uneven-aged stands of loblolly and shortleaf pines: the current state of knowledge. *Forest Ecology and Management* **129**:177-193.
- Smolander, H. and P. Stenberg. 1996. Response of LAI-2000 estimates to changes in plant surface area index in a Scots pine stand. *Tree Physiology* **16**:345-349.
- Sneath, P. H. A. and R. R. Sokal. 1973. Numerical taxonomy; the principles and practice of numerical classification. Freeman, San Francisco,.
- Snyder, R. A. and C. L. Boss. 2002. Recovery and stability in barrier island plant communities. *Journal of Coastal Research* **18**:530-536.
- Sokal, R. R. and F. J. Rohlf. 1995. Biometry : the principles and practice of statistics in biological research. 3rd edition. Freeman, New York.
- Spurr, S. H. and B. V. Barnes. 1980. Forest ecology. 3d edition. Wiley, New York.
- Stenberg, P., S. Linder, H. Smolander, and J. Flowerellis. 1994. Performance of the Lai-2000 Plant Canopy Analyzer in Estimating Leaf-Area Index of Some Scots Pine Stands. *Tree Physiology* **14**:981-995.
- Van Laar, A. and A. Akça. 2007. Forest Mensuration. 2<sup>nd</sup> Edition. Springer, The Netherlands.
- Veblen, T. T., K. S. Hadley, M. S. Reid, and A. J. Rebertus. 1991. The Response of Sub-Alpine Forests to Spruce Beetle Outbreak in Colorado. *Ecology* **72**:213-231.

- Webb, S. L., M. G. Glenn, E. R. Cook, W. S. Wagner, and R. D. Thetford. 1993. Range Edge Red Spruce in New-Jersey, USA - Bog Versus Upland Population-Structure and Climate Responses. *Journal of Biogeography* **20**:63-78.
- Whittaker, R. H., F. H. Bormann, G. E. Likens, and T. G. Siccama. 1974. Hubbard Brook Ecosystem Study - Forest Biomass and Production. *Ecological Monographs* **44**:233-252.
- Xu, M. G. and T. B. Harrington. 1998. Foliage biomass distribution of loblolly pine as affected by tree dominance, crown size, and stand characteristics. *Canadian Journal of Forest Research-Revue Canadienne De Recherche Forestiere* **28**:887-892.
- Zampella, R. A., G. Moore, and R. E. Good. 1992. Gradient Analysis of Pitch Pine (*Pinus-Rigida* Mill) Lowland Communities in the New-Jersey Pinelands. *Bulletin of the Torrey Botanical Club* **119**:253-261.

### **III. Sea level forcing, and relationships of freshwater availability and barrier island forest biophysical structure**

#### **Abstract**

Assateague Island National Seashore (AINS) and Parramore Island, Virginia Coast Reserve (PIVCR) upland forests are understudied systems. This chapter characterizes the ecohydrological system here in a broad manner to address the dearth of baseline information, and to assess vulnerabilities of the forests to sea level rise (sea level rise is occurring at a relative rate of about  $3\text{mm year}^{-1}$  according to Hayden *et al.* 1995). A simple functional relationship is developed that can be applied to the assessment of forest structure change with sea-level forcing of barrier island freshwater tables.

As the substrate of the islands is sand down to a commonly found peat layer (acting as an aquatard) it is hypothesized that there is a near 1:1 relationship (with the peat layer as a confounding variable) between the rising of average sea level and that of average island freshwater tables. It is assumed that the upland forests here are water-limited systems. Based on theoretical work by Hayden *et al.* (1995), a generalized water availability to vegetation communities is estimated by depth to water table measurements. This is feasible because of the generally low water holding capacity of sand and low capillary strength of water in sand soil. Depth to water table (DWT) is hypothesized to negatively correlate with biophysical structural values – of loblolly pine (*Pinus taeda* L.) in particular – because vegetation structure is sensitive to water availability. Detection of

a spatial gradient relationship in water and structure can aid in determining likely trajectories of rising water on temporal basis.

The structure of the *P. taeda*-dominated forest varies at the coarse and fine scales across environmental gradients including DWT at AINS. Capturing leaf area changes associated with general water availability will provide a circumstantial reference to anticipate and better model production and growth trajectories under changing water levels. The relationship of plant area index (PAI), a variable conveniently collected with a light sensor instrument that integrates leaf area, is found to only weakly correlate ( $r_s=0.46$ ,  $p=0.133$ ) with DWT. The scaling of DWT with a ratio of soil texture (STI) improves the relationship up to  $r_s=0.54$ ,  $p=0.004$ . Shrub canopy dripline area (SCA) is found to be a reliable indicator of hydrology (correlates with DWT at  $r_s=-0.80$ ,  $p=0.009$ ), and its continued monitoring is recommended at a variety of scales to track structural changes due to water table rise.

Evapotranspired groundwater ( $ET_G$ ) is estimated to quantify an underlying flux that can be helpful in determination of variation in physiological feedbacks in the above-ground structure/below ground water storage balance, and in derivation of better predictions of effects of water table rise. This exercise also contributes evidence from a unique habitat to the ecohydrological paradigm of evapotranspiration as a conservative process. Dendrochronological analysis of initial-condition development supports a rooting depth and DWT interactive constraint theory of forest growth.

At AINS, a wind/wave-dominated barrier, the peat layer does hamper attempts at tidal forcing descriptions of the freshwater lens systems. There are feasible theories, however, based on local geomorphology, of the variation in forcing functions and low

cross-correlations of the tide and water table time series. PIVCR appears more readily described by standardized functions due to its nature as a mixed-energy-dominated barrier. In general, there is evidence that seawater rise is currently a measurable force on water tables.

Combination of results from these analyses allows for drafting of a chronological development theory. It is expected that in most cases on AINS, a permanent water table rise could force roots to reside in coarser soil than current, reducing water availability. This will be detrimental to growth of forests at the higher elevations if they do not adjust rooting habits sufficiently. Lower elevation sites, apparently accessing vadose precipitation water preferentially over groundwater, may be most affected by encroachment of shrubs or alternately, inundation and salt stress.

### **3.1. Introduction**

The study is designed to derive a basic understanding of the ecohydrological system of the upland forests of barrier islands, and thus propose an underlying mechanism that can explain forest development patterns here. Depicting adequately the soil-plant-atmosphere circuit is paramount to understanding the likely reaction of above-ground forest structure and related development to increased freshwater table heights expected with sea level rise. Chapter 2, “Mid-Atlantic barrier island forest structural properties and site gradient expression” provides the raw data for correlation analyses of structure and moisture variables. Perhaps most essential to predictions of forest structural

change are a combination of the records of past growth provided by dendrochronological analyses, and the records of daily water use by vegetation type in site water level records.

The specific goals of this chapter are: 1) develop a simple site water availability index that is indicative of structural change along hydrological gradients; 2) compare sites along biophysical and environmental gradients in magnitude of groundwater evapotranspiration; 3) assess vulnerability of freshwater sources to forcing by sea levels through time series analysis of sea tides and site water tables; and 4) synthesize the findings into a general predictive theory of likely ecophysiological adjustment, and the effects to above-ground structure of rising waters.

With these results, small-scale structural changes are illustrated across existing hydrological gradients that could feasibly be ascribed to rising sea levels later. The opportunity exists to apply these theories to monitoring programs of coastal change with rising seas, and Chapter 4 “The application of the EAARL (Experimental Advanced Airborne Research Lidar) to measurement and monitoring of barrier island forest structure in an ecohydrological change scenario” details how a lidar program could provide robust, fine-scale verification of the ecohydrological mechanism proposed in the current chapter. It is also apparent, through the analyses here, that there is a potential to create highly detailed time series models of site water levels and forest productivity with some increased field data sets (E.g., site leaf area change timed with moisture availability).

In general, this work will also aid in planning for change, and managing natural and human coastal landscapes; provide more evidence in the debate over the effects of anthropogenic atmospheric change; enhance methodologies to monitor ecohydrological

relationships; and promote the coordinated use of standard technologies to arrive at verifiable conclusions in issues of global change.

## **3.2. Background**

### **3.2.1. General barrier island upland forest ecohydrology**

The significance of understanding the physical structure of forests in the context of ecological processes involving material and energy exchange has long been recognized. Monsi *et al.* (1973) note “...morphological features... have a great influence upon the processes of action and reaction between plants and their environment through the modification and interception of fluxes of radiation, heat, carbon dioxide, etc.” Consequently, productivity is determined in substantial part by canopy structure (Monsi *et al.* 1973). It follows that these same morphological properties should play an important role in site water relations through interception of precipitation and as an interacting surface (leaf area) in transpiration (Gholz *et al.* 1990).

Shugart (2000) notes “structural dynamics can strongly alter the process-based predictions of such features as ecosystem productivity” at timescales similar to those of concern in the present study. As will be shown later, the effect of canopy flora on subcanopy flora and vice versa is evident in groundwater evapotranspiration ( $ET_G$ ) across a shrub:canopy tree gradient. Knowledge of a suite of biophysical characters along environmental gradients can aid in development of predictive and conceptual models of changes in water use with associated structural change. Environmental gradients

developed in this study allow for a spatial-for-temporal scale substitution to investigate the consequences of sea level rise to island upland forest.

Barrier islands are highly dynamic systems, and hence provide a unique opportunity for the study of vegetation dynamics and structure, and the controls exerted by various environmental factors. Though relatively protected from direct overwash impact, the loblolly pine (*Pinus taeda* L.) forests of AINS and PIVCR can be affected by changing availability of freshwater resources and related interactions like those described in Hayden *et al.* (1995). Here, the researchers describe the interplay of three changeable surfaces: land, sea and fresh water tables. Vertical changes in one or more of these will affect the distance to ground water for vegetation communities and associated general water availability as determined by groundwater storage capacity and average matrix potentials. Ehrenfeld (1990) writes the effects on “species diversity, community structure, and ecosystem function are likely to be profound.” Incremental shifts in physiology may also be occurring as the saline-fresh water interface rises and vegetation stomatal conductivity is reduced by exposure of the rooting zone to greater salinity levels (Johnson and Young 1993).

The sources of fresh groundwater on the barrier islands are lenses of freshwater that float on the denser salt water with a fluctuating zone of mixing between the bodies. The size of the freshwater lens “depends primarily on landmass width, permeability, recharge and tidal range” (Urish 1980). Adherence of freshwater bodies of the mid-Atlantic barrier island forests to the Ghyben-Herzberg (Urish 1980) principle of aquifer morphology is likely rare. This model predicts a 1:40 relationship between the height of the water table above mean sea level and the thickness of the lens. It is expected that

Assateague and Parramore freshwater lenses are localized, and their morphologies and dynamics dependent to a degree upon: vegetation, through variation in transpirational demands (Ruppel *et al.* 2000); and the presence and thickness of impeding marshland-derived peat layers (Anderson *et al.* 2000) at the base of site soil profiles.

### 3.2.2. Water availability and structure

Leaf area index (LAI) is largely assumed to be a determinant and result of the forest stand processes of interest in the present study. Hebert and Jack (1998) note its applicability as an index of site productivity in *P. taeda* stands “because it affects interception of radiation, assimilation of carbon, carbohydrate storage, transpiration of water and accumulation of nutrients.” It follows to reason that changes in LAI may significantly affect productivity and water availability (Gholz *et al.* 1990). Vose and Allen (1988) find a linear relationship ( $r^2=0.75$ ,  $p<0.01$ ) between LAI and stemwood production across some coastal plain (North, South Carolina) stands of *P. taeda*. Phillips and Oren (2001) find that seasonal LAI and changes in maximum LAI explain significant variation in *P. taeda* canopy evapotranspiration when combined with vapor pressure deficit. In their seminal paper, Grier and Running (1977) find that LAI clearly varies across vegetation zones with a precipitation gradient in Oregon. They posit that where sufficient leaf water potential can not be maintained through stomatal control and available water, leaf area is adjusted to balance evaporative demands. Water stress can therefore limit LAI, and reduce – more significantly than any other site factor – tree growth in general (Spurr and Barnes 1980).

There is little known, however, concerning the relationship between LAI and site water for individual species (Vose *et al.* 1994). The degree to which the relationship is significant in barrier island habitats is unknown, but Day *et al.* (2001), working in herbaceous vegetation on Hog Island of the Virginia Coast Reserve (VCR), determine that above-ground biomass may in large part be determined by position of the water table.

Pines of the Southeastern U.S. undergo multiple foliage flushes during a growing season, the number of which is determined by environmental variables – “especially moisture” (Spurr and Barnes 1980); *P. taeda* commonly displays a two-fold difference in LAI in a growing season (Vose *et al.* 1994). This indeterminate growth makes it difficult to estimate a temporal pattern in *P. taeda* LAI (Sampson *et al.* 2003; see Chapter 2), thus requiring very specific site information and regular surveys to make accurate characterizations of change and causal relationships. Better modeling of leaf area changes with water availability will provide for fine-scale growth predictions. Hebert and Jack (1998) were unable to directly relate a moisture gradient and LAI in loblolly plantations, but they note the range in precipitation may have been too small for them to observe significant LAI change within the experimental design.

### **3.2.3. Tidal forcing**

It is clear that sea levels would force barrier lens hydrology and water tables. There is heightened concern regarding the effects of sea level rise to vegetation on barrier islands because of the possible loss of island stability at an accelerated pace with vegetation decline. The current work is not concerned with explicit description of the

physical system, only in gauging the sensitivity of areas and detecting a general tidal signal in freshwater tables.

Dusterhoff (2001), working on the forest upland/marsh wetland transition zone (about 70 meters from the shoreline) on the Delmarva Peninsula mainland southwest of PIVCR, detected a clear bay tidal signal lagging about 65 minutes. Tidal signals attenuate as they traverse sandy barriers (Rotzoll *et al.* 2008) becoming more difficult to tease out of water table time series. Accurate assessments of local sensitivities to sea level influence can also be used in the near-term for modeling and predictive efforts on storm surge and variation in depths to saline mixing. There are hydrological disparities between AINS and PIVCR due to a variety of factors (which are covered below), but they are likely most reliant on the alternate geomorphologies of the two island systems: AINS is a microtidal wave-dominated strip, and PIVCR a mixed-energy (wave and tide) ‘drumstick’ (Krantz *et al.* in review).

#### **3.2.4. Evapotranspiration**

It seems logical to assume that  $ET_G$  should vary with leaf area levels, however, research has frequently shown a lack of dependence between the two variables. Phillips and Oren (2001) find that *P. taeda*-mixed forest canopy transpiration (per unit ground area) “tended to dampen, rather than amplify, variation in evaporative demand or annual water availability, and there was no significant temporal increase in [canopy transpiration per unit ground area] with a net increase in [leaf area].” Some do find a relationship between expressions of water availability and ET (Bond *et al.* 2007; Ford *et al.* 2005) to an extent. But, more studies in more areas are showing that evapotranspiration is a

“conservative process” (Roberts 1983; Roberts 2000) with “water use not exceeding the water holding capacity of a deeply rooted soil [barring additional rain]” (Roberts 1983). A trend toward methods of drought avoidance (Retzlaff *et al.* 2001) by rooting growth and physiology also appears in examples, as does maintenance of a constant root area to leaf area ratio (Hacke *et al.* 2000, Torreano and Morris 1998) in *P. taeda*. These adjustments are coupled with the interaction of physical structure of all site species in which shrubs and other subcanopy flora compensate (Phillips and Oren 2001) for lower canopy stomatal density/activity.

ET<sub>G</sub> data is used to place structural expression on a scale of water use, and create another explanatory variable in the physiological control of fine structure. ET information helps characterize the hydrological Soil Plant Atmosphere Continuum or SPAC (Bond *et al.* 2007) on a site-to-site basis, and aids in assessing likely effects of perturbations to water availability and the constituents of the evapotranspiration function used in the present study (the White, 1932, method of groundwater use estimation). Studies often find quite low variation in ET as detailed above, yet perhaps it can be enough to reflect the adjustments by flora (in leaf area, for instance) to counteract the “loss of hydraulic contact” (Hacke *et al.* 2000) in the rhizosphere. The results are an important aspect of crafting predictions of effects to canopy and whole forest community structure of rising water at AINS and PIVCR.

### **3.2.5. Synthesis**

Site water baselines must be determined because of the assumed influence of sea level rise on island fresh water table levels (Ehrenfeld 1990). Technically, water

availability is the amount of water in a soil between field capacity and permanent wilting point of the site vegetation (Lee 1980; Cassel and Nielsen 1986). Freshwater availability is estimated at AINS through continuous water level monitoring and soil textural description. A standard selection of forest biophysical features and a suite of environmental parameters are used in alternating fashion here to cluster sites and draw out relationships of structure to water. In addition, dendrochronological analysis bolsters theories about site limitations, and predictions concerning water table rise.

Vegetation has long been studied for hydrological gradient expression (E.g., Waring and Major 1964). The challenge presently – with no prior data sets at AINS – is to find that relationship expressed at the scales monitored in this study. Fineness of the vegetation data is limited to plant area index (PAI): an index of plant area (the sum of one-sided leaf area and stem/branch area) per unit ground area ( $\text{m}^2\text{m}^{-2}$ ). Biophysical structural measures are employed, as opposed to species presence and abundance identification typical of phreatic vegetation stratification, in part to coordinate this study aspect with the lidar (Light Detection and Ranging) remote sensing project detailed in Chapter 4 of this volume. Also, species association analysis may not be the best stratification method in certain environments. Roman *et al.* (1985), in a test of the reliability of ‘wetland indicator’ species in the New Jersey pinelands – similar to AINS in its low relief and sand soils – find most species intergrade, disrupting cluster analysis and other attempts to have hydrological groups fall out.

### **3.3. Methods**

The following methods pertain mainly to research activities performed at AINS. PIVCR was studied for water level fluctuation, coarse structure, and evapotranspiration estimates only. At the time of study, the forest canopy had recently been largely decimated following a series of natural disturbances.

#### **3.3.1. Site and biophysical stratification**

In the preceding chapter, data collection of the biophysical structure of pine forests of the islands and their associated site environments was described in detail. Sites are prescribed to groups by the results of principal components analysis (PCA) and cluster analysis of biophysical and environmental measures. Structural measures are: tree heights and crown lengths; trunk diameters at breast height (dbh); and shrub canopy dripline area (SCA). Individual tree crown lengths were integrated over plots to arrive at heights of peak canopy density (technically, peak foliated canopy presence frequency), HPCD. Plot-level values were computed of basal area (BA):  $\pi*(dbh/2)^2$ ; and the Whittaker *et al.* (1974) parabolic volume estimate (Vol):  $(0.5(PTH)\pi(dbh/2)^2$  where PTH is the plot average tree height.

The hand-held “LAI-2000” Plant Canopy Analyzer (Li-Cor Biosciences) that derives PAI through calculation of canopy light extinction was used to collect PAI estimates at all sites, and characterize in-season foliage changes. The LAI-2000 was determined to be the most appropriate means of estimating LAI after a review of the literature, though it is noted that it “systematically” underestimates LAI in coniferous

forests (Scurlock *et al.* 2001). The deficiencies arise from pine species violating the condition of evenly distributed reflecting surfaces in the Beer-Lambert Law by “clumping” their foliage. However, the LAI-2000, in providing instantaneous results of PAI (integration of woody and foliar area), may be most appropriate in “estimat[ing] seasonal patterns in LAI when LAI varies continuously over the course of the year” (Sampson *et al.*, 2003). Destructive harvesting to derive a stand-specific dbh to LAI regression (Vose *et al.*, 1994) may result in better accuracy (though possibly not in the harsh and heterogeneous barrier island environment) but it is very labor-intensive, and the National Park Service (NPS) and VCR prohibit resource destruction. Litterfall estimates of LAI are also very labor-intensive and must be measured throughout at least one year. The LAI-2000 offers ease of replication for monitoring purposes, and fast and precise ground-truthing of the lidar surveys described in Chapter 4 of this volume. Rather informal litter traps were installed at the 11 AINS water level-monitoring plots to develop a relative leaf loss scale coordinated with PAI measures, and investigate the leaf loss and water availability relationship.

The environmental variables soil texture, soil organic matter, distance from ocean shoreline (distshore), maximum tree age (maxage; approximates the time since disturbance), average depth to water table (DWT), and bare earth elevation (BEE) were input to a PCA that separated sites into six “site types” after cluster analysis. These types are used throughout this study in making site-level interpretations of environmental forcing on biophysical responses. Two major PCA-clusters (4 subclusters) were developed with the major biophysical parameters. These “bio-types” were used to frame the structure-dependant analyses. Clusters were developed by regression of PC1 on PC2,

and results grouped with the unweighted pair-group method in SAS (SAS Institute, 2002-2003) statistical software. SAS was used for all statistical procedures.

### **3.3.2. Water availability and structure**

Continuous monitoring of sub-hourly to hourly water levels was accomplished with Ecotone (Intermountain Environmental Inc.) automatic capacitance water level monitoring instruments at the “water plots”: 11 AINS plots and 4 PIVCR sites. As initially designed, and as explained above per the Hayden *et al.* (1995) theory, long-term measures would supply a dynamic approximation of ‘water availability’ with simple DWT. Soil texture measurements were taken to account for differences in soil water holding capacities and matric potentials as variation in these would confound purely depth-driven characterizations. Effects of nutrient capacity and leaching variations can similarly be accounted for by particle size analysis as shown in a study of sandy Cape Cod, MA soils by Seely *et al.* (1998). AINS Samples were drawn regularly (about every 10cm) through profiles until water tables were encountered. Soil organic matter (SOM) was measured by ignition (see Chapter 2) of samples drawn from the top 10cm of soil profiles.

Initial data analyses showed that site soils differed mainly in the proportions of fine and medium sands. Fraction values were derived for each site and a ratio or soil texture index (STI) of fine to medium sand calculated for every sample depth. Profiles of texture fineness values were calculated and an average STI figured for each site.

The interaction of DWT and STI was tested to see if it characterized relative water availability within an ecosystem type better than simple depth to water. An

exploratory ANOVA (analysis of variance by general linear model, proc glm, SAS Institute 2002-2003) and correlations confirmed that a multiplicative combination of DWT and STI (DWST) performs very well compared to both original variables in signifying structural change. The simplified model of water availability afforded by a majority-sand soil profile, the assumption of an aquatard at depth, and the sensitive water tables due to generally high hydraulic conductivity of sand, together preclude more intensive water and soil analyses for obtaining relative association of moisture and above-ground vegetation structure.

PAI is tested as a plot-level variable in determining effects of relative water availability on above-ground structure. Changes in PAI and more coarse structural measures are assessed for correlation to water availability gradients. Holst *et al.* (2004) found that the LAI-2000 instrument reliably detected metered changes in beech (*Fagus sylvatica* L.) stand PAI when silvicultural treatments across sites were replicated. They calculated an error of about 15% throughout treatments. PAI was collected at AINS throughout 2005 to develop an average spatial gradient in PAI across site types, and capture seasonal and moisture-mediated leaf area change. DWT and PAI values were lagged by about two weeks in correlation exercises.

Tree radial growth rates determined in dendrochronological analyses are utilized as developmental evidence in interpreting structure-water interactions. The method (K. Hadley, pers. comm.) compares 20-year trends of growth from samples of the two bio-types. Composite trends were developed from several plots in each bio-type subgroup (see Chapter 2), initiated at one or two years after breast height. Aligned with site data, guiding principles of site effects on growth were developed.

### 3.3.3. Evapotranspiration

The Loheide *et al.* (2005) modification of White's (1932) groundwater evapotranspiration equation was applied to AINS water level data. The White equation (from Loheide *et al.* 2005) is:

$$ET_G = S_Y (\Delta s/t + R) \quad (1)$$

where  $\Delta s/t$  is the change in storage for a day of time  $t$  found by linear change in water table depth; and  $R$  is the recovery rate: the rate of night time (transpiration-free) positive change in water table height.  $S_Y$  is the specific yield for each site's soil computed as the average of associated changes in water table height for three precipitation events. Of the possible sources of  $S_Y$  described by Loheide *et al.* (2005), this derivation was deemed most appropriate for the data available. See Figure 1 for a chart of a sample water table and derived statistics for the period of measure.

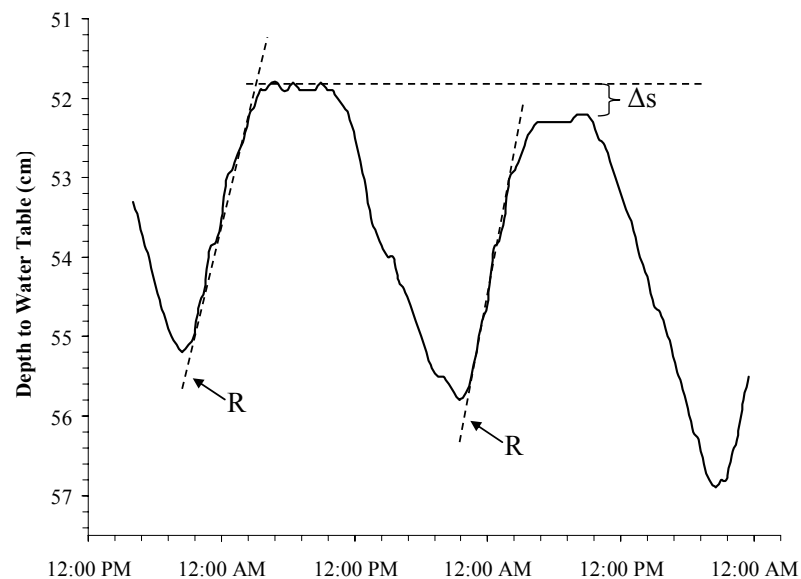


**Figure 1.** An example of water table fluctuation data used in the White ET equation from AINS plot 29803. The 24 hour change in storage ( $\Delta s$ ) is 0.01m; the approximate recovery period is 11PM to 3AM; and the two-day (day of, and day after July 20, 2005) average daily recovery rate ( $R$ ) is 0.13 m.

Consecutive near-transpiration-free (Loheide 2008) times used to compute the average recovery rate  $R$ , varied from plot to plot. In Figure 1 it is from 11PM to 3AM of both the day of and the day after the period of interest (7/20/2005). Depth to the water table (cm) is plotted over time.  $S_Y$  for a site will vary with PAI and the associated interception rates. Interception is unquantified, but differences in transpiration due to leaf boundary layer conditions of wetness should be controlled in our current results as the canopies are all comprised mainly of *P. taeda*. For a representative daily  $ET_G$  estimate, July 20, 2005 was determined to be sufficiently removed from precipitation events, with weather typical of a Mid-Atlantic coast hot and humid summer day (Table 1).

The strength of association between  $ET_G$  and biophysical and environmental variables was tested to characterize direct and indirect controls of  $ET_G$ . This would enable more robust interpretations of structural differences (spatially and temporally) over physical gradients. Differences in  $ET_G$  that may be due to variable advection by site are not investigated. Roberts (2000) details this process as a main cause of variation in ET among vegetation types. The extent to which it may cause variation within a small landscape such as barrier island uplands is likely insignificant on a rather calm day like July 20, 2005.

Variable	Daily July 20, 2005	Annual Average 2005
Rainfall daily (cm)	0	N/A
Rainfall year (cm)	25	40
Min air temp (C)	23	9
Max air temp (C)	34	18
Avg wind speed (km/hr)	7	11
Max wind speed (km/hr)	24	34
Avg wind direction (degrees)	236	184
Min rel. humidity (%)	58	57
Max rel. humidity (%)	93	91
Min baro. pressure (mb)	1024	1023
Max baro pressure (mb)	1027	1029
Avg fuel moist (%)	14	20
Min fuel moist (%)	11	14
Avg fuel temp (C)	31	16
Max fuel temp (C)	47	26

**Table 1.** Meteorological measurement values for July 20, 2005 and annual average values for 2005 collected at Assateague Island National Seashore.

### 3.3.4. Tidal forcing

The Influence of sea levels on freshwater tables was investigated through time series analyses of available tides and the site water table records. In a three-tier process of simple correlation, ARIMA (autoregressive integrated moving average), and SPECTRA (spectral density analysis) iterations, site-specific qualitative estimates of connectivity with near-term sea level forcing were developed. A period of relative dryness (<0.5cm rain) in winter – February 12, 2006 to March 19, 2006 – was chosen for analysis to reduce confounding effects of transpiration on periodicity of the time series, although there will likely be some evapotranspiration on warmer, sunny days in winter (Martin 2000).

AINS freshwater lens height fluctuations absent transpiration are a result of Sinepuxent Bay (Fig. 2) and oceanside sea levels. The verified Ocean City (OC), MD inlet data (NOAA CO-OPS website archive) alone were utilized in lieu of verified ocean

tides. The tide slowly fills the bay as there is a single inlet at Ocean City and single outlet at Chincoteague, VA. Winds, precipitation, and coastal drainage combine to make tide levels and timing irregular and unpredictably modulated at any spot along the island's bayside. PIVCR site water fluctuations are somewhat more readily described by the predicted (only unverified data were available for the time period) ocean tide because of the generally consistent lag time from ocean levels due to the highly flushed nature of the salt marsh, channels and inlets.

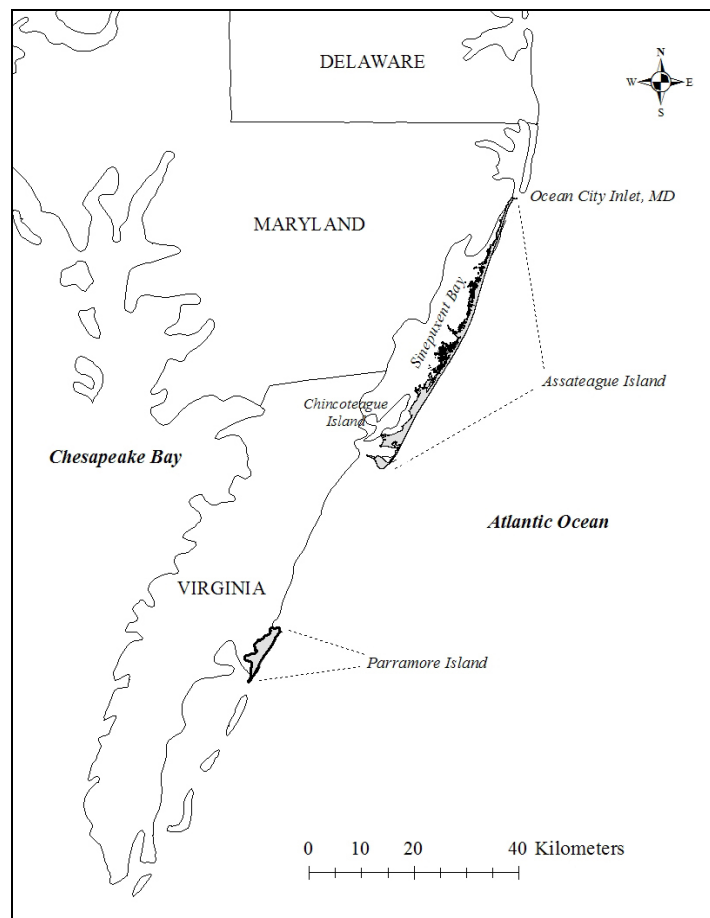


**Figure 2.** Assateague and Parramore Islands of the Delmarva Peninsula.

A diurnal tide signal is not immediately apparent in the water table series, and it is likely that distance and substrate (especially the peat layer) are nonlinear dampeners of water table reaction to the changing salt-water levels. Analyses progressed from simple correlations between time series of tide and water table in order to identify significant lags due to these site conditions in addition to distance from the Ocean City Inlet (Fig. 2). The interference and cancellation by the two tidal signals (Rotzoll *et al.* 2008) at island interiors is also hampering detection of a clean signal.

Data were averaged at 12 (AINS) and 24 hours (PIVCR) (hourly results were poor) and input to simple correlation procedures. Then these average time series were assessed with the ARIMA procedure in SAS (SAS Institute, 2002-2003). Ford *et al.* (2005) methodology, in which they determined lag functions of water deficits on evapotranspiration, was followed in constructing the ARIMA. The tide is the 'x', or independent variable and the water table is the 'y', or dependent variable. The great advancements here from simple correlation include the removal of autocorrelation ("prewhitening") prior to testing for a transfer function from x to y (Pack 1977), and the ability to test all possible lag times in the cross-correlation function of the procedure.

Reed *et al.* (2008) provide a model for the application of the SPECTRA (SAS Institute, 2002-2003) procedure. They apply findings of cross-spectral density to determining cyclic time signatures in estuary levels due to winds and coastal sea level. The SPECTRA procedure (SAS Institute, 2002-2003) decomposes raw data series with the finite fourier transformation forming a "periodogram" that is then smoothed by weighted moving averages. The two periodograms are cross-correlated. The SPECTRA procedure was performed on hourly AINS and PIVCR site water level and associated tide

data of the dry winter period to determine the most common cycles in spectral coherence as data are lagged. This analysis provided site-relative evidence of repeating patterns that were linked to a tidal signal.

PIVCR tidal forcing analysis was limited to SPECTRA and simple correlation. The predicted ocean tide at the VCR could not be made to conform to the stationarity principal needed in creating transfer functions (Pack 1977) in ARIMA.

The Sinepuxent Bay wind field data were tested for cross-correlation with water tables using SAS ARIMA as above because it was hypothesized that bay water retention time and volume may create measurable pulses to island water tables. Sustained winds from the SSW can impede drainage of the bay and impound water. Alternately, perpendicular to the AINS bayshore, sustained wind from the longest fetch (WNW) could cause impoundment directly on the shore. Per the Reed *et al.* (2008) method, all wind was converted to a vector of direction and speed, then rotated relative to the long axis of Sinepuxent bay ( $22.5^{\circ}\text{E}$ , “v-relative axis”), and perpendicular to this (“u-relative axis”) to form two wind force time series.

ARIMA functions were processed, unless otherwise noted, as 2<sup>nd</sup> order autoregressive, with a moving average of 1 (where a unit is 12 hours), or 5 (single hours) in the wind vector analysis. The tide is differenced by 1 unit (12 hours) to achieve stationarity and the wind vector is differenced by 1 hour. Upon initial testing, no ARIMA wind analyses yielded meaningful results and they will not be covered further.

### **3.4. Results**

#### **3.4.1. Site and biophysical stratification**

Full results of the AINS environmental and biophysical typing are in Chapter 2. Table 2 lists the values by plot for both sets of stratifying categories. Note that the DWT is a point-in-time measure. Table 3 lists the environmental cluster results and Table 4 the sub-type biophysical groupings. The broad 1 and 2 bio-types of Table 4 were mainly applied in the respective biophysical analyses. The outliers of the biophysical PCA are distinguished by their relatively large numbers of deciduous woody plants or extensive shrub component. See Chapter 2 for island maps of respective clusters.

Plot	BIOPHYSICAL							ENVIRONMENTAL				
	PAI	Vol	MCH	HPCD	SCA	BA	Maxage	DWT	SOM	STI	Distshore	BEE
19001	1.8	258.5	17.7	12.0	13.1	34.4	65	0.43	0.95	0.09	806	0.57
19002	2.1	230.3	13.9	9.9	179.9	40.0	58	0.18	1.01	0.13	705	0.42
20901	3.3	---	---	---	---	---	24	0.21	1.08	0.08	679	0.36
21801	1.7	57.6	8.1	3.4	175.0	19.0	21	0.33	1.31	0.06	346	0.34
21901	2.1	241.5	22.8	13.5	5.9	29.7	63	0.71	1.58	0.16	1013	1.34
21902	1.4	191.0	14.1	9.3	40.0	34.1	61	0.21	2.13	0.13	932	0.40
21903	3.2	199.8	16.3	10.8	847.4	29.9	64	0.29	1.18	0.12	1079	0.18
27701	2.7	118.2	11.2	6.0	57.1	28.3	23	0.33	1.25	0.10	329	1.18
27703	2.7	198.9	15.4	10.5	1.8	32.9	40	0.55	0.87	0.10	631	1.03
27704	3.0	406.7	22.9	15.5	149.3	41.9	42	0.32	1.01	0.13	691	0.77
28304	4.7	134.8	17.9	4.5	836.3	20.8	11	0.36	3.59	1.00	1389	0.41
28307	3.0	368.1	24.4	18.0	18.5	35.2	54	0.57	7.62	1.13	1327	0.53
28506	3.3	469.6	29.2	18.8	326.0	38.2	90	0.37	22.09	0.72	1015	0.46
28702	2.7	188.2	14.6	9.0	0.0	31.1	56	0.54	2.82	0.09	421	0.51
28703	2.2	144.9	10.1	7.3	106.2	33.8	29	0.39	4.43	0.10	294	0.92
28704	1.9	92.2	12.4	4.8	62.7	28.2	13	0.22	1.30	0.10	268	0.91
29201	1.9	150.0	10.9	7.2	41.6	33.9	44	0.23	3.70	0.14	390	0.73
29202	2.6	292.6	22.5	10.5	0.0	39.5	67	1.20	2.29	0.17	509	1.36
29203	1.8	181.3	15.5	8.7	0.0	31.6	54	0.45	0.97	0.16	475	0.75
29205	1.1	82.1	11.7	6.3	0.0	20.3	34	0.51	1.50	0.13	383	0.86
29503	3.5	280.0	17.1	13.6	24.2	39.1	51	0.23	4.27	0.54	502	0.27
29504	1.5	89.7	10.7	5.1	67.8	21.8	33	0.41	1.74	0.11	448	0.22
29505	3.0	220.2	16.8	6.8	198.8	34.7	44	0.53	2.72	0.22	598	0.51
29506	1.7	108.3	12.2	6.3	246.1	27.3	26	0.29	1.63	0.12	369	0.52
29801	1.3	69.2	8.6	5.0	206.4	20.2	28	0.25	1.01	0.09	444	0.04
29802	3.1	373.4	22.8	16.5	18.0	39.5	64	0.45	13.22	0.14	548	0.14
29803	1.8	113.5	12.1	5.5	238.6	25.0	29	0.33	0.59	0.08	437	0.15

**Table 2.** The variables and plot values (n=27; plot 20901 was not measured for most biophysical traits) that were used to derive principle components (PC) and group sites into biophysical and environmental types by cluster analyses of PC scores. PAI is study period (2004-2006) average plant area index in  $m^2m^{-2}$ ; Vol is parabolic volume ( $m^3$ ); MCH is the maximum canopy height (m); HPCD is the height (m) of the peak canopy density; SCA is cumulative area ( $m^2$ ) of shrub dripline; BA is basal area ( $m^2$ ); Maxage is the maximum age of trees in years; DWT is depth to water table (m; point-in-time); SOM is soil organic matter (%) from the top 10 cm of soil; STI is the soil texture index (fine sand:medium sand); Distshore is distance (m) from the ocean shoreline; BEE is bare earth elevation (m).

	Environment Site-Types					
	1A	1B	2	3	4	5
Plots	19001	27701	20901	19002	21901	28307
	27704	27703	21801	21902	29202	28506
	28702	28703	28704	21903		
	29201	29205	29504	28304		
	29203		29506	29503		
	29505		29801	29802		
			29803			

**Table 3.** Site types derived of environmental variable principal components analysis, and the cluster analysis of PC scores by individual plots.

		Biophysical Types				
		1A	1B	2A	2B	Outliers
Plots		19001	27704	21801	27701	21903
		19002	28307	28704	28703	28304
		21901	29503	29504	29506	
		29202	29802	29801	29803	
		21902	28506	29205		
		29201		20901*		
		29203				
		27703				
		28702				
		29505				

**Table 4.** Biophysical sub-types derived by principal components analysis of structural variables and cluster analysis of PC scores. The Outlier group is excluded from most analyses. \*This plot is included in 2A based on visual estimation only.

### 3.4.2. Plant area index

Of the biophysical variables, PAI is most likely to change at short monitoring scales with moisture, thus providing an ecohydrological indicator of SPAC adjustment to rising water. Figure 3 shows the integrative nature of the PAI measurement through strong Pearson correlations ( $r$ ) with coarse structure. These are due in part to the fact that the LAI-2000 does not distinguish between woody or foliar material, and in part to these measures being physiologically interdependent. Basal area did not conform to normal distribution after log transformation. Its Spearman correlation rank ( $r_s$ ) with PAI is 0.51,  $p=0.008$ .

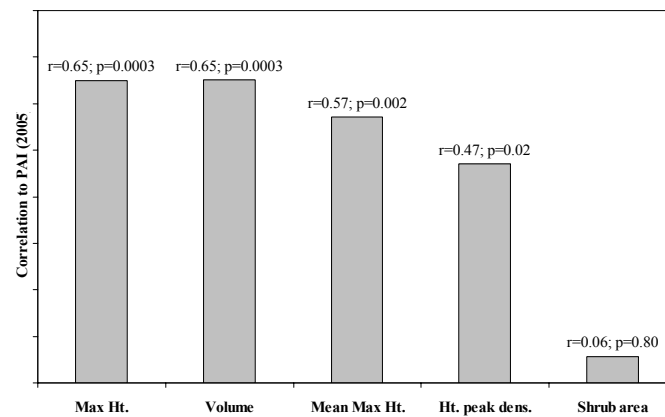


**Figure 3.** Pearson correlations between PAI from 2005 and coarse structural metrics collected in all plots,  $n=26$ . Data were log-transformed to normal distributions.

PAI changed throughout the study year (2005) in the major bio-types in a few common seasonal patterns seen in Figure 4. The proportional changes in PAI from peak to lowest foliated points in 2005 are in Table 5. Coefficients of variation of PAI loss are 35% and 48% for bio-types 1 and 2, respectively.

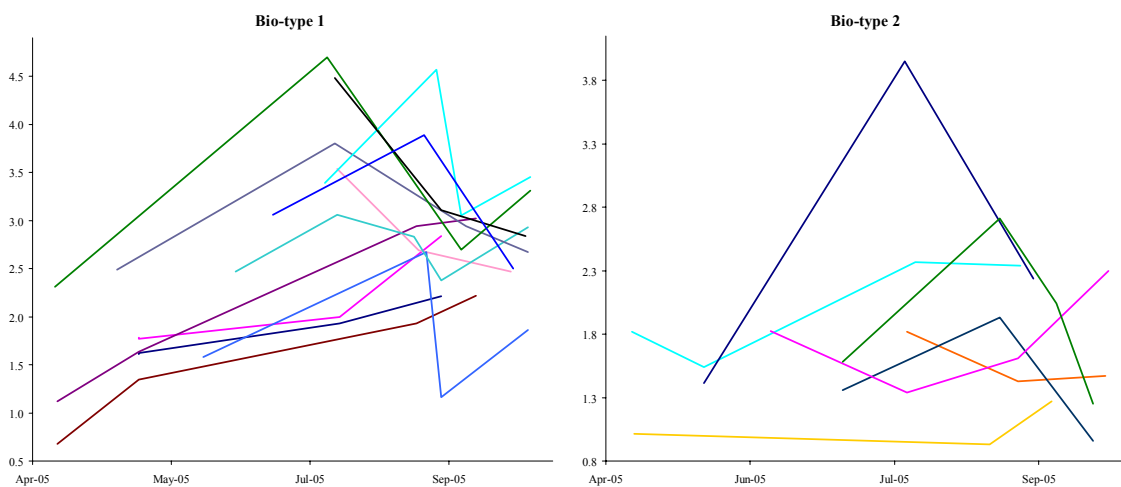


**Figure 4.** PAI values across 2005 study period for plots in the biophysical bio-types 1 ( $n=15$ ) and 2 ( $n=10$ ).

2005 Annual PAI Change			
Bio-Type	n	Average % Reduction in PAI	Standard Dev.
1	15	41	14
2	10	36	17

**Table 5.** The proportional reduction of PAI in 2005 for major bio-types.

Of utmost interest in predicting growth patterns is change to PAI effected by moisture status. *P. taeda* leaf area is sensitive to drought, and noted for dropping leaves relatively quickly under moisture stress (Vose and Allen 1991), and for flushing new foliage in good conditions. The leaf litter collections of summer and fall 2005 at the 11 water plots yield the patterns seen in Figure 5. PAI and leaf litter correlations were conducted to determine if there is a regular differential with PAI and litter-driven LAI loss. Lagging the total litter weight gain and coincident PAI change by approximately 14 days, the correlation analyses resulted in opposite directional relationships for bio-types (Table 6). The analysis was not constrained with meteorological data like wind and rain which could explain some variation.

It is likely that it would take multiple consecutive seasons of gathering PAI and groundwater information to derive an accurate function of dependence between the two. However, as discussed later, this interaction may only be an indirect relationship involving plot-wide vegetation transpirational dynamics.

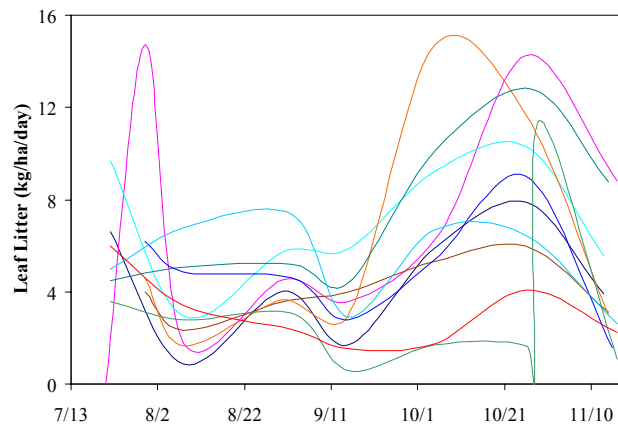


**Figure 5.** The average litterfall (leaves only) through 2005 monitoring, in  $\text{kg ha}^{-1}\text{day}^{-1}$  for individual sites ( $n=10$ ). 21903 (bio-type outlier) is not represented here as it skews the chart by a very large needle drop late in the year.

PAI and Litterfall		
	Bio-type 1	Bio-type 2
Spearman Corr. Coeff.	-0.40	0.62
<i>p</i> -value	0.286	0.102
<i>n</i>	9	8

**Table 6.** The correlation results of change in PAI and litterfall in the biophysical types. The *n* values reflect the number of unique sets of measures across each bio-type in the study period.

### 3.4.3. All biophysical structure

All structure measures were tested for relationships with the moisture-related site factors STI and DWT to develop inferential statistics of ecohydrological mechanisms. As stated previously, it may be reasonable to assume that DWT in sand soils will indicate general available moisture within a vegetation type, with shallower DWT indicating greater availability. In addition, finer sands (higher STI) will hold moisture longer than more coarse sands, likely providing an advantage during drought and in low nutrient conditions.

The results of the moisture indices and structural parameters correlations are in Table 7. Unclustered, and with only 10 samples from instrumented plots, PAI correlates somewhat weakly positively with average DWT ( $r_s=0.46$ ), yet shrub canopy dripline area (SCA) and maximum age (maxage) correlate significantly ( $r_s=-0.80$  and  $0.63$ , respectively). Height of peak canopy density (HPCD) is weakly positively correlated with DWT. STI, on the other hand, correlates more significantly with PAI, vol, maximum canopy height (MCH), and BA; all plots ( $n=26$ ) are considered here (Table 7).

The sites are clustered into respective bio-types to develop more specific relationships of fine plant area change and moisture limitation through DWT. These results are in Table 8; note the change in correlative direction from bio-type 1 to bio-type 2. Note, however, that this does not improve upon the results in Table 7 from unclustered sample groups. Together, these results are evidence that deeper plots are generally more likely than shallow plots to have higher PAI.

Soil Texture Index (STI) and Forest Structure (n=26)							
	PAI	Vol	MCH	HPCD	SCA	BA	Maxage
Spearman Corr. Coeff.	0.52	0.58	0.68	0.47	-0.06	0.49	0.38
p-value	0.007	0.002	0.0001	0.015	0.764	0.011	0.056
Average Depth to Water Table (DWT) and Forest Structure (n=10)							
	PAI	Vol	MCH	HPCD	SCA	BA	Maxage
Spearman Corr. Coeff.	0.46	0.37	0.43	0.53	-0.80	0.00	0.63
p-value	0.133	0.332	0.244	0.145	0.009	1.000	0.053

**Table 7.** The correlation results for the site moisture indices STI and DWT with forest structure across site and biophysical types.

Depth to Water Table and PAI		
	Bio-type 1	Bio-type 2
Spearman Corr. Coeff.	0.46	-0.37
p-value	0.179	0.239
n	10	12

**Table 8.** The correlation results for DWT and PAI within biophysical types at an average two-week lag from time at DWT to time at PAI. n refers to sets of average measurements from the bio-type grouped by time of year.

#### 3.4.4. Shrub analysis

Shrub analysis is emphasized because of the apparent potential of SCA as an independent site moisture indicator at AINS (Table 7). Conn and Day (1993) document *Myrica cerifera* (bayberry) association with relatively shallow DWT at the VCR, and Tolliver *et al.* (1995) note *M. cerifera*'s common successional status on the barrier islands as intermediate between herbaceous vegetation and trees. SCA is free of high intercorrelation with the other coarse structure measures in our study, with a maximum Pearson correlation of  $r=-0.40$ ,  $p=0.07$  ( $n=26$ ) with HPCD. Figure 6 is a chart of average shrub heights and canopy area by site type.

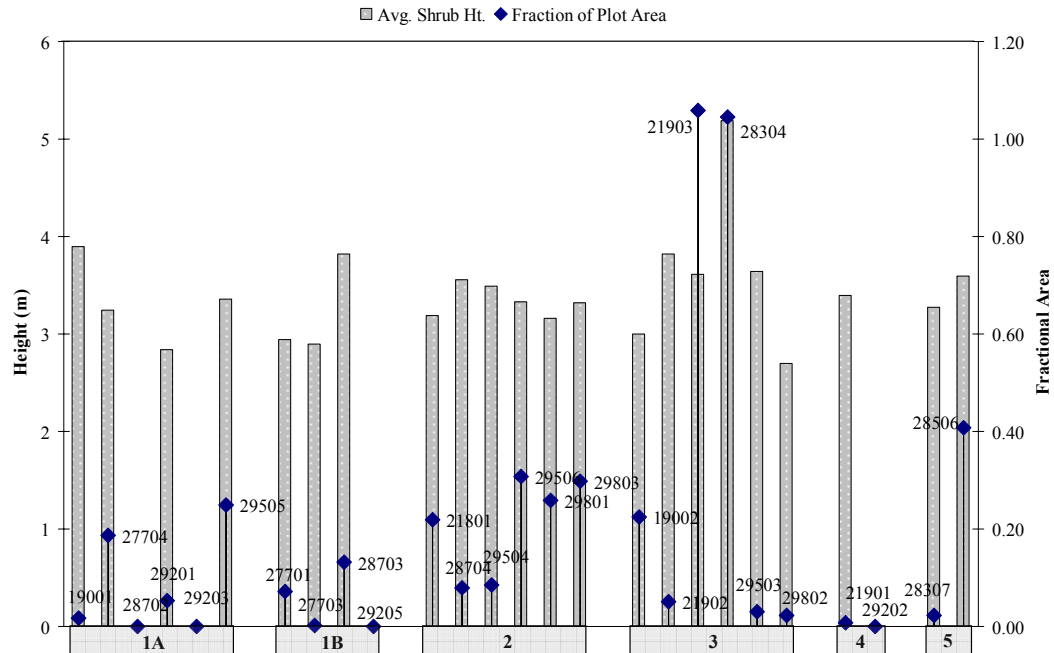


**Figure 6.** Shrub canopy area (◆) and average height (■) of the shrub layer in plots at AINS. All sites are grouped into their respective environmental site types, 1a-5.

### 3.4.5. Soil texture index and water availability

In an ANOVA of DWT in the four subgroup bio-type clusters (1a, 1b, 2a, 2b for a total of 25 sites), bio-type does not account for significant variation in DWT ( $r^2=0.15$ ,  $p=0.433$ ) while bio-type does impart significant variation ( $r^2=0.46$ ,  $p=0.007$ ) to average STI (with a fair amount of unexplained variation). This new result led to the testing of a combination of the measures to utilize the information in STI as needed and develop a more dynamic and hydrologically meaningful ordinate: DWST (DWT•STI). The soil texture descriptions at regular intervals through the soil profiles (Fig. 7a-7c), allow for water availability estimates around the water table, and upward through the profile. In the correlation analysis with forest structural measures, average DWST performance generally mirrors that of STI (Table 7), except for a more significant and negative

association with SCA ( $r_s=-0.32$ ,  $p=0.12$ ), and a reduced positive relationship with BA ( $r_s=0.32$ ,  $p=0.11$ ).

A new DWT variable was modeled using the linear regression function of point-in-time (PIT) measures of Table 2 and the respective values of verified, long-term automatic well-collected averages ( $n=11$ ). The regression model is:

$$\text{DWT}=0.96(\text{PIT})+0.14 \quad (2)$$

for which  $r^2=0.69$ , and root mean square error (RMSE) is 0.19m. Using the modeled DWT to derive DWST, and the annual 2005 PAI (as opposed to the study length average of 2004-2006, as this may be skewed by long intervals between the main set of measures and preceding or succeeding ones, see Figure 4), the PAI-DWST correlation over  $n=24$  (outliers removed) plots is significantly better ( $r_s=0.49$ ,  $p=0.02$ ) than that for DWT only ( $r_s=0.22$ ,  $p=0.29$ ) and improves upon STI only ( $r_s=0.37$ ,  $p=0.08$ ).

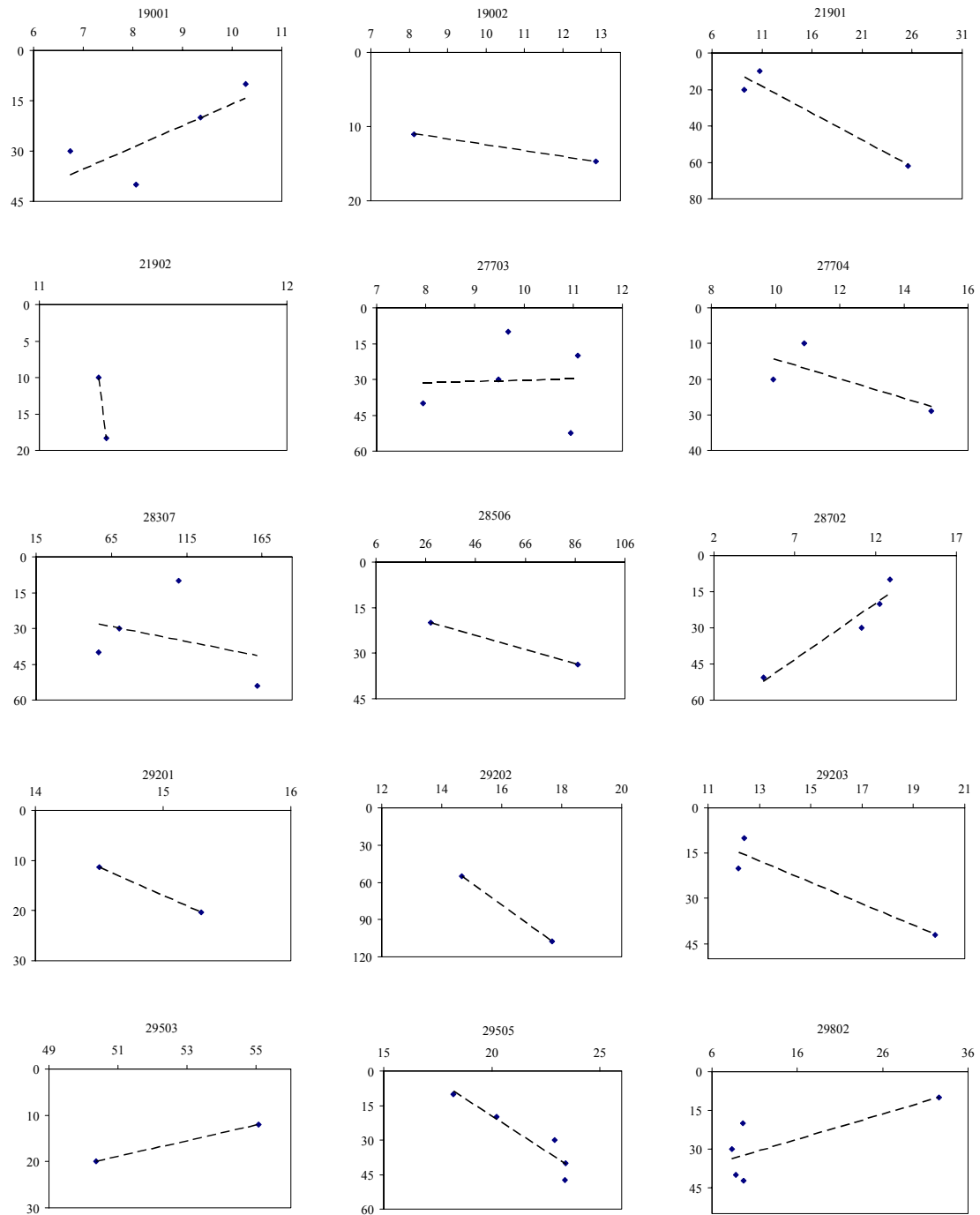


**Figure 7a.** The STI profiles of plots in bio-type 1 with a linear best-fit trendline (---). STI in percent (fine sand/mediums sand X 100%) is on the x-axis and soil depth from surface is on the y-axis.

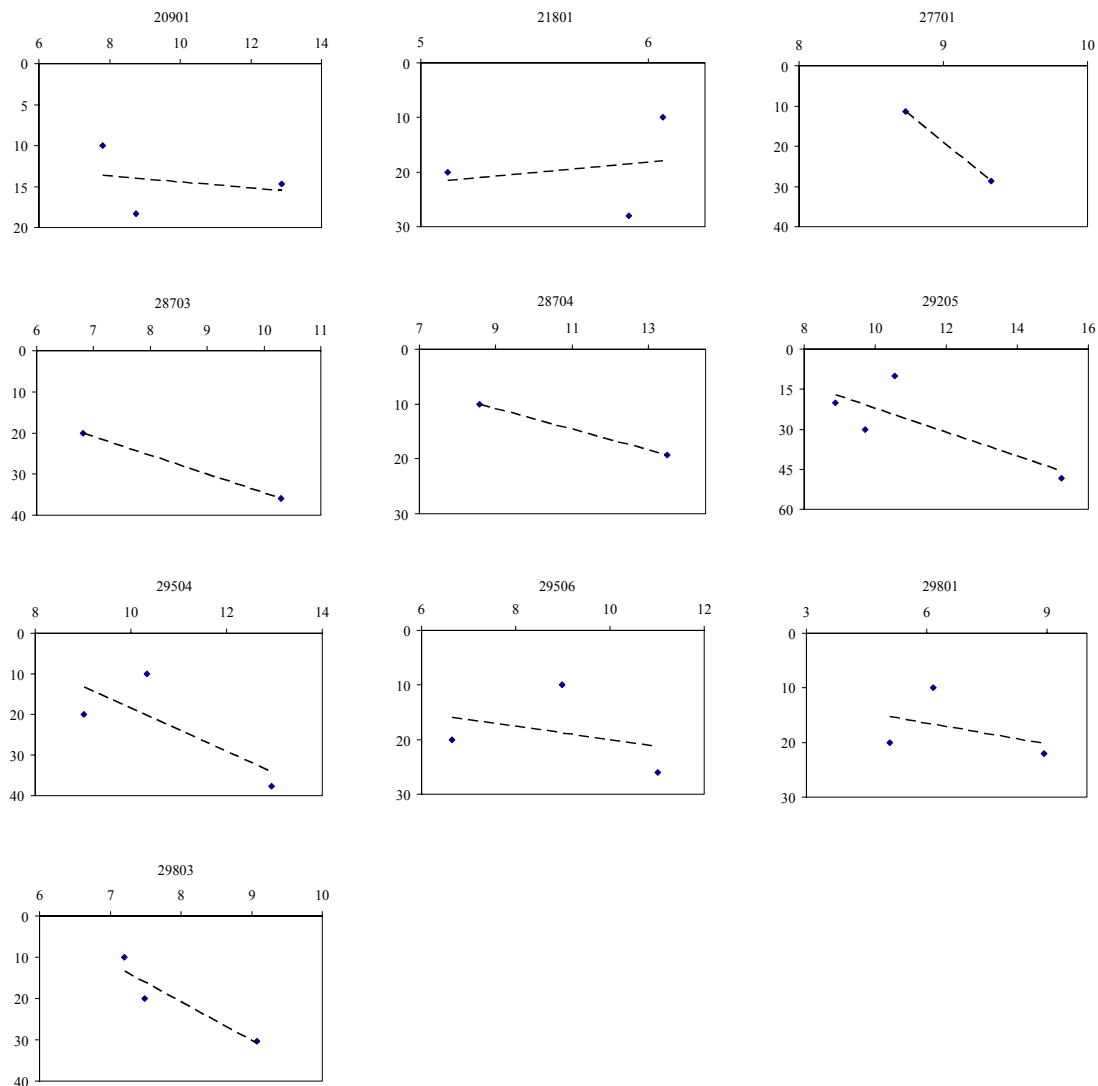


**Figure 7b.** The STI profiles of plots in bio-type 2 with a linear best-fit trendline (---). STI in percent (fine sand/mediums sand X 100%) is on the x-axis and soil depth from surface is on the y-axis.

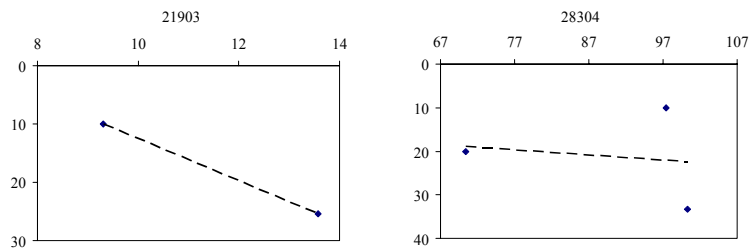


**Figure 7c.** The STI profiles of plots in bio-type outliers with a linear best-fit trendline (---). STI in percent (fine sand/mediums sand X 100%) is on the x-axis and soil depth from surface is on the y-axis.

### 3.4.6. Evapotranspiration

Table 9 lists the factors and results for the groundwater evapotranspiration analysis. The standard deviation (s) of  $ET_G$  over all sites (n=10) is  $2.63\text{mm day}^{-1}$ , with a coefficient of variation (CV) of 56%. There is no correlation between transpired groundwater and concurrent PAI measures. However, all PAI readings were generally taken above the influence of most shrub canopy. Of all correlations with biophysical variables,  $ET_G$  trends significantly only with SCA ( $r_s=0.67$ ,  $p=0.03$ ). This and the other correlations among the White equation elements and the important biophysical and environmental variables are listed in Table 10. Exploratory simulations (not shown) of the Shao *et al.* (1995) barrier island shrub transpiration (MCHOG) model with *M. cerifera*, and a separate permutation with *P. taeda*, result in a *M. cerifera* transpiration  $0.9\text{mm day}^{-1}$  greater than *P. taeda*, or about 50% higher.

In the test of environmental factor significance in  $ET_G$  trends, BEE (bare earth elevation) is the only significant correlation at  $r_s=-0.55$ ,  $p=0.1$  (DWT correlation is insignificant but also inverse at  $r_s=-0.42$ ). BEE is a major inversely varying factor in the recovery rate, R ( $r_s=-0.71$ ,  $p=0.02$ ) as a result of general topographic effects, and the general condition that R tends to be lower in higher elevations because a source to generate recovery needs to have a higher hydraulic head (Loheide 2008). This condition is often not met at higher elevation sites, hence a periodic R of 0 (Table 9) results.

Loheide *et al.* (2005) note that fine soil textures will produce greater R, however no relation is found between the AINS STI and R data. A significant negative correlation of average DWST and R:  $r_s=-0.78$ ,  $p=0.01$  (n=9) does result.  $S_Y$  (specific yield) as

mentioned earlier is reduced by greater above-ground biomass through interception, hence the significant inverse correlation with PAI ( $r_s=-0.57$ ,  $p=0.09$ )

Assateague Site	$\Delta s$	R period	R	$S_y$	$Et_G$	Shrub Area	Herb, vine layer
29803	0.01	11PM-3AM	0.129	0.07	9.94	0.28	grass, TORA
19002	0.02	7:30-9:00PM	0.081	0.07	6.93	0.21	grass, SMRO, fern
21901	0.02	12-2:30AM	0.049	0.10	6.40	0.01	grass, SMRO
21801	0.01	12-2:00AM	0.072	0.07	5.88	0.21	grass, PHAU
20901	0.02	12-2:00AM	0.048	0.08	5.12	missing	grass (sparse)
28307	0.02	9PM-1:00AM	0.087	0.05	5.10	0.02	grass, SMRO
21903	0.03	12-4AM	0.054	0.05	4.00	1.00	N/A
28703	0.02	11PM-12:00AM	0.036	0.05	2.75	0.13	grass, SMRO (sparse)
29202	0.02	11PM-2:00AM	0	0.10	2.03	0	grass (sparse), SMRO
29205	0.03	7AM-9AM	0	0.07	1.75	0	grass
27703	0.03		0	0.05	1.27	0.002	grass
<b>Average</b>	0.02		0.051	0.07	4.65		
<b>Standard Dev.</b>	0.01		0.041	0.02	2.63		
<b>CV</b>	0.27		0.811	0.27	0.56		
Parramore Site	$\Delta s$	R period	R	$S_y$	$Et_G$	Shrub Area	Herb, vine layer
91	0.01	N/A	0	0.56	6.78	mature MAVI, MYCE	SMRO
6580	0.01	N/A	0	0.32	4.05	BAHA, PITA regen.	grass
12	0.02	N/A	0	0.11	2.05	MYCE (sparse)	grass, SMRO regen
6540	0.01	variable	0.001	0.10	1.42	BAHA, PITA regen.	grass
<b>Average</b>	0.01		N/A	0.27	3.58		
<b>Standard Dev.</b>	0.00		N/A	0.22	2.41		
<b>CV</b>	0.23		N/A	0.80	0.67		

**Table 9.** The White groundwater evapotranspiration equation values for July 20, 2005.  $\Delta s$  is the daily change in water storage of the site soil (m in depth); R period is time span of freshwater influx to water table after active transpiration ends; R is recovery rate (m recovery period<sup>-1</sup>);  $S_y$  is specific yield of site soil (dimensionless);  $Et_G$  is daily evapotranspiration of groundwater (mm day<sup>-1</sup>); Shrub area is a relative value of shrub species' canopy area in plots. For Parramore plots, shrub canopy was not measured, and listed are shrub and tree species presence in the understory; Herb and vine layer are characterized by species presence only; grasses were not identified, BAHA is *Bacchus halmifolia*, MAVI is *Magnolia virginiana*, MYCE is *Myrica cerifera*, PHAU is *Phragmites australis*, PITA is *Pinus taeda*, SMRO is *Smilax rotundifolia*, TORA is *Toxicodendron radicans*. Sites are listed in descending order of total daily evapotranspiration.

Plot 29803 (Table 9) has a significantly higher  $Et_G$  than the next highest reading. Its water table is significantly more stationary than the others (Fig. 9a) which may indicate a reliable recharge source at a higher head as mentioned above. Its fairly high total SCA is also a factor.

Evapotranspiration, Biophysical, and  
Environmental Variables

	<b>S<sub>Y</sub></b>	<b>Et<sub>G</sub></b>	<b>R</b>	
<b>PAI</b>	-0.57	-0.27	-0.06	<b>r<sub>s</sub></b>
	0.085	0.446	0.879	<b>p-value</b>
<b>SCA</b>	-0.32	0.67	0.72	<b>r<sub>s</sub></b>
	0.369	0.035	0.018	<b>p-value</b>
<b>BEE</b>	0.31	-0.55	-0.71	<b>r<sub>s</sub></b>
	0.381	0.098	0.020	<b>p-value</b>
<b>DWST*</b>	0.37	-0.57	-0.78	<b>r<sub>s</sub></b>
	0.321	0.112	0.013	<b>p-value</b>

**Table 10.** The Spearman correlation results of White groundwater evapotranspiration constituents and a selection of site environmental and biophysical variables. S<sub>Y</sub> is specific yield of site soil; ET<sub>G</sub> is daily evapotranspiration of groundwater; R is recovery rate of ground water table; PAI is plant area index; SCA is a relative value of shrub species' canopy area in plots; BEE is average plot bare earth elevation; and DWST is the water availability index DWT•STI (depth to water table X soil texture index). n=10. \* n=9.

### 3.4.7. Developmental forces

Dendrochronological samples of both bio-types decline at similar rates in their respective clusters (Fig. 8), but bio-type 2 declines about 27% faster than bio-type 1 (see Chapter 2). An ANOVA of all of the slopes of radial growth decline results in significant difference ( $p=0.006$ ) between the groups at  $r^2=0.63$ . Obviously, developmental pressures – competition for water, for instance – are greater in the years depicted (20 years post-breast height for each sample) for bio-type 2.

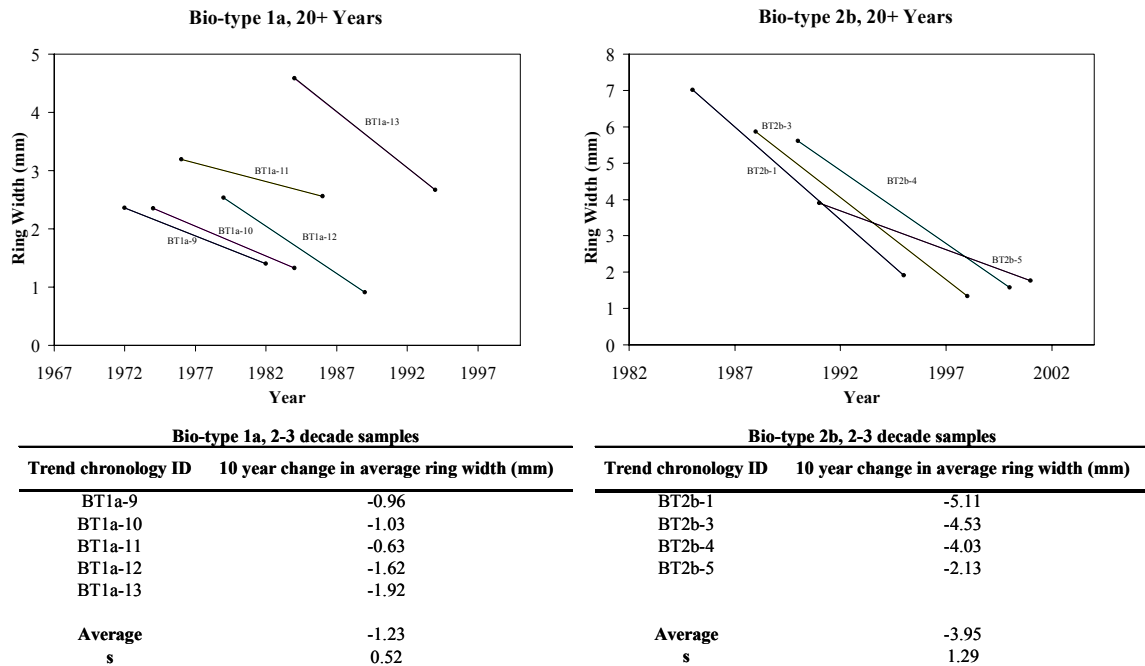


**Figure 8.** Results of a dendrochronological analysis of radial growth rates performed on two bio-type subgroups at AINS of similar age and comparable canopy crown class positions. Average raw percentage declines are 42% for bio-type 1a and 69% for bio-type 2b.

### 3.4.8. Tidal forcing

Figures 9a-9b depict the 12-hour water table and tidal levels for AINS, and 24-hour levels for PIVCR, respectively, used in the simple correlation and prewhitened, lagged crosscorrelation. These were the most successful configurations after testing hourly, 6, 12 and 24-hour iterations at both islands. Results of the exploratory simple, hourly correlations are charted in Figure 10. PIVCR time series correlate at a greater magnitude than AINS series. Both sets are inversely (less plot 29803 of AINS) correlated, yet the discrepancy in magnitude between sets necessitates more refinement of the possible difference in lag from sea to water table.

In the assessment of SPECTRA procedure results (Figures 11a-11b), it is apparent that the two tide data series (hourly data here) are limiting the shapes of the cross spectral density courses. The AINS OC inlet tidal level is subject to several non-linear inputs,

hence the lack of dramatic peaks and the presence of slowly decaying spectral density on either side of the visible peaks. The 13 and 27-hour signals are common, as is the steady climb of relative cross-spectral density to the strong peak at hour 86.4 (approx. 3.5 days). Figure 12 charts the OC Inlet tide over the study period, and an approximate 3-day rise and fall pattern can be detected. Note the presence of *diurnal inequality* during this time of alternating amplitude or “mixed” tides (NOAA CO-OPS Tides and Currents website). Plot 29803 has the only positive simple correlation (insignificant) (Fig. 10), and an especially muted spectral density plot (Fig. 11a) in the SPECTRA analysis.

The predicted, unverified Wachapreague, VA tide at PIVCR is artificially regularly-variant, producing strong 13 and 27-hour spectral cycles at the three northern sites. The highly variable pattern (Fig. 9b) of the water table at PIVCR 91 (an isolated upland island surrounded by marsh) leads to a focusing of the spectral densities around 13 and 27 (Fig. 11b).

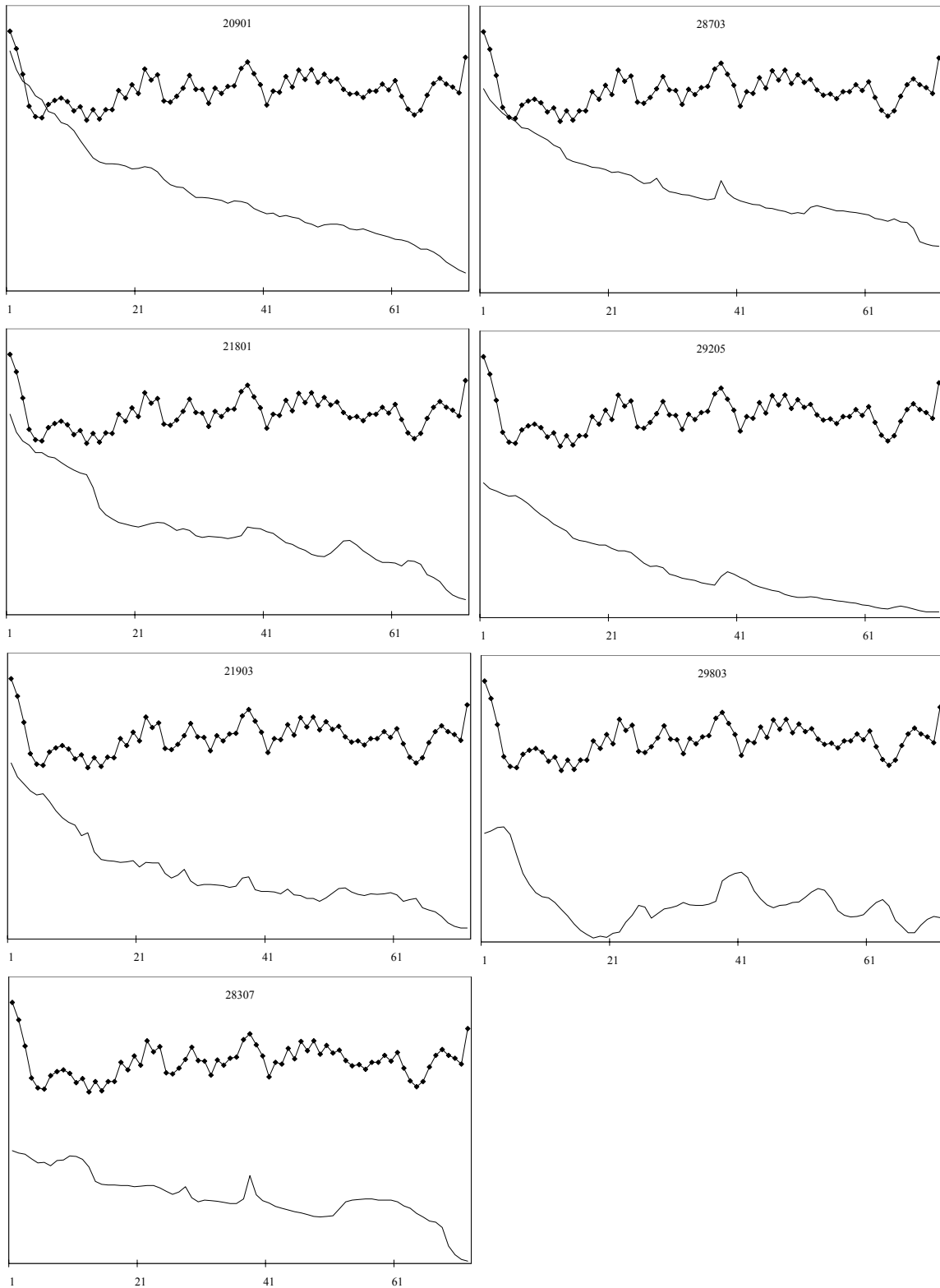


**Figure 9a.** 12-hour average tide (♦) and fresh water table levels (—) at AINS plots in the winter dry period of February 12, 2006 to March 19, 2006. Time (x-axis) is in 12-hour increments.

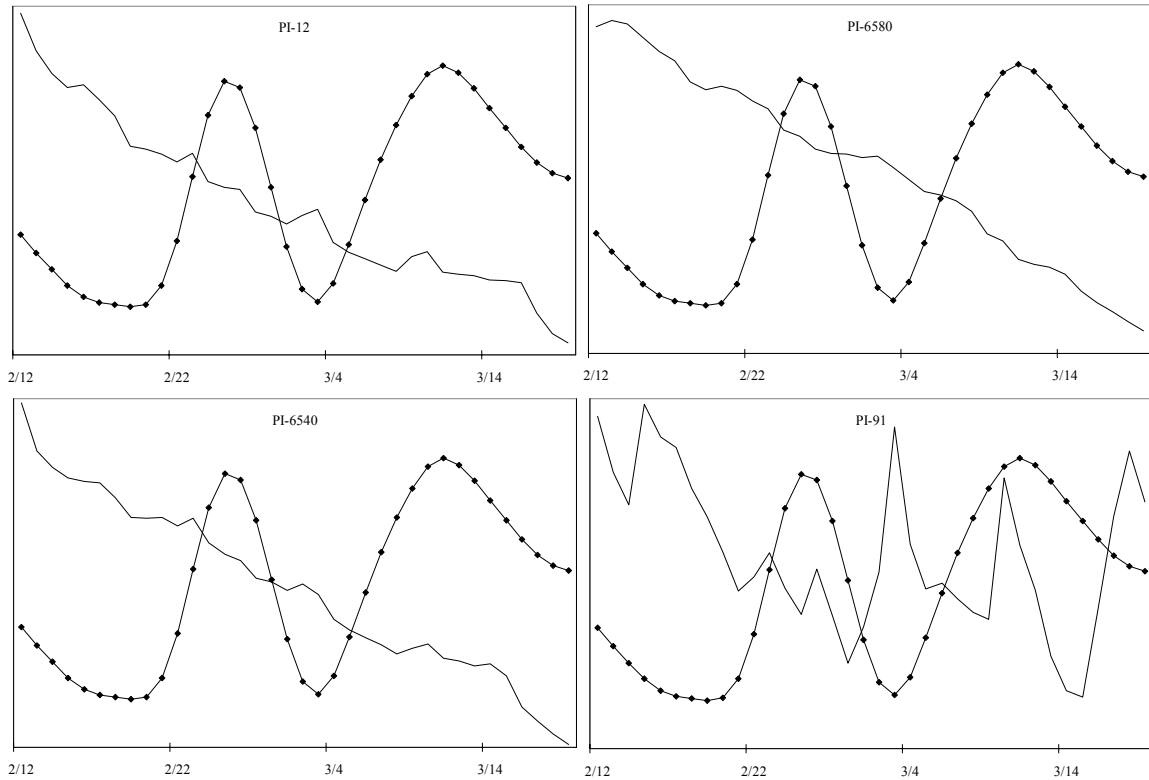


**Figure 9b.** 24-hour average tide (◆) and fresh water table levels (—) at PIVCR plots in the dry winter period of February 12, 2006 to March 19, 2006. Time (x-axis) is in 24-hour increments.

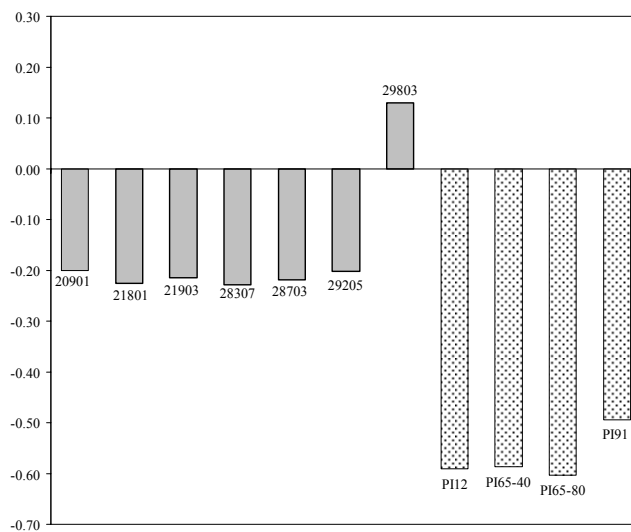


**Figure 10.** The Spearman correlation ranks ( $r_s$ ) of the tide and water tables for AINS (■) and PIVCR (▨) in the winter dry period of February 12, 2006 to March 19, 2006.

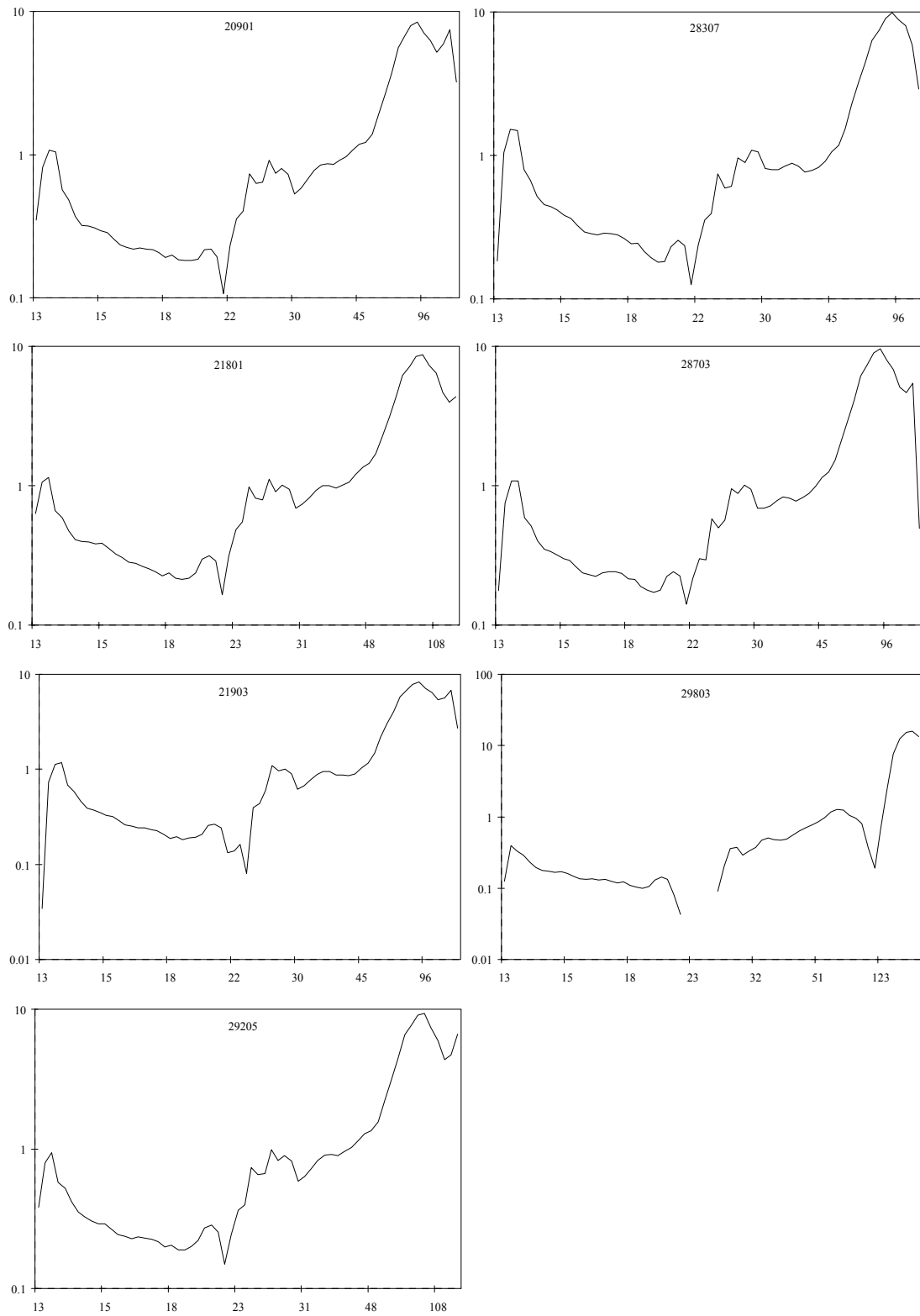


**Figure 11a.** The SPECTRA procedure results for AINS plots in the dry winter period. The y-axis is log-adjusted and denotes the estimates of the smoothed cross-spectral density of tide and fresh water table levels at hourly time steps. Time (x-axis) is in 1-hour increments.

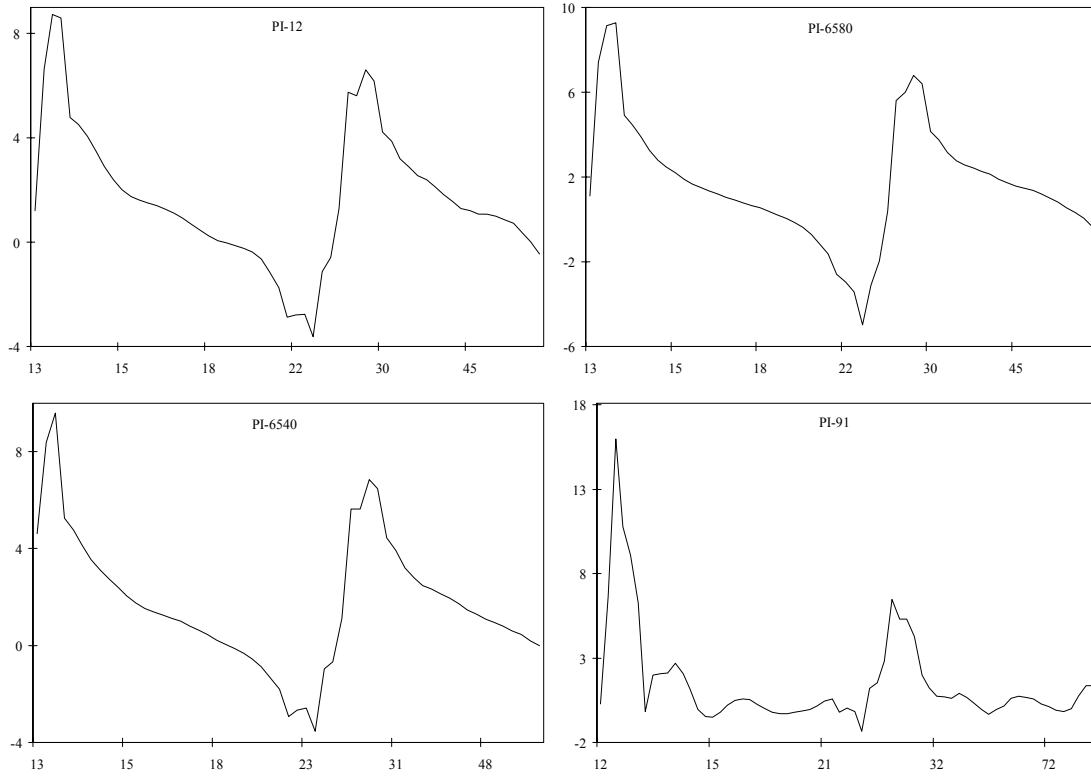


**Figure 11b.** The SPECTRA procedure results for PIVCR plots in the dry winter period. The y-axis is log-adjusted and denotes the estimates of the smoothed cross-spectral density of tide and fresh water table levels at hourly time steps. Time (x-axis) is in 1-hour increments.

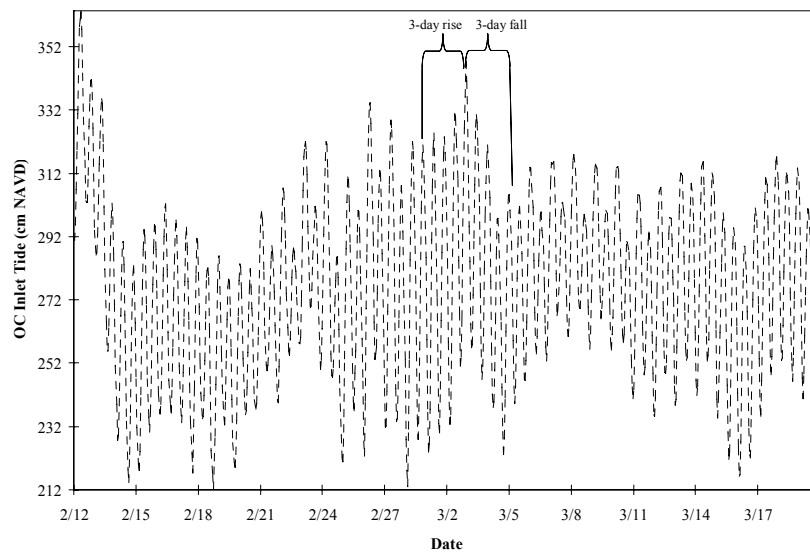


**Figure 12.** Hourly OC Inlet tide for the winter dry period. The approximate 3-day half-cycle repeating pattern is illustrated.

ARIMA processing allows for making informed estimates of the lag from saltwater tide to freshwater table fluctuation. These are the most interesting of the tidal forcing results in that they are unique to each site, and can provide the best prospect to derive meaningful sea level action on uplands from a limited data set. Figure 13 is the chart of the most significant lag cross-correlations at AINS. There is likely error introduced by applying a differencing of 12 hours to the tide in the stationarity adjustment of ARIMA, as the real tidal regime is about 12.42 hours. The time separation will unavoidably grow. SAS software (SAS Institute 2002-2003) allows only whole numbers for the differencing correction.

It is logical to choose as explanatory the lag of the greatest direct (positive) correlation (i.e., shift tide series ahead  $n$  lags for direct effect on water table). However, geomorphic and tidal interaction conditions may combine to require a negative lag (of OC inlet tide) because of the difference in ocean-side and bayside level times. Downshore bay levels normally lag behind ocean levels up to several hours – and more if winds are from the south or west. The ARIMA results from each site (Fig. 13) are interpreted individually in Figures 14a-f with maps and site knowledge as support. “Dual propagation” in Figures 14a-f text refers to the influence of ‘asynchronous’ tidal propagation from opposite sides of the island (Rotzoll *et al.* 2008).

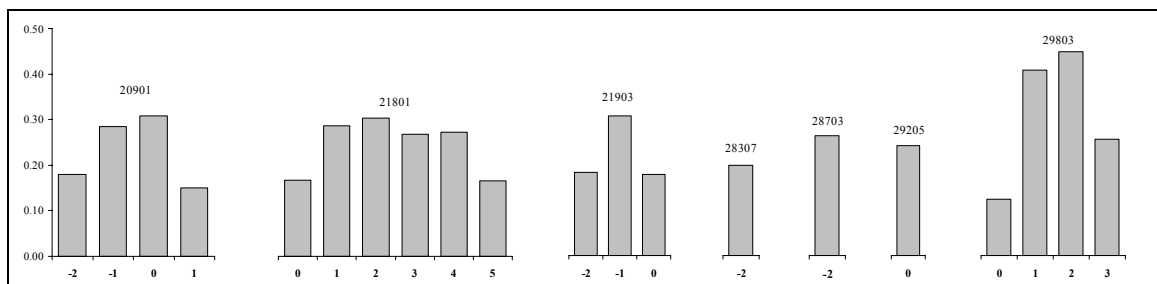


**Figure 13.** The best cross-correlation values (y-axis) between “prewhitened” tide and fresh water table levels at various lags (x-axis, 12-hour units) for 7 AINS plots.

**Figures 14a - 14f; all plots denoted by  $\blacklozenge$  and plot number.**

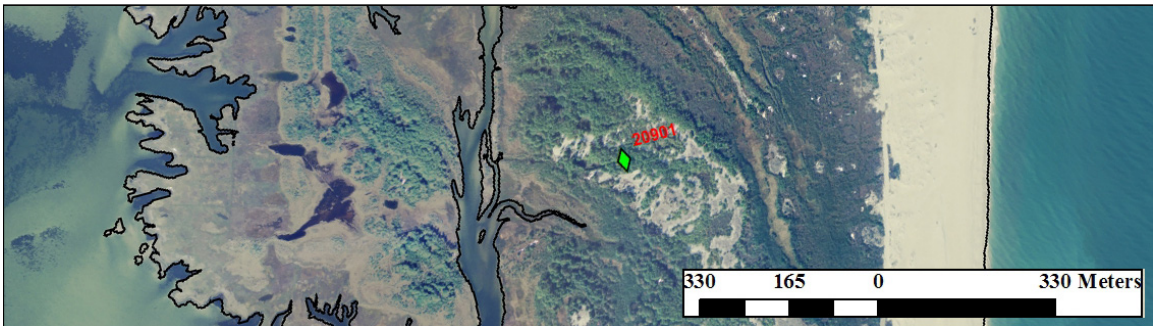


**Figure 14a.** Map excerpt of AINS plot 20901. 0 (12hr) lag.  $r=0.31$ ; grades out to -2 and 1 lags. There may be a sub-12 hour response to bay tide with the proximity to a bay gut, a shallow soil, and perhaps less winter transpiration than occurs at other sites because of several hardwood dominants in dormancy.

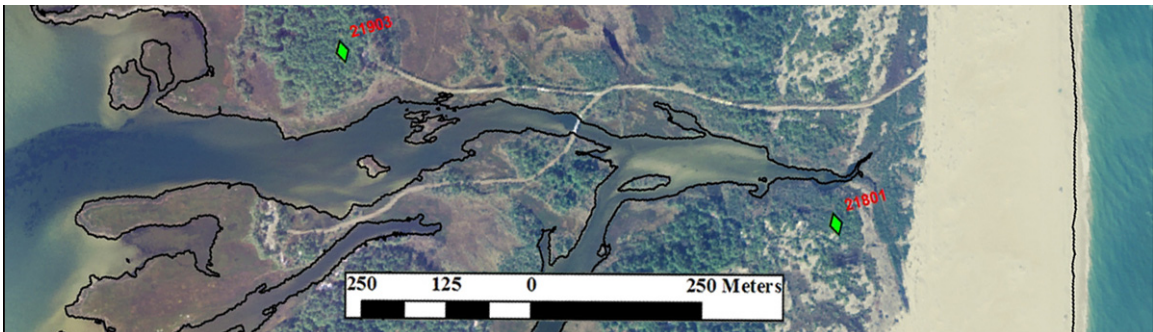


**Figure 14b.** Map excerpt of AINS plot 21903 (left). -1 (12hr) lag. A negative lag may imply a greater influence by ocean side tide signal that propagates prior (up to 3-4 hours) to the inlet tide reaching the island bay side. The transverse gut here may be forced by ocean propagation as this is a geomorphic weak point. Alternately, there could be dual propagation causing feedback. Plot 21801 (right): 2 12hr lag. Dual propagation negating a dominant signal appears likely here, and this is supported by the wide lag window in figure 13. Alternately, it may be a 12-24 hour bayside propagation, though this seems unlikely.

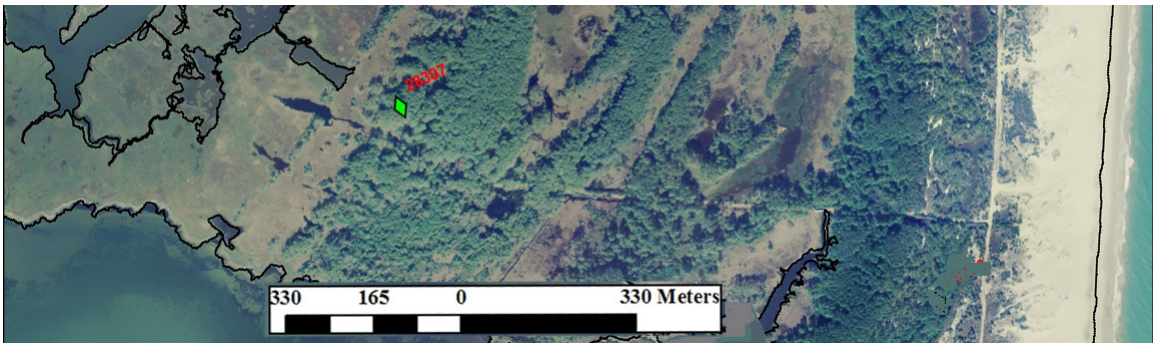


**Figure 14c.** Map excerpt of AINS plot 28307. -2 (12hr) lag. A longer negative lag; at these low correlation levels this could indicate spurious effects ( $r=0.20$ ). The 'Green Run' area here is geomorphically distinct from the main ocean side spit formation. It is plausible that a main ocean signal would take up to 24 hours to propagate through the areally extensive marsh peat. The diurnal inequality of the tide at this time of year can be producing a consistent 24 hour 'average' level upon attenuation.

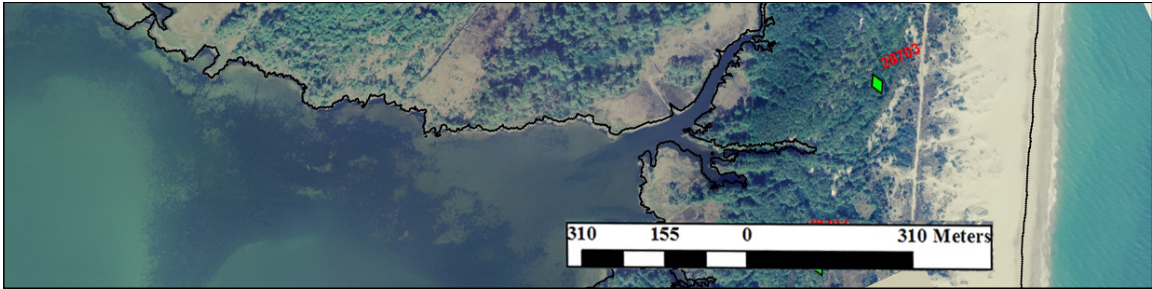


**Figure 14d.** Map excerpt of AINS plot 28703. -2 (12hr) lag. As in 28307, it appears that the diurnal inequality and geomorphic attenuation may lead to a 24 hour stabilization.

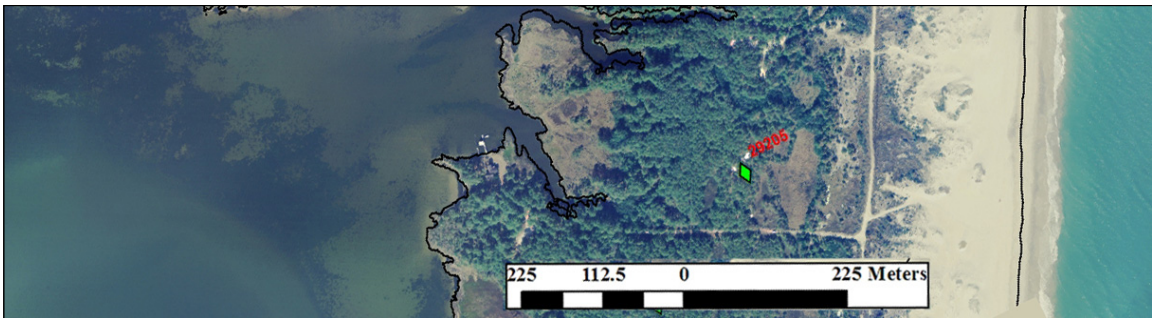


**Figure 14e.** Map excerpt of AINS plot 29205. 0 (12hr) lag. With its central position, and its proximity to open drainage to marsh, the decline is flat in this sparsely wooded plot. The small range may lead to insignificant correlation results, or the freshwater lens is forced by the ocean at a sub-12hr phase.

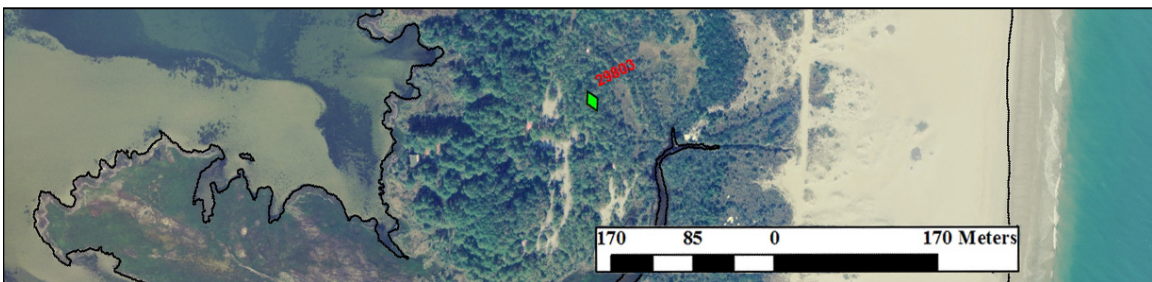


**Figure 14f.** Map excerpt of AINS plot 29803. 2 (12hr) lag. Within 24 hours of the tide level reading at the OC inlet, the plot water table corresponds at an  $r$  of 0.45 – the highest of all plots tested. There are some washover fan formations relatively close to the eastern side, and to the north of the gut termination. This may indicate a preferential pulse flow path from the ocean side, or the configuration of the terminating gut forces a defined amplitude pulse.

### 3.5. Discussion

#### **3.5.1. Plant area index**

Roberts (2000) notes that reduction in leaf growth – not stomatal closure – in species of indeterminate-growth (like *P. taeda*) is the “first indication of development of water stress.” As seen in other studies, *P. taeda* leaf area change through the annual course is substantial (Fig. 4; Table 5). Hennessey *et al.* (1992) find that *P. taeda* needle fall is greatly reduced following a dry year – because production is reduced in the dry year – and that current-year climate (precipitation and temperature) shifts timing of peak monthly needle falls with drought reducing leaf duration.

That PAI may increase with litterfall in the lower biomass bio-type 2 (Table 6), while possibly decreasing in bio-type 1 could indicate the leaf area change and climate relationship varies among developmental classes and differing moisture regimes (see dendrochronology-climate analyses, Chapter 2). Also, the opposite (though not significant) directional correlation found for PAI and DWT between the bio-types (Table 8: bio-type 1:  $r_s=0.46$ ,  $p=0.179$ ; bio-type 2:  $r_s=-0.37$ ,  $p=0.239$ ) may indicate alternate water strategies in different sites by *P. taeda*. In fact, growth trajectories differ markedly (Fig. 8) between the bio-types due, apparently, to site elevation and depth to water source. *P. taeda* adapts its root energetics to the water source timing and configuration (Retzlaff *et al.* 2001; Torreano and Morris 1998) that are products of soil texture and depth.

### 3.5.2. Developmental forces

Early radial growth rate is significantly different between the major biophysical types of AINS as seen in the direct comparison example of Figure 8. It is likely that the trajectories within type (bio-type 2 trends, CV=33%, are more homogeneous than those of bio-type 1, CV=42%) result from shared patterns of root growth as constrained by site, and flora competition. Torreano and Morris (1998) found intra-season change in *P. taeda* seedling root growth to be a result of changes in soil water and transpirational demand, and found that seedlings exhibited significant reductions in root development and proportional decreases in above-ground biomass with short-term reductions in water potentials. Flatter rates of decline seen in bio-type 1 compared to bio-type 2 indicate a more stable development (Johnson and Young 1992) as would result from root-tapping of average tables at a plentiful source (see Chapter 2).

Hacke *et al.* (2000) find that *P. taeda* root area to leaf area ratios are significantly different from loam to sand sites, with the ratio increasing with increasing soil porosity (lower overall matric potential). Torreano and Morris (1998) determine that this ratio remains fairly constant among differentially water-treated seedlings. This inherent characteristic can be very important in continued studies on the barrier islands such as remote sensing monitoring (see Chapter 4), and related modeling of structural relationships to moisture indices.

Generally, bio-type 1 sites are greater than bio-type 2 sites in all the standard biophysical metrics except SCA (Table 11). Note they are also at greater average elevation: 1.01m (s=0.54, n=15) to 0.78m (s=0.24, n=9) for bio-type 2. In sand soils at time of colonization, individuals that can access the water table capillary fringe (Zahner

1968) are at a clear advantage. Successful bio-type 1 individuals gained access to groundwater quickly. Bio-type 2 individuals were stocked more densely and, at generally lower elevation, had easier water table access. The better adapted individuals here preferentially accessed precipitation water in the unsaturated zone.

Water lenses of lower elevation sites are necessarily thinner and more ephemeral as trees will draw down tables quickly. There can thus also be a disadvantage to having permanent roots much deeper in bio-type 2 stands where they may be in a more saline zone.

	Bio-type 1 (n=15)		Bio-type 2 (n=9)		Ouliers (n=2)	
	Mean	St. dev.	Mean	St. dev.	Mean	St. dev.
PAI	2.54	0.63	1.77	0.48	3.95	1.05
MCH	18.70	5.06	10.79	1.57	17.06	1.15
BA	35.72	3.72	24.86	4.94	25.36	6.39
Vol	270.01	94.39	97.29	26.85	167.28	45.93
SCA	67.81	98.65	128.88	89.65	841.82	7.86

**Table 11.** Summary statistics of biophysical properties of the AINS bio-types. PAI is Plant Area Index ( $\text{m}^2\text{m}^{-2}$ ); MCH is maximum canopy height (m); BA is Basal Area ( $\text{m}^2 \text{ha}^{-1}$ ); Vol is parabolic volume in  $\text{m}^3 \text{ha}^{-1}$ ; SCA is shrub canopy dripline area in  $\text{m}^2$ .

### 3.5.3. New water availability index

The need for a more appropriate water availability estimate evolved from the initial low PAI-DWT correlation of 0.46 (Table 7). Having collected STI among other environmental site variables to account for confounding and interacting factors in the original depth-driven model, it is shown to be a better overall direct predictor of biophysical characteristics (Table 7).

It is commonly acknowledged that “water availability” is a result of a dynamic interaction between rooting pattern and the concurrent soil matrix (Cassel and Nielsen 1986). STI, as a proxy of standard soil particle size distribution and associated matric

potential is important to water retention and movement (Brady and Weil 2008) at any one depth in the soil column. It can be used in tandem with DWT over time to characterize water availability to the *P. taeda* forests at AINS. When average modeled DWT is multiplied by mean site STI – forming the DWST variable – there is an improvement over either variable separately in correlations with average 2005 PAI ( $r_s=0.49$ ,  $p=0.02$ ). This correlation improves further when the PIT (single daily depth to water table) depth measures are used ( $r_s=0.54$ ,  $p=0.004$ ). The PIT measures, though made in late 2006, may better reflect variation across all sites.

Improved correlations with PAI may indicate that DWST acts on a more meaningful time scale here than does DWT – a result consistent with our intent of deriving a more dynamic estimate of water availability (hourly at the water table if needed). Figure 15 is a conceptual model of the soil water system dependent on DWT and its intersection in the soil profile along an STI gradient (recall figures 7a-7c of individual plot STI profiles). The implications of the model are discussed within a sea level rise scenario below. Texture sample replicates should be assessed for average nutrient (N, P, K) concentrations in future work to control for these effects on biophysical variables.

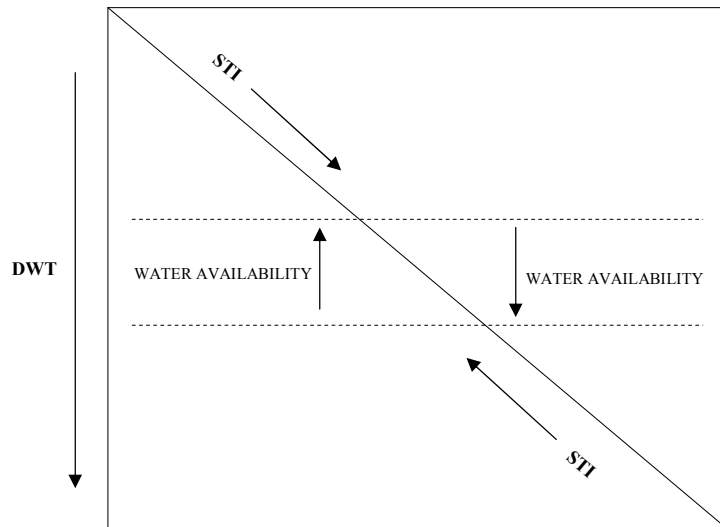


**Figure 15.** Diagram of current water availability scale in an idealized Assateague Island soil column. Arrows indicate direction of increase, and the upper and lower bounds of an average water table over time are represented by the dashed (---) horizontal lines. In the top right half, STI increases downward through the profile, and water table rise will result in lower water availability. In the bottom left half, STI increases upward through the profile so that water table rise will lead to greater water availability.

#### 3.5.4. Shrub analysis

Figure 6 represents shrub structure for individual plots. It is noteworthy that SCA correlates strongly negatively with DWT ( $r_s = -0.80$ ,  $p = 0.01$ ) as it is a further indication of developmental and successional control, and structural determination (as well as PAI variation as seen above) by DWT. SCA is also an important variable for continued monitoring that will yield greater insight into the relationship of structural heterogeneity and  $ET_G$ .

*M. cerifera* appears to transpire at higher rates than *P. taeda*. It is possible that *M. cerifera* is making some shallow sites amenable to *P. taeda* by drying otherwise flooded sands. This would work in tandem at longer times scales with elevation addition by island migration (rollover), making succession to forest more likely at accreting spots (Johnson

and Young 1992). It has been shown that a site's maxage correlates rather strongly positively with DWT ( $r_s=0.63$ ,  $p=0.05$ ; Table 7). Through glasshouse experiments, Tolliver *et al.* (1997) also show that *P. taeda* is probably more sensitive than *M. cerifera* to flooding duration and frequency.

### 3.5.5. Evapotranspiration

It was hypothesized that transpired groundwater ( $ET_G$ ) would vary with structural differences at AINS, and that a relationship would emerge between PAI and  $ET_G$  because of the reactivity of *P. taeda* foliage, and the generally lowered stress-buffering ability of coarse, quickly-drained soil. Specifically, it was anticipated that  $ET_G$  was predicted by PAI to an extent that would help explain water table and foliage relationships, and hence, provide a physiological mechanism in adjustments of structure to altered water availability (and possibly increased inundation). Modeling of *P. taeda* transpiration with the adapted Shao *et al.* (1995) model (not shown) predicts a small but measurable increase in transpiration with a 50% increase in LAI value. Some have found no relationship or a non-linear one at best between canopy leaf area and  $ET_G$  (Roberts 2000). Our final result is of no relationship between PAI and  $ET_G$  (Table 10).

As for coarse structure, Calder (1998) found basal area to correlate significantly with transpiration, while BA at AINS is unrelated ( $r_s=-0.06$ ) to  $ET_G$ . SCA on the other hand, is a consistent positive factor in  $ET_G$  ( $r_s=0.67$ ,  $p=0.03$  overall; see Tables 9, 10). This result is consistent with Philips and Oren (2001) in that a "main cause of conserved forest  $E_c$  [canopy ET per unit ground area] is subcanopy compensations for water losses occurring from forest canopies of varying [leaf area]." It is apparent in smaller stature

stands, that *M. cerifera* or other shrubs when present, act to increase ET totals to a relatively low total variation (CV at AINS of 37% among plots with shrubs) over the study area (table 9). The CV of  $ET_G$  in PIVCR plots is 67%, due to the regenerating condition of most of these sites and increased exposure of subcanopies to light and atmospheric demands due to dominant canopy decline.

In site-level evaluation terms, AINS plot 29803 is biophysically unremarkable being near the bottom of canopy volume, and with a slightly above-average shrub areal coverage of 28%, yet its  $ET_G$  rate is well above the next greatest (Table 9). All of the shrubs here are *M. cerifera*, while the plot with the highest shrub area, 21903, has a mid-range  $ET_G$ . The vast majority of the subcanopy here is *Vaccinium corymbosum* L (highbush blueberry) a broad-leaf deciduous shrub with transpiration quite sensitive to water stress (Mingeau *et al.* 2001). *M. cerifera* has a maximum simulated rate of about 8 mm day<sup>-1</sup> at the barrier islands (Shao *et al.* 1995), but it is also fairly sensitive to drought. The overstory at plot 21903 is more developed and may partly explain the discrepancy with the sparsely canopied plot 29803 (compensation effects noted earlier). It also seems likely that *M. cerifera* is more salt-tolerant than *V. corymbosum*, thus possibly contributing to the site-level  $ET_G$  difference.

Site effects to  $ET_G$  rates are evident in the recovery rate (R) (Table 9) which lends a large portion of variation to the White equation (equation 1) results (Table 10). Perhaps proximity to marshes, in combination with shrub presence leads to the higher calculated groundwater use because of nighttime inflow (Loheide *et al.* 2005) if marshes are under greater hydraulic head. Figures 14e-f illustrate that, though similarly near marsh, 29205 does not recover like 29803 perhaps due to its deeper soil. It is instructive that BEE and

$ET_G$  correlate somewhat strongly negatively ( $r_s=-0.55$ ,  $p=0.1$ ) (Table 10). This is, as was shown earlier, probably related to shrub compensation with their increased presence at lower elevation sites. It also reflects the fact that deeper sands commonly do not have notable recovery influx because of a lack of recharge from sources of higher hydraulic head in the vicinity.

Site moisture limitations as may be imposed on transpiration by more coarse soil, can not be determined from one day's measure of  $ET_G$ . Hacke et al (2000) examined loam versus sand soils, and extending their finding to gradations in sand, one would expect the coarser soils to limit overall water uptake as hydraulic conductivity declines faster than in finer sands (Brady and Weil 2008). In fact there is no relationship ( $r_s=-0.12$ ,  $p=0.7$ ) between  $ET_G$  and soil texture index (STI) at AINS. There results a significant negative relationship ( $r_s=-0.57$ ,  $p=0.1$ ) between  $ET_G$  and the average water availability in DWST, but this is probably a result of the overriding effect of decreasing R with greater elevation (Table 9) as discussed above. An exploratory correlation (not shown) using the *daily* July 20, 2005 DWST (by finding the STI at the average daily DWT through regression of the profile information, figures 7a-c) was inconclusive. Roberts (2000) expects reductions in highly transpiring (>9mm/day) systems with water deficits, and little change in lesser transpiring types; and Ford *et al.* (2005) state “usually only under very low soil moisture availability does ET show a strong relationship with soil moisture”. Standard water availability measurements – though not foolproof (Cassel and Nielsen 1986) – may be required to better develop these relationships for AINS.

The result of an inverse correlation between  $ET_G$  and BEE supports the developmental paradigm of water use detailed earlier, that: vegetation of shallow soil

sites (generally lower DWST) compete for the more fleeting vadose precipitation sources here, and thus operate at higher ET per ground area; and the vegetation with well developed root systems at deeper sites preferentially access the stable average groundwater tables, transpiring at a more metered pace. There are also the feedbacks mentioned earlier of canopy and community structure-specific microclimate conditions maintaining the  $ET_G$  differential along the elevation gradient.

### 3.5.6. Tidal forcing

Results from tidal and water table time series analyses have affirmed a general presence of tidal forcing in the water table data. A qualitative view of sensitivity to sea level rise by site is developed by comparing final crosscorrelation strengths of prewhitened tide and water table series. There is much nuance to discussion of the results (see accompanying text to Figures 14a-f) for the AINS ARIMA lag allocations (Fig. 13). Note that PIVCR cannot be effectively managed by the ARIMA process because the tide is not verified. PIVCR simple correlation results were stronger than AINS, perhaps indicating a greater sensitivity, but they could be inflated because autocorrelation is still present in each time series (Ford *et al.* 2005).

The SPECTRA results offer a general confirmation, in all sites at AINS and PIVCR, of pulse cycles that are tide-related. The peaks of cross-spectral density are at about 13 and 27 hours (Figures 11a-b), approximating the diurnal tide cycle (12.42 hour period). AINS plots also share the large spectral density peak at about 3.5 days or 86 hrs that appears to be a result of the alternating phase of rise and fall of the OC inlet tide depicted in Figure 12.

The longer diffusion of cross-spectral density at AINS compared to PIVCR is likely a result of the already attenuated nature of the OC inlet signal through the bay. PIVCR water tables are more conducive to change detection because tides are more synchronized from one side of the island to another as a result of the ‘mixed energy’ nature of the barrier system here with a greater overall tidal range. It seems that the Sinepuxent Bay water levels at AINS are a non-linear combination of effects of: distance from inlet; drainage processes from riverine inputs; drainage from the single outlet to open water at Chincoteague (up to 30km to the south); unpredictable effects of winds; interference of both ocean and bay tide signals at island interiors; protracted hydraulic forcing (saturation and saturated hydraulics of peat layer) and drainage of heterogeneous layers (sand, peat); varying rates of rise and fall in homogeneous sand (Nielsen 1990); and the averaging of the mixed tide (alternating amplitude) nature of the tide which introduces a drift in the average and could affect the allocation of lag initially.

Perhaps the most significant local determinant of forcing by rising and lowering of the salt-fresh interface is the non-linear hydraulic dampening by the intact peat layer traversing significant portions of sites and the island as a whole. The peat layer is treated as a constant throughout the study area. A layer was encountered at many sites during soil sampling and ecotone well installations. At its least dense, the layer will have hydraulic conductivity similar to very fine sand (Knott *et al.* 1987). Density will increase – creating an aquatard situation – with compaction by topping sand layers. It is recommended that future work on sea level forcing characterize the layer thoroughly.

## **3.6. Conclusions**

### **3.6.1. General conclusions**

It is important to monitor structure and moisture status to develop predictive relationships that provide insight into ecohydrological functioning of these rare forested habitats of Mid Atlantic barrier islands. Short-term sea levels force island water table levels and, hence, water availability. A relatively precise inferential relationship between forest biophysical structure and water availability estimates is determined. This will be useful to managers of natural *P. taeda* forests of barrier islands and other landscapes where water sources are subject to alteration.

### **3.6.2. System description and factor synthesis**

Forests of the barrier islands are structured by constraints associated with site elevation, BEE. Forest bio-type 1 (see Table 11), is at an average yearly DWT of 0.76m (n=4) and bio-type 2 at 0.39m (n=4). As a result of island migration processes ('rollover'), BEE will also determine soil texture profiles to an extent. STI is a significant source of variation in bio-typing ( $r^2=0.46$ ,  $p=0.01$ ), with values largely trending up with depth from ground surface. Dendrochronological analysis shows that tree radial growth trajectories are significantly different between bio-types, with bio-type 1 declining at a much slower rate than bio-type 2.

PAI, an easily measured fine-scale structural metric, can be used to quantify in-season foliar changes at AINS resulting from a combination of factors including soil moisture. PAI correlates significantly (up to  $r_s=0.54$ ,  $p=0.004$ ) with a hybrid of DWT and

STI: DWST, a flexible, easily measured site moisture availability estimate. This has improved upon the individual relationships of PAI with either soil metric (STI only slightly) mainly because DWT needs to be scaled by a meaningful representation of the soil's matric potential to better reflect general probability of available water.

These are site-level measures that reflect the moisture capacity of the entire vadose zone; and are related to the annual average PAI. For fine-scale growth impacts (as may be ascertained with changing foliage levels) due to changing water levels with sea level rise, the unexplained variation in the PAI and DWST relationship needs to be addressed.

The PAI-DWST function can be further developed to a fine scale time series that would allow very precise modeling of leaf area change and associated productivity with water tables. A predictive transfer function would require additional PAI measures and calibration of the DWST with soil moisture analyses. PAI monitoring with remote sensing tools like lidar can be used now (see Chapter 4) to determine fine-scale changes occurring in natural vegetation associated with rising water tables. Multi-year study appears necessary to capture the effects of previous-year moisture levels on current-year foliage (see Hennessey *et al.* 1992), and explain the variation due to indeterminate growth of *P taeda*. Continued dendrochronological analysis can relate foliage levels to stemwood production.

Change in tree canopy PAI over multiple years may signify adjustment to community succession related to DWT. Changes in the proportion of canopy tree biomass and subcanopy (shrubs, especially) biomass over time may be the first significant indicators of ecohydrological change with sea level rise. Shrubs are indicative

of site types at AINS, and their density can signify the successional status of the community. Shrub density (or SCA) determines total groundwater evapotranspiration to a greater extent than any other biophysical metric, and remains independent of these other structural metrics (except HPCD). Evapotranspired groundwater, determined with water table and other site data, is very much a property of community structure and tends to increase where *M. cerifera* is present. With this knowledge, another constraint can be applied to the feedback loop of the SPAC, and physiological adjustment can be indirectly detected with structural change. Chapter 4 details how a remote sensing system can populate simple regression models and, potentially, run productivity models with structure data to monitor and analyze these feedbacks.

### 3.6.3. Predictions of effects to bio-types

Our simple model of water availability on barrier islands illustrated in Figure 15, and the supporting relationships, together guide some fundamental predictions of effects to above-ground structure. The degree to which these are observed may be very dependent on *P. taeda*'s ability to adjust water uptake strategies on applicable time scales. In general, tree leaf area is expected to decrease on a ground area basis with rising water tables, and:

In **bio-type 1**, *P. taeda* seedling establishment could be temporarily enhanced by higher water tables, yet overall water availability in drought could decrease with rooting residency in lower STI strata. Seedling maturation may lead to lower overall site growth rates. This bio-type may also experience increased invasion from woody shrubs at some of the

more shallow sites and increased competition for water, thus reducing canopy tree growth rates.

In **bio-type 2**, if the rooting zone in lower areas of the islands are progressively submerged this could reduce water absorption (Spurr and Barnes 1980) and limit growth through reduced gas exchange (Johnson and Young 1993). It is unclear if direct salinization of rooting zone water will be an issue in the forest stands – this will depend on local lens depth to saline mixing. Johnson and Young (1994) observed reduced stomatal conductance in coastal loblolly with temporary salt inundation but found the trees recovered quickly. In general, *M. cerifera* will out-compete *P. taeda* for water in the shrinking vadose zone.

### **3.7. References**

- Anderson, W. P., D. G. Evans, and S. W. Snyder. 2000. The effects of Holocene barrier-island evolution on water-table elevations, Hatteras Island, North Carolina, USA. *Hydrogeology Journal* **8**:390-404.
- Bond, B. J., J. R. Brooks, and F. C. Meinzer. 2007. How trees influence the hydrological cycle in forest ecosystems. In: Wood, P. J., D. M. Hannah, and J. P. Sadler (eds). *Hydroecology and Ecohydrology: Past, Present and Future*. John Wiley & Sons Ltd. pp.7-35.
- Brady, N. C. and R. R. Weil. 2008. *The nature and properties of soils*. 14th edition. Prentice Hall, Upper Saddle River, N.J.
- Calder, I. R. 1998. Water use by forests, limits and controls. *Tree Physiology* **18**:625-631.
- Cassel, D. K. and D. R. Nielsen. 1986. Field capacity and available water holding capacity: In A. Klute (ed). *Methods of soil analysis, Part 1. Rev. Physical and Mineralogical Methods*. Amer. Soc. Of Agron. Monogr. 9. pp.901-929.
- Conn, C. E. and F. P. Day. 1993. Belowground Biomass Patterns on a Coastal Barrier-Island in Virginia. *Bulletin of the Torrey Botanical Club* **120**:121-127.
- Day, F. P., E. R. Crawford, and J. J. Dilustro. 2001. Aboveground plant biomass change along a coastal barrier island dune chronosequence over a six-year period. *Journal of the Torrey Botanical Society* **128**:197-207.
- Dusterhoff, S. R. 2002. Controls on near-surface soil moisture dynamics in coastal environments. Thesis (M S ). University of Virginia.

- Ehrenfeld, J. G. 1990. Dynamics and Processes of Barrier-Island Vegetation. *Reviews in Aquatic Sciences* **2**:437-480.
- Ford, C. R., C. E. Goranson, R. J. Mitchell, R. E. Will, and R. O. Teskey. 2005. Modeling canopy transpiration using time series analysis: A case study illustrating the effect of soil moisture deficit on *Pinus taeda*. *Agricultural and Forest Meteorology* **130**:163-175.
- Gholz, H. L., K. C. Ewel, and R. O. Teskey. 1990. Water and Forest Productivity. *Forest Ecology and Management* **30**:1-18.
- Grier, C. C. and S. W. Running. 1977. Leaf Area of Mature Northwestern Coniferous Forests - Relation to Site Water-Balance. *Ecology* **58**:893-899.
- Hacke, U. G., J. S. Sperry, B. E. Ewers, D. S. Ellsworth, K. V. R. Schafer, and R. Oren. 2000. Influence of soil porosity on water use in *Pinus taeda*. *Oecologia* **124**:495-505.
- Hayden, B. P., M. C. F. V. Santos, G. F. Shao, and R. C. Kochel. 1995. Geomorphological Controls on Coastal Vegetation at the Virginia-Coast-Reserve. *Geomorphology* **13**:283-300.
- Hebert, M. T. and S. B. Jack. 1998. Leaf area index and site water balance of loblolly pine (*Pinus taeda* L.) across a precipitation gradient in east Texas. *Forest Ecology and Management* **105**:273-282.
- Hennessey, T. C., P. M. Dougherty, B. M. Cregg, and R. F. Wittwer. 1992. Annual Variation in Needle Fall of a Loblolly-Pine Stand in Relation to Climate and Stand Density. *Forest Ecology and Management* **51**:329-338.

- Holst, T., S. Hauser, A. Kirchgassner, A. Matzarakis, H. Mayer, and D. Schindler. 2004. Measuring and modelling plant area index in beech stands. *International Journal of Biometeorology* **48**:192-201.
- Johnson, S. R. and D. R. Young. 1992. Variation in Tree-Ring Width in Relation to Storm Activity for Mid-Atlantic Barrier-Island Populations of *Pinus-Taeda*. *Journal of Coastal Research* **8**:99-104.
- Johnson, S. R. and D. R. Young. 1993. Factors Contributing to the Decline of *Pinus-Taeda* on a Virginia Barrier-Island. *Bulletin of the Torrey Botanical Club* **120**:431-438.
- Knott, J. F., W. K. Nuttle, and H. F. Hemond. 1987. Hydrologic Parameters of Salt-Marsh Peat. *Hydrological Processes* **1**:211-220.
- Krantz, D. E., C. A. Schupp, C. C. Spaur, J. E. Thomas, and D. V. Wells. *In review*. Dynamic Systems at the Land-Sea Interface. In: Dennison, W. C. *et al.* (eds). *Shifting Sands: Environmental and cultural change in Maryland's Coastal Bays*. pp.194-230.
- Lee, R. 1980. *Forest hydrology*. Columbia University Press, New York.
- Loheide, S. P. 2008. A method for estimating subdaily evapotranspiration of shallow groundwater using diurnal water table fluctuations. *Ecohydrology* **1**:59-66.
- Loheide, S. P., J. J. Butler, and S. M. Gorelick. 2005. Estimation of groundwater consumption by phreatophytes using diurnal water table fluctuations: A saturated-unsaturated flow assessment. *Water Resources Research* **41**:-

- Martin, T. 2000. Winter Season Tree Sap Flow and Stand Transpiration in an Intensively-Managed Loblolly and Slash Pine Plantation. *Journal of Sustainable Forestry* **10**:155-163.
- Mingeau, M., C. Perrier, and T. Ameglio. 2001. Evidence of drought-sensitive periods from flowering to maturity on highbush blueberry. *Scientia Horticulturae* **89**:23-40.
- Monsi, M., Z. Uchijima, and T. Oikawa. 1973. Structure of Foliage Canopies and Photosynthesis. *Annual Review of Ecology and Systematics* **4**:301-327.
- National Oceanic and Atmospheric Administration (NOAA), Center for Operational Oceanographic Products and Services (CO-OPS), Tides and Currents. 2009. <http://tidesandcurrents.noaa.gov/>.
- Nielsen, P. 1990. Tidal Dynamics of the Water-Table in Beaches. *Water Resources Research* **26**:2127-2134.
- Pack, D. J. 1977. Revealing Time Series Interrelationships. *Decision Sciences* **8**:377-402.
- Phillips, N. and R. Oren. 2001. Intra- and inter-annual variation in transpiration of a pine forest. *Ecological Applications* **11**:385-396.
- Reed, R. E., D. A. Dickey, J. M. Burkholder, C. A. Kinder, and C. Brownie. 2008. Water level variations in the Neuse and Pamlico Estuaries, North Carolina due to local and remote forcing. *Estuarine Coastal and Shelf Science* **76**:431-446.
- Retzlaff, W. A., G. K. Blaisdell, and M. A. Topa. 2001. Seasonal changes in water source of four families of loblolly pine (*Pinus taeda* L.). *Trees-Structure and Function* **15**:154-162.

- Roberts, J. 1983. Forest Transpiration - a Conservative Hydrological Process. *Journal of Hydrology* **66**:133-141.
- Roberts, J. 2000. The influence of physical and physiological characteristics of vegetation on their hydrological response. *Hydrological Processes* **14**:2885-2901.
- Roman, C. T., R. A. Zampella, and A. Z. Jaworski. 1985. Wetland Boundaries in the New-Jersey Pinelands - Ecological Relationships and Delineation. *Water Resources Bulletin* **21**:1005-1012.
- Rotzoll, K., A. I. El-Kadi, and S. B. Gingerich. 2008. Analysis of an unconfined aquifer subject to asynchronous dual-tide propagation. *Ground Water* **46**:239-250.
- Ruppel, C., G. Schultz, and S. Kruse. 2000. Anomalous fresh water lens morphology on a strip barrier island. *Ground Water* **38**:872-881.
- Sampson, D. A., T. J. Albaugh, K. H. Johnsen, H. L. Allen, and S. J. Zarnoch. 2003. Monthly leaf area index estimates from point-in-time measurements and needle phenology for *Pinus taeda*. *Canadian Journal of Forest Research-Revue Canadienne De Recherche Forestiere* **33**:2477-2490.
- SAS Institute Inc. 2002-2003. *Statistical Analytical Software Version 9.1 for Windows*. Cary, NC.
- Scurlock, J. M. O., G. P. Asner, and S. T. Gower. 2001. Worldwide historical estimates of leaf area index, 1932–2000. Oak Ridge National Laboratory Technical Report ORNL/TM-2001/268.
- Seely, B., K. Lajtha, and G. D. Salvucci. 1998. Transformation and retention of nitrogen in a coastal forest ecosystem. *Biogeochemistry* **42**:325-343.

- Shao, G. F., H. H. Shugart, and D. R. Young. 1995. Simulation of Transpiration Sensitivity to Environmental-Changes for Shrub (*Myrica-Cerifera*) Thickets on a Virginia Barrier-Island. *Ecological Modelling* **78**:235-248.
- Shugart, H. H. 2000. Importance of structure in the longer-term dynamics of landscapes. *Journal of Geophysical Research-Atmospheres* **105**:20065-20075.
- Spurr, S. H. and B. V. Barnes. 1980. *Forest ecology*. 3d edition. Wiley, New York.
- Tolliver, K. S., D. M. Colley, and D. R. Young. 1995. Inhibitory Effects of *Myrica-Cerifera* on *Pinus-Taeda*. *American Midland Naturalist* **133**:256-263.
- Tolliver, K. S., D. W. Martin, and D. R. Young. 1997. Freshwater and saltwater flooding response for woody species common to barrier island swales. *Wetlands* **17**:10-18.
- Torreano, S. J. and L. A. Morris. 1998. Loblolly pine root growth and distribution under water stress. *Soil Science Society of America Journal* **62**:818-827.
- Urish, D. W. 1980. Asymmetric Variation of Ghyben-Herzberg Lens. *Journal of the Hydraulics Division-Asce* **106**:1149-1158.
- Vose, J. M. and H. L. Allen. 1988. Leaf-Area, Stemwood Growth, and Nutrition Relationships in Loblolly-Pine. *Forest Science* **34**:547-563.
- Vose, J. M. and H. L. Allen. 1991. Quantity and Timing of Needlefall in N and P Fertilized Loblolly-Pine Stands. *Forest Ecology and Management* **41**:205-219.
- Vose, J. M., P. M. Dougherty, J. N. Long, F. W. Smith, H. L. Gholz, and P. J. Curran. 1994. Factors influencing the amount and distribution of leaf area of pine stands. *Ecological Bulletins* **43**:102-114.

- Waring, R. H. and J. Major. 1964. Some Vegetation of the California Coastal Redwood Region in Relation to Gradients of Moisture, Nutrients, Light, and Temperature. *Ecological Monographs* **34**:167-215.
- White, W. N. 1932. A method of estimating ground-water supplies based on discharge by plants and evaporation from soil, Washington, DC.
- Whittaker, R. H., F. H. Bormann, G. E. Likens, and T. G. Siccama. 1974. Hubbard Brook Ecosystem Study - Forest Biomass and Production. *Ecological Monographs* **44**:233-252.
- Zahner, R. 1968. Water Deficits and Growth of Trees. In: *Water Deficits and Plant Growth* (edit. by Kozlowski, T. T.), 2, 191. Academic Press, London and New York.

**IV. The application of the EAARL (Experimental Advanced Airborne Research Lidar) to measurement and monitoring of barrier island forest structure in an ecohydrological change scenario**

**Abstract**

The EAARL (Experimental Advanced Airborne Research Lidar) is investigated for accuracy in making detailed forest structural measurements and producing inferential statistics for remote monitoring and change detection of barrier island forest ecohydrology. Barrier island hydrology is likely to be affected by sea level rise associated with rising air and ocean temperatures. Physiology and structure of associated vegetation will respond according to depth to average water table and sand textural distribution in the rooting zone. Specifically, the major goals of the project are: a) intensively ground-truth EAARL for forest structure characterization on the Mid-Atlantic barrier island habitats of Assateague Island National Seashore, MD (AINS) and Parramore Island, Virginia Coast Reserve (PIVCR); b) derive standard and unique lidar waveform metrics and test them in the estimation of field-measured metrics related to hydrological gradients; and c) apply the findings in a and b to development of a draft remote monitoring routine of the effects of sea level rise on island freshwater resources and dependant forest structure.

The EAARL can be deployed with high confidence in loblolly pine (*Pinus Taeda* L) and similar forest mensuration projects as done here for baseline biophysical description. These structure data are correlated with environmental gradients on AINS, thus providing an important reference state for continued ecological study. EAARL

significantly predicts in multiple regressions: plot-level volume, height indices, and basal area at coefficients of determination ( $R^2$ ) from 0.72 to 0.95. The system measures the directly-derived one-dimensional vertical metrics: maximum canopy height (MCH), height of peak canopy density (HPCD), and bare earth elevation (BEE) at standard errors of 1.8m, 1.3m, and 0.3m respectively or, 11.8, 13.9 and 45.8 nominal percent errors. Of special interest here is the introduction of a potential surrogate of MCH (canopy tops are routinely difficult to measure with small footprint lidars) in HPCD. The latter is better predicted by EAARL at an  $r^2$  of 0.89 compared to 0.80 for MCH while in the field, HPCD can predict true MCH at  $r^2=0.77$  ( $p<0.0001$ ).

Unique approaches to lidar analyses in ecological studies are developed in this Chapter. A flexible total-canopy variation PCA (principal components analysis) is shown in an exploratory test to be an appropriate method for wide-scale vegetation typing by lidar full-waveform returns. In ecohydrological analyses, the lidar integrative three-dimensional stand metric CRR (Canopy Reflection Ratio) models ground-collected PAI (Plant Area Index; measured with the common Li-Cor LAI-2000) by simple regression at an  $r^2$  of 0.73 ( $p<0.0001$ ). It is apparent that PAI changes with leaf area change in the study area. *P. taeda* foliage levels are generally known to be relatively sensitive to water shortage, abscising leaves in drought. A soil water availability estimate based on depth to water table (DWT) and soil texture index (STI) is well correlated with PAI up to  $r_s=0.54$ ,  $p=0.004$ . Regular surveys for EAARL CRR and continued field measures of PAI and DWT/STI will help improve the relationship. Ideally, more intensive physiological measurements can be implemented for better assessments of direct effects, but as seen in

Chapter 3, this basic ecohydrological function can be applied now to making specific predictions of structural change to expect with rising water.

#### **4.1. Introduction**

As part of the larger study researching the structural changes in forests across freshwater availability gradients for application to forecasting changes with sea level rise on barrier Islands of the Delmarva Peninsula – Assateague Island National Seashore (AINS) in Maryland and Parramore Island of the Virginia Coast Reserve LTER (Long Term Ecological Research) Site (PIVCR) – a lidar (Light Detection and Ranging) system is tested in predicting forest structure. This chapter constitutes the first comprehensive ground-verification of the EAARL (Experimental Advanced Airborne Research Lidar) in measurement of above-ground forest structure. A test in 2002 provided a relatively limited study of forest metrics, from which there is only qualitative assessments of predictive performance (A. Nayegandhi, unpublished data). Large-scale vegetation types were identified at the present study site using three-dimensional metrics, though it has not been thoroughly ground-truthed (A. Nayegandhi, unpublished data). Recently, Nayegandhi *et al.* (2006) found good agreement ( $r^2$  of 0.73 to 0.91) between ground and remote EAARL measures in the average heights of trees in informal plots.

The initial stages are presented in development of a monitoring protocol in which waveform lidar metrics are linked to water availability and hydrologic factors of wooded areas to assess vegetation differences due to sea-level change. Typical freshwater sources in sandy barrier island substrates are lenses of freshwater floating atop saltwater. Sea

level change could force shifts in water availability patterns as freshwater lens morphologies and elevations change. Plant area index (PAI) ( $\text{m}^2$  plant woody and foliar area: $\text{m}^2$  ground area) and traditional forest metrics have been tested for their relationship to site moisture status at the plot scale; EAARL data products are analyzed for prediction of PAI and coarse structure to determine a remotely sensed metric sensitive to counterpart changes in moisture indicators.

Depth to water table (DWT) was originally hypothesized to negatively correlate with structural values. This was based on the theory that in sandy soils, height above water table can be a reliable predictor of water availability (Hayden *et al.* 1995), and findings that structure (leaf area in particular) depends on water availability (Grier and Running, 1977). CRR (Canopy Reflection Ratio) was the lidar waveform metric hypothesized to most closely approximate field-collected PAI (integrates foliar area), the most sensitive plot-level structural measure. These factors make for a simple remote monitoring framework where EAARL CRR predicts PAI which in turn indicates water availability. However, as seen in Chapter 3, there is a significant measure of unexplained variation in PAI changes as related to DWT.

With the addition of a soil texture factor, STI (soil texture index), some of the unexplained variation is resolved and an overall clearer depiction emerges of effects of rising average water tables. The soil profile needs to be described to allow for robust inferences from remote biophysical data that is circumstantially related to site moisture. And, as also seen in Chapter 3, community structure description (ratio of shrub area to tree area in a plot, for instance) enhances the indirect indication of site moisture status.

This mensuration capability is assessed for EAARL, and sources of error are shown to be explainable.

This project represents a step forward in what Omasa *et al.* (2007) describe as the thus far under-explored potential of lidar in monitoring vegetation for responses to stressors and obtaining “more accurate dynamic estimation of plant properties.” Other foreseeable applications of work started here include production forestry resource mensuration and studies of ecosystem carbon flow. Loblolly pine (*Pinus taeda* L) is an extensively studied species because of its economic importance. Results of this research will be useful to land managers and conservationists interested in forecasting changes in biomass and structures in a changing environment. Ecologists interested in system productivity can apply findings of coarse structural types to identify developmental stages. Shugart (2000) describes the importance of developmental dynamics and general biophysical structure in modeling the responses of physiological relationships to inputs in most forested ecosystems. For instance, differences in crown length – a plot-level index of which is replicated with EAARL – will signify developmental processes and “result in different light regimes that may influence ecophysiological leaf traits” (Nagel and O’Hara 2001) such as gas exchange, leaf Nitrogen, and specific leaf area (SLA - leaf area/unit leaf mass).

## **4.2. Background**

### **4.2.1. Lidar remote sensing**

Lidar is the application of a metered laser pulse to a target and the digitization of the return path position and timing through three-dimensional space. An “active” as opposed to “passive” form of remote sensing of radiance, self-contained Lidar systems emit quantified energy packets at known angles, distances, rates and energies. This condition lends itself to less art in interpretations as these data are more readily directly-truthed with traditional ground methods.

Early airborne lidars were discrete-return Altimeter Topographic Mapping (ATM) instruments. Still in use, these collect ranging data only while waveform-returning models measure the intensity of backscatter energy from all surfaces through the canopy at intervals determined by the system digitization rate (Fig. 1). Or as Nayegandhi *et al.* (2006) write, the waveform comprises “a time history of the return backscatter photons within the laser footprint.” This allows for the relative indexing of material density and area through a pulse’s path.

An airborne small-footprint lidar with full-waveform return capability (the EAARL) is employed in the present study to measure forest structure, and detect changes in structural metrics with gradients in site environmental qualities. The literature on waveform analyses is dominated by research with large-footprint lidars. Researchers have successfully predicted field-verified stand variables from lidar-derived information. Lefsky *et al.* (1999a) reliably inferred LAI (leaf area index) and biomass from lidar data, and others have found strong correlations between ground-collected basal area, mean

stem diameter (Drake *et al.* 2003), canopy height and leaf biomass (Means *et al.* 1999) and the related lidar metrics. The canopy height profile (CHP) and the canopy volume method (CVM) (reliable in estimating LAI) of Lefsky *et al.* (1999a) have proven instructive to analyses of whole-canopy data by providing ecologically significant, integrative metrics describing distribution of vegetation surfaces within a canopy.

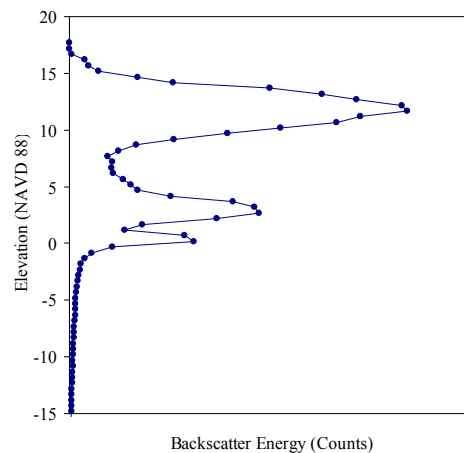


**Figure 1.** An example of a lidar waveform returned from a 0.08ha land surface plot on Assateague Island National Seashore, August 2004. Digital counts of backscattered photons are resolved to 50cm vertical resolution.

Similar objectives are pursued with small-footprint discrete-return lidar. Lim *et al.* (2003a), utilizing the first/last range and intensity returns of a 20cm footprint lidar (ALTM 1225) found agreement with their ground measures of, for example, LAI (hemispherical photo-derived), and biomass. The same instrument was successfully applied to the prediction of foliage distribution and light transmittance (Todd *et al.* 2003). Naesset (2002), in a stand assessment of standard production forestry metrics (with an ALTM 1210) found good agreements between the remote and ground data sets (lidar data

could explain 84-92% of the variation in the field data) where predictions of stem number were the least reliable of the measures.

Small footprint lidars can be limited in their ability to penetrate canopies at high scan angles (Means *et al.* 1999). Canopy height estimates are low in some coniferous forests, as there is lower probability of scanning a conical tree top with a smaller footprint (Gaveau and Hill 2003). This may be overcome to a degree by adjusting sampling density, and it would be reasonable to assume that the problem is less significant with the more rounded canopies of *P. taeda* at the AINS and PIVCR study sites. Lim *et al.* (2003a) write that lidar could indeed be more accurate than field measures with traditional instruments in determining canopy height because of inconsistent technique in the latter, including the common inability to see the top of the individual crown from the ground. The georeferencing and mensuration of all stems in this study was planned to enhance the power of validation tests.

#### **4.2.2. The EAARL lidar**

The lidar instrument employed in this study is the NASA EAARL (Fig. 2) developed by Wayne Wright at NASA's Wallop's Island, Virginia facility. The survey and processing was conducted in cooperation with the USGS (United States Geological Survey) Center for Coastal and Watershed Studies (CCWS) (St. Petersburg, FL). USGS researchers developed the Airborne Lidar Processing System (ALPS) (Nayegandhi *et al.* 2006) processing and visualization environment, and developed all processing code for EAARL data collected over AINS and PIVCR in 2004.

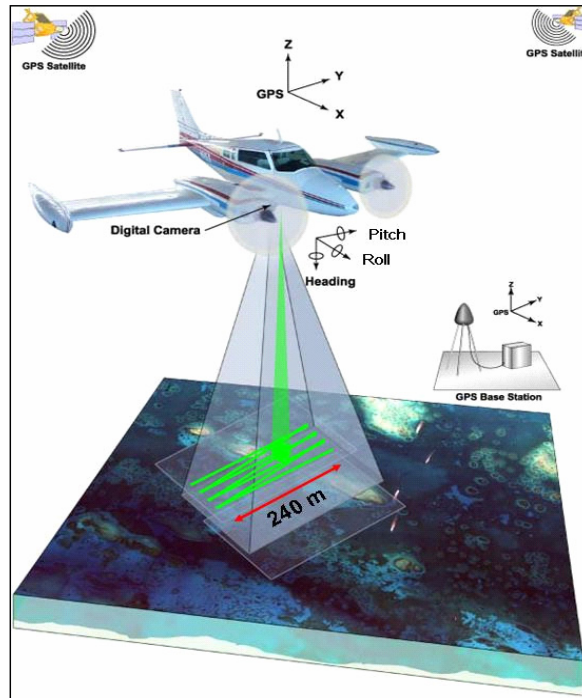


**Figure 2.** General EAARL survey configuration. The platform is a fixed wing Cessna aircraft. Flight positional data are corrected with kinematic differential GPS. Image courtesy of USGS.

EAARL is an example of a relatively new variety of airborne laser instrument – the full waveform-returning small-footprint lidar. EAARL’s footprint is 20cm, the spacing between each pulse is 2-4 meters (depending on flightline densities), and its swath width is approximately 240 meters. The one-nanosecond digitization rate corresponds to a vertical resolution of about 15cm. Nilsson (1996) introduced a similar instrument, yet the data storage available allowed for only about 17% of the waveforms. Though the EAARL wavelength (green: 532nm) is considerably less reflective in vegetation than that typical of terrestrial lidars (NIR: 900-1064nm), the information retrieved is unlikely degraded unless, perhaps, scene species vary widely in their brightness at that wavelength. The EAARL technical summary is (W. Wright, <http://lidar.net> ca. 2005):

The EAARL system is the first airborne lidar to simultaneously map submerged, subaerial, and vegetation covered topography. It uses a 5kHz 532nm 1.2-NS laser, a wide dynamic range high speed optical receiver, and a pair of multi-channel 4-Giga Sample/second waveform digitizers. The system digitizes 192 million samples each second and, using adaptive real-time processing, edits each waveform to accommodate and retain only the complex back-scatter of interest greatly reducing the amount of data which must be stored. The system effectively auto-adapts to the terrain, vegetation covered earth, or bathymetry being mapped.

### **4.3. Methods**

#### **4.3.1. General considerations**

The following methods were designed with four main goals in mind. First is a detailed ground verification of EAARL at the plot scale. Second and ancillary to another area of study in this volume is the building of a strong correlative relationship between vegetation structural attributes and general hydrological status. Third is the association of ground-based and remotely-sensed changes in moisture-sensitive structural metrics. Last is the inclusion of guidance for monitoring this and similar natural systems utilizing the information-rich waveform to draw inferences of effects of environmental change.

### 4.3.2. Data collections

Refer to Chapter 2 for study area and field methodologies common to the project. An EAARL survey of AINS and PIVCR (Figure 3) was flown in August 2004. The raw horizontal resolution of about 3m is a function of flightline density, and the raw vertical resolution of 15cm is a function of the backscatter digitizing rate. High resolution (14cm) CIR imagery was collected coincident with the lidar data, yet it is not available due to technical problems.

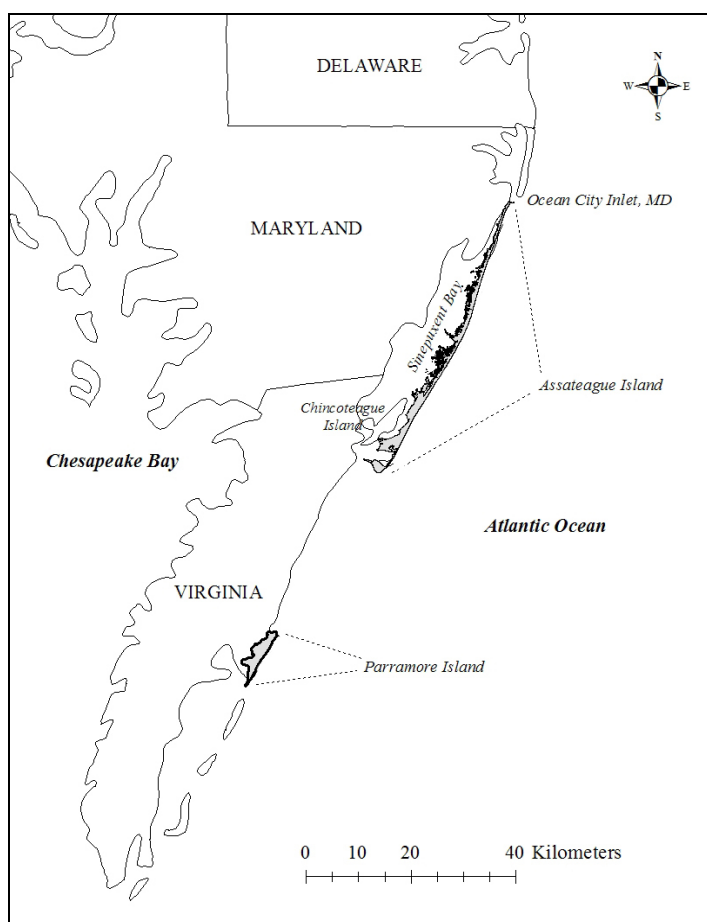


**Figure 3.** Assateague and Parramore Islands of the Delmarva Peninsula.

Ground biophysical structure and environmental surveys of the 26 AINS plots were completed in 2005 as described in Chapter 2. These included the collection of continuous PAI measurements in the AINS plot network with the electronic LAI-2000 (Li-Cor Biosciences), and, horizontal positions of plot centers and tree stems and average plot elevations with sub-meter accuracy survey-grade GPS and a total station survey instrument. The PIVCR ground surveys were abbreviated in comparison to AINS due to the extremely degraded condition of the canopy and the complicated logistics of reaching the island with due frequency.

#### **4.3.3. EAARL data descriptions**

16.3m radius composite large footprint waveforms (LFPW) (Figure 4) were synthesized at ground plot centers by averaging raw waveforms in the NASA/USGS ALPS environment. Laser returns are georeferenced using aircraft GPS and attitude information. Conversion to the desired coordinate system, and the processing of five standard metrics (Fig. 4) for composite waveforms at desired center points, was programmed in ALPS: bare earth elevation (BEE), maximum canopy height (MCH), ground reflection ratio (GRR), canopy reflection ratio (CRR), and height of median energy (HOME). The LFPW's resultant centroid location is a function of laser posting separation distance (raw horizontal resolution) and random IFOV (instantaneous field of view) location.

BEE is determined with an iterative random consensus filter (IRCF) process algorithm (Nayegandhi, unpublished), and MCH is the maximum canopy height gleaned from the zero-crossing at the second derivative of the top of the waveform (Nayegandhi

et. al., 2006). CRR, GRR, HOME are then computed from the energy return profile between BEE and MCH. Resultant vertical resolution is 50cm. Large-scale geotiff coverages (2km X 2km) of MCH and BEE metrics (2002 data) at about 1.5m raw horizontal resolution (1m resampled final resolution) have been produced by USGS CCWS. Five-meter resolution layers were produced in the present study that were later found to be inaccurate. The problem appears to be within the coverage generation commands, though it has yet to be identified. GIS (Geographic Information Systems)-ready data layers will be developed with the corrected methods when adapting the research to wider monitoring operations.

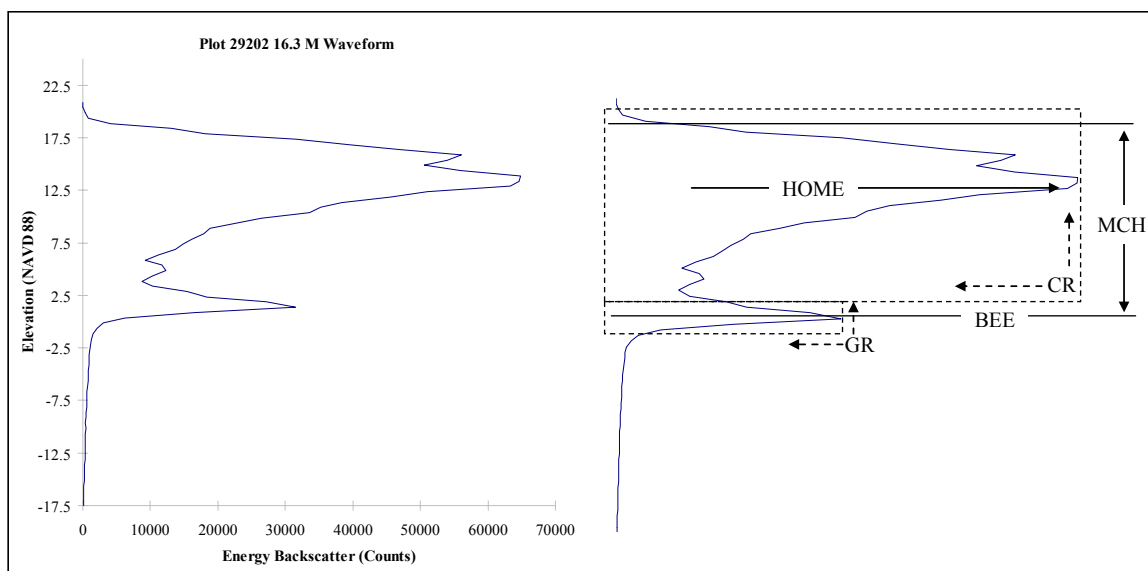


**Figure 4.** A raw EAARL composite waveform (left) and graphical metric descriptions (right). MCH=maximum canopy height; BEE=bare earth elevation; CR=total canopy reflection (energy backscatter counts); GR=total ground reflection; HOME=height of median energy. CRR=canopy reflection ratio:  $CR/(CR+GR)$ . GRR=ground reflection ratio:  $GR/(CR+GR)$ .

#### 4.3.4. Analyses

All statistical analyses described in this section are performed with SAS software (SAS Institute, 2002-2003). EAARL and field measures of plot location, BEE, MCH, and

height of peak tree canopy density/reflection energy (HPCD) are directly compared. Shrub (dripline) canopy area (SCA) can not be directly compared between field and remote data sets. Field-collected tree crown lengths were combined for each plot into a foliated crown presence histogram (Fig. 5). As there are unmeasured gaps in foliation, these only represent the maximum likelihood of finding foliated branches at 10cm vertical segments (see Appendix C). The EAARL HPCD values were taken as the height of the peak backscatter count in the canopy return of the waveform (Fig. 5), and field HPCD as height of the peak frequency in the crown presence histograms. This metric of a maximum density-height will vary among sites according to developmental stage, moisture and microclimate. Development of HPCD as a metric is undertaken to compensate for expected loss of canopy top information in MCH as measured by EAARL. It is expected that across a broad study area, HPCD could be as effective as maximum height in site quality indication (see Chapter 2).

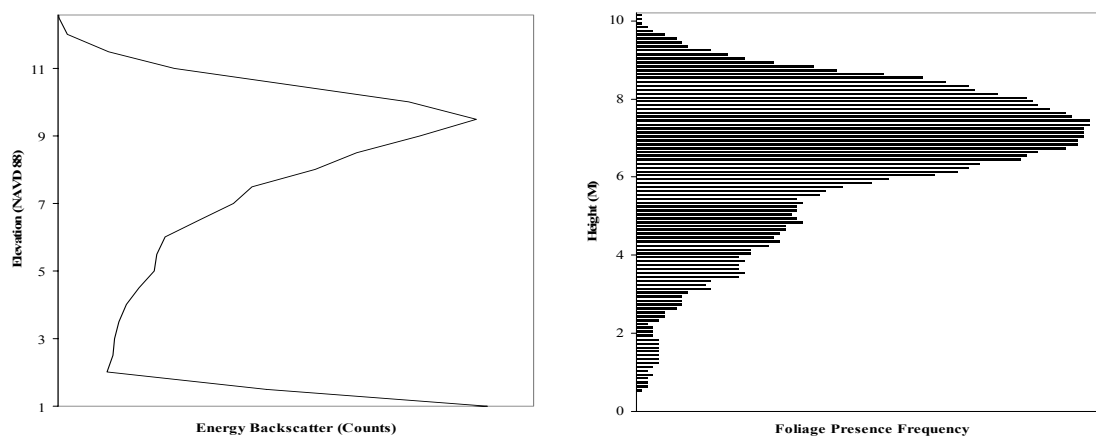


**Figure 5.** A comparison of an EAARL backscatter count spectrum (left) and a field plot canopy foliage presence histogram (right).

Standard field measures were processed to plot-level values of basal area (BA):  $\pi \cdot (\text{dbh}/2)^2$ , where dbh is the cumulative diameter at breast height of all plot trees, and

volume:  $(0.5(PTH)\pi(dbh/2)^2)$  (Whittaker *et al.*, 1974, parabolic volume estimate) where PTH is average plot tree height. While these and the field one-dimensional measures were assumed to strongly intercorrelate, inclusion of variable levels of structural organization offer greater probability to develop functional relationships for precise remote monitoring of the structure-water interaction.

All field biophysical variables were tested for correlations with the hydrological indicators STI (a ratio of fine to medium sand fractions), average DWT, and the product of these two variables: DWST (see Chapter 3). Recommendations for EAARL-based monitoring of the ecohydrology of the dynamic barrier island forest system follow from these results. PAI is the most temporally sensitive metric to be related to variations in site moisture. It is for this reason all EAARL metrics are regressed on PAI to develop a model that will enable remote monitoring of plant (and leaf) area change.

As detailed in Chapter 2, field plot measures of PAI, MCH, HPCD, SCA, BA and Maximum Age (maxage; by tree ring analysis) are used to develop two major “bio-types” from PCA (Principal Components Analysis) and subsequent cluster analysis on the results of the regression of plots’ PC1 and PC2 scores. The environmental variables STI, soil organic matter (SOM), distance from ocean shoreline (distshore), maxage (approximates the time since disturbance), average DWT, and BEE are similarly processed into six “site types” through cluster analysis. These classifications are necessary here to focus structural monitoring schemes and to qualify the wider ecohydrological predictive theories.

To explore a quantitative assessment of the similarities in patterns of canopy density in remote and field data sets, a methodology by Caylor *et al.* (2004) was adapted

to this study. Principal components (PC) were derived from all field canopy density frequency distributions and EAARL reflection counts by vertical one-meter intervals. PC's were assessed for the original vertical segments contributing significant amounts of variation to the new PCA variable set. Plots were grouped into site types; their scores in PC1 and PC2 of the respective (field, lidar) canopy representations were then used to graph a qualitative comparison between field and lidar PC clustering.

This procedure appears likely to provide another means of fine-tuning assessments of effects of changing water availability on vegetation communities. Caylor *et al.* (2004) used the technique to differentiate sites on a moisture gradient by vertical locations of highest total variance in leaf area, and to tailor productivity models. As they note, PCA offers an improvement in precision because “simple means and variances of vegetation [structure] are poor representatives of structural heterogeneity in semi-arid ecosystems.”

Finally, a conceptual model of a monitoring and research project with the tools and products described here is diagrammed per recommendations in Fancy *et al.* (2009).

## **4.4. Results**

### **4.4.1. Direct comparisons**

Results indicate that EAARL can often reliably estimate standard forest metrics at the scale of ground plots (0.08ha or 835 m<sup>2</sup>). Table 1 lists the mean absolute errors of directly-derived EAARL metric values. MCH – a good overall indicator of site quality (Spurr and Barnes, 1980) – is in error by 1.9m on average at the plot level. As expected,

EAARL underestimated MCH in most cases. This bias is widely reported in the lidar literature and occurs because individual tree tops are often missed, especially by the more sharply-focused small footprint models. This could also be explained by low stocking density or by the LFPW offset from plot boundaries in some cases; however, less overall error was originally expected because of the relatively broad tops of *P. taeda* “oval”-shaped (Gilman and Watson 2006; visual confirmation) crowns.

The LFPW’s are displaced from ground plot centers up to 3m (about 1 raw pixel width) and generally to the southeast (Table 1). This implies a possible 4m offset at plot geolocation when the internal EAARL error range of about 1m is included. For plot-level statistics this may introduce a comparability issue. BEE, however, is within about one-half meter. This is a good result and points to EAARL’s fine-scale capabilities.

Assateague’s relict dune-derived topography changes at very short spatial scales with plots ranging up to 2.3m in elevation (complete slope placements were avoided). Fairly precise BEE also supports the assumption that the bulk of MCH error is due to simple canopy exclusion by the pulse IFOV as opposed to an overriding geolocation issue.

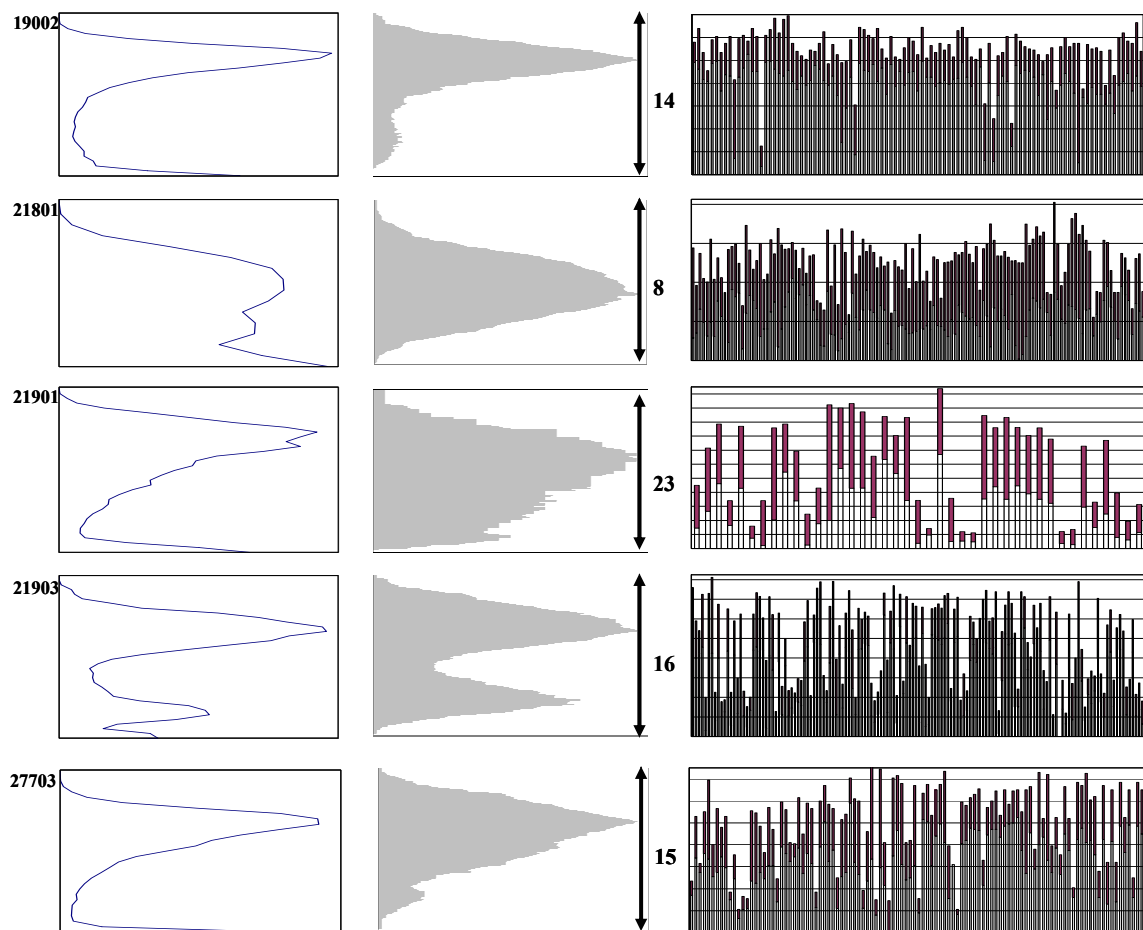
<i>Assateague Island, n=26</i>						
	16.3m Plot Center Easting	16.3m Plot Center Northing	Total Centroid Displacement	BEE	MCH	HPCD
<b>MAE</b>	0.8	2.6	2.8 (Southeast)	0.4	1.9	1.2
<b>Standard Error</b>	0.4	0.4	0.5	0.3	1.8	1.3
<i>Parramore Island, n=4</i>						
<b>MAE</b>	0.6	2.2	2.3 (Southeast)	1.1	1.8	2.4*
<b>Standard Error</b>	1.0	0.6	0.9	1.2	2.7	0.5*

**Table 1.** The mean absolute error (MAE) and standard deviation of MAE (standard error) between directly measured field values and EAARL values in the 16.3m field plots and LFPW’s. Centroid displacement is generally directed to the Southeast. BEE=bare earth elevation (m), MCH=maximum canopy height (m), and HPCD=height of peak canopy density (m).

\*  $n=2$ .

At AINS, accuracy improves from MCH to HPCD by about 0.7m, though standard error (SE) is still relatively high. Note that sample size is much smaller at PIVCR so that most standard errors are greater than those from AINS. HPCD in ground-collected crown lengths are from only 2 sites at PIVCR. The SE here (0.5m) is quite low compared to AINS due to the very denuded canopy in the plots, so that *occlusion* (Lefsky *et al.* 1999a) of laser energy by higher canopy material to lower reaches is less likely. PIVCR analyses are limited to these direct comparisons because of the rapidly changing canopy. Figure 6 displays the graphical qualitative comparisons of EAARL and field canopies and the field stem profiles of the ten plots equipped with automatic water table recorders (the ‘water plots’), and the three permanent PIVCR plots; Appendix A contains these figures for the entire plot network. All graphics are depicted relative to average ground level for the 0.08ha plots.

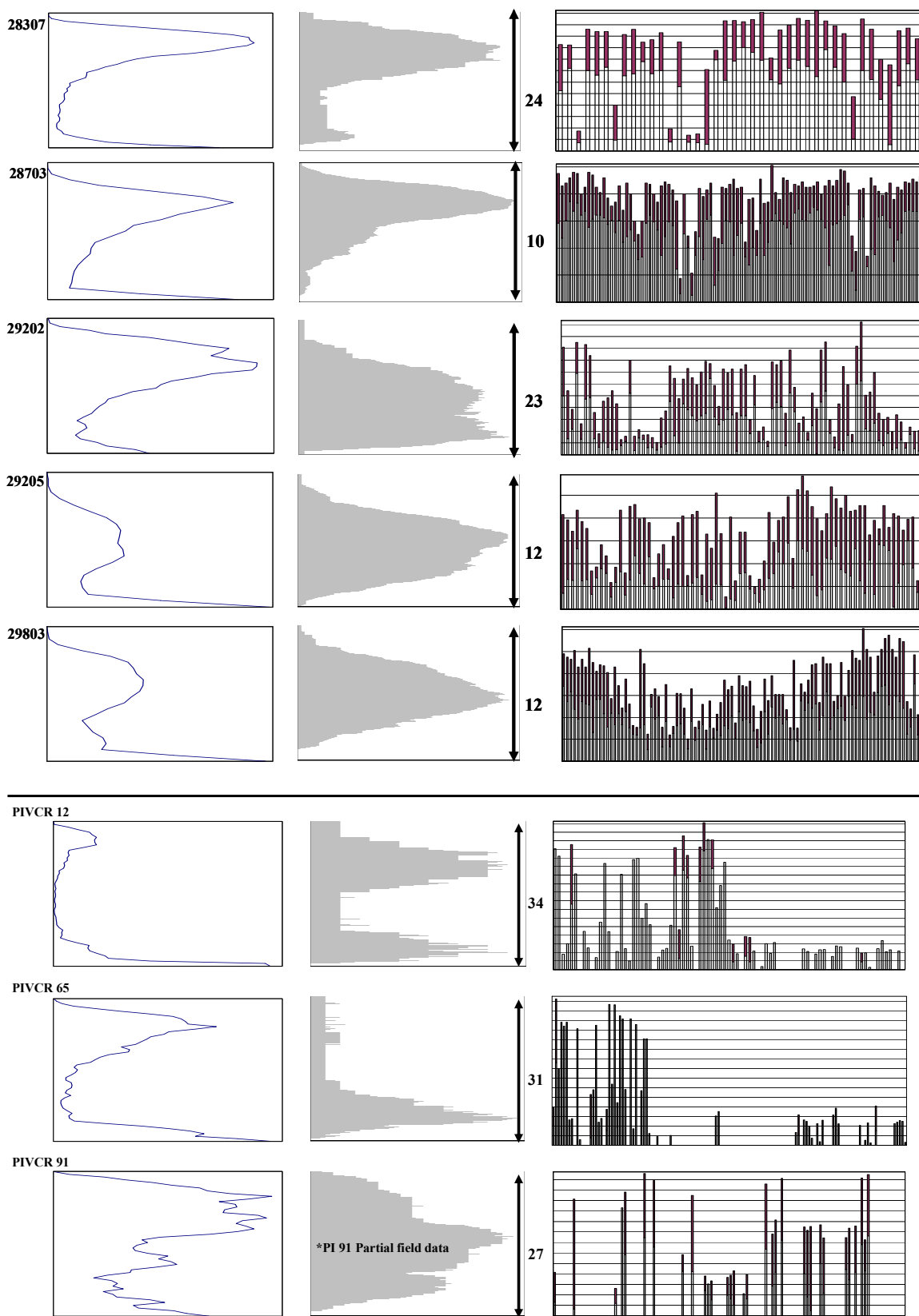
Results of the simple regression models (general linear model procedure, “proc glm”, SAS Institute 2002-2003) of EAARL metrics and the field parameters are shown in Figure 7. The field parameter values are charted against EAARL-predicted values for AINS plots only (n=26). The EAARL MCH results in a prediction of plot maximum height at an  $r^2$  (coefficient of determination) of 0.80 and RMSE (root mean square error) of 2.44. Predictions of HPCD are better at  $r^2$  of 0.89 and RMSE of 1.45. AINS field HPCD predicts field MCH at an  $r^2$  of 0.77, and RMSE of 2.67. Elevations for BEE are predicted with a RMSE of 0.31, yet an  $r^2$  of only 0.67. BEE comparisons are based on the 19 samples for which average field elevation values were collected.



**Figure 6.** From left: plot number, the EAARL waveform, field crown presence frequency histogram, maximum field height (m), and stem profile (crown length is shaded) for the 10 instrumented *water plots* at AINS and 3 measured PIVCR plots. All figures are referenced to plot average bare earth elevation.

*\*Note: PIVCR 91 field data are not complete.*

Figure 6. Continued from above.



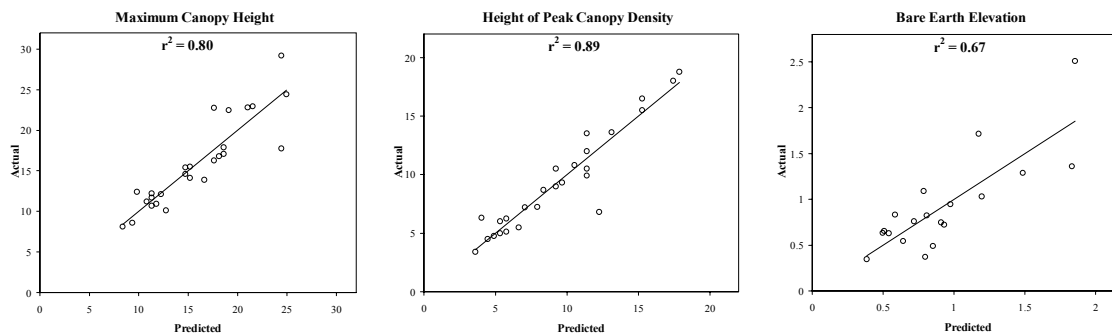


**Figure 7.** Regressions of the field-collected parameters against EAARL-predicted values. From left the metrics of interest are: maximum canopy height (MCH), height of peak canopy density (HPCD), and bare earth elevation (BEE). Units are in meters.

#### 4.4.2. Multiple regressions for stand-level metrics

To test applicability of the EAARL in basic forestry mensuration needs, stepwise regressions, using the SAS (SAS Institute, 2002-2003) “reg” procedure, were developed in the manner of Lefsky *et al.* (1999a) for several typical stand metrics including volume (vol) and BA (Fig. 8). MCH and HOME were retained in predicting BA; and CRR and HOME were retained for tree Mean Maximum Height (MMH-tree), MMH-all (includes shrub heights), and vol. As CRR does not significantly improve the model for vol, and decreases the significance, it is not included in the final model. All final models are significant to  $p < 0.07$ .  $r^2$  values range from 0.72 for BA to 0.95 for vol. The respective RMSE values are included in the individual regression graphs of Figure 8.

#### 4.4.3. PAI, and relationships of structural variables to site moisture

PAI represents the finest structure currently resolved on a plot-space and temporal basis as it incorporates leaf area change. PAI is also significantly positively correlated to coarse structure measures for the 26 AINS plots (Table 2). Though the collections were not timed equally among plots, the index clearly changes with seasonal influence in the

major bio-types (Figure 9). Bio-type 1 is comprised of plots of greater biomass and height; bio-type 2 sites are shorter with generally underdeveloped form.

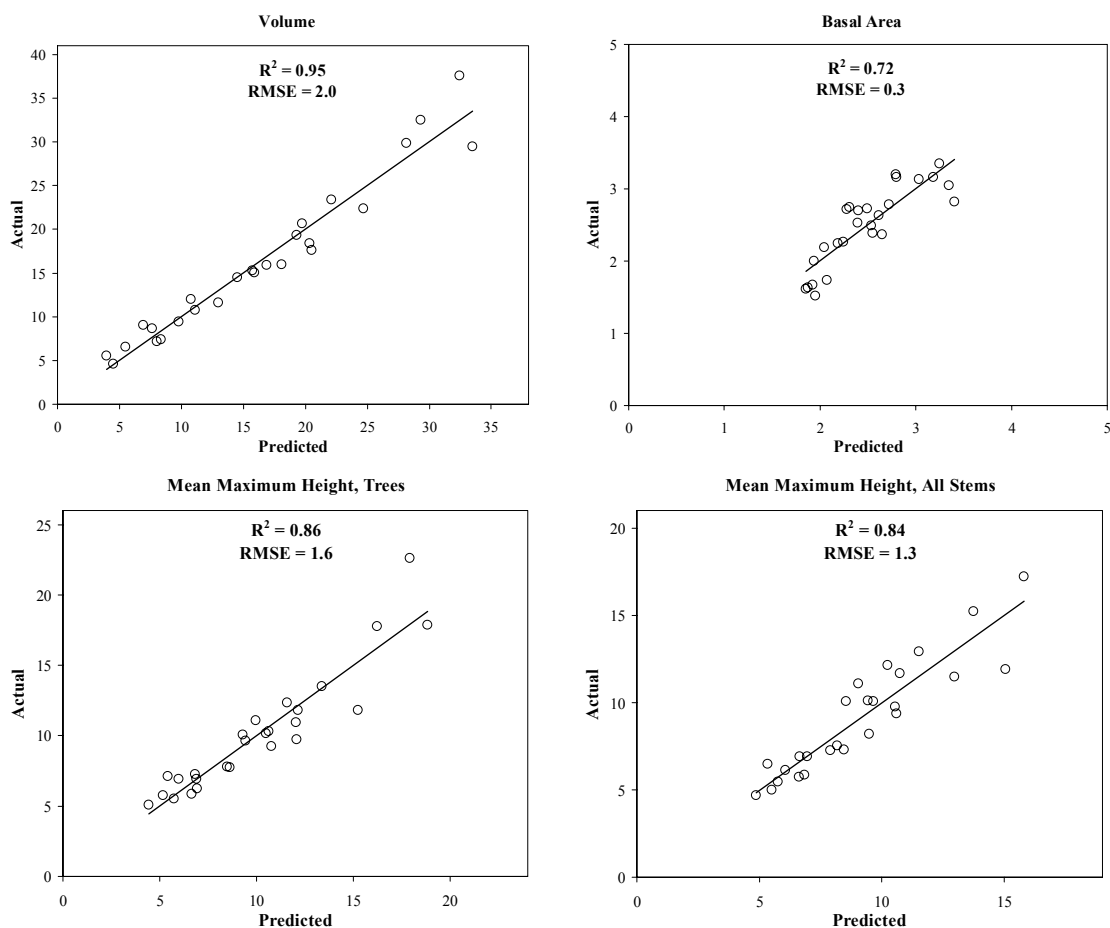


**Figure 8.** Predictions of stand variables from multiple stepwise regressions with standard EAARL metrics MCH, CRR and HOME. Note coefficients of determination ( $R^2$ ) and root mean square error (RMSE) values in graph spaces.

Average PAI (2005) and Forest Structure						
	Mean Maximum Height, Trees	Maximum Height	Height of Peak Canopy Density	Basal Area	Volume	Maximum PAI
Spearman Corr. Coeff.	0.58	0.71	0.52	0.51	0.66	0.95
p-value	0.002	<0.0001	0.007	0.008	<0.0005	<0.0001

**Table 2.** Correlations among average PAI from 2005 and structural metrics collected in all plots,  $n=26$ . Maximum PAI is included as a consistency check.

*P. taeda* foliage is sensitive to drought, and noted for abscising leaves relatively quickly under moisture stress (Vose and Allen 1991). PAI and leaf litter correlations were

conducted to determine if there is a regular differential with PAI and litter-driven LAI loss. Lagging the total litter weight gain and coincident PAI change by approximately 14 days, the correlation analyses resulted in an insignificant negative correlation (Spearman rank correlation,  $r_s$ ) in bio-type 1 ( $r_s=-0.40$ ) and weakly significant positive correlation in bio-type 2 ( $r_s=0.62$ ,  $p=0.10$ ) as detailed in Chapter 3.

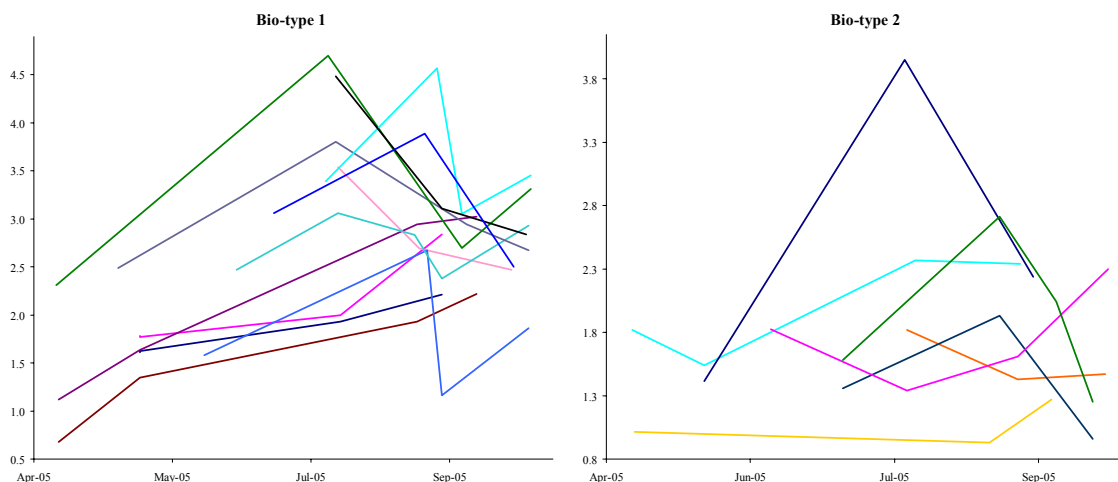


**Figure 9.** PAI values across 2005 study period for plots in the biophysical bio-types 1 ( $n=15$ ) and 2 ( $n=10$ ).

PAI correlates weakly positively with average DWT ( $r_s = 0.46$ ,  $p=0.13$ ), yet SCA and maxage correlate strongly ( $r_s = -0.80$ ,  $p=0.01$  and  $r_s = 0.63$ ,  $p=0.05$ , respectively), and HPCD is weakly positively correlated. STI, on the other hand correlates more significantly with all the other structural metrics.

#### 4.4.4. The EAARL correlates for moisture status monitoring

PAI is modeled well by EAARL CRR over the entire range at  $r^2=0.73$ ,  $p < 0.0001$ . At the biophysical cluster level, the coefficient of determination diverges significantly, as bio-type 2 (generally shorter, younger) PAI is more confidently predicted than bio-type 1 (generally taller, older) PAI. Figure 10 shows the model results for the

network-wide, bio-type 1 and bio-type 2 PAI-CRR functions, for which RMSE is, respectively, 0.47, 0.53, and 0.21.

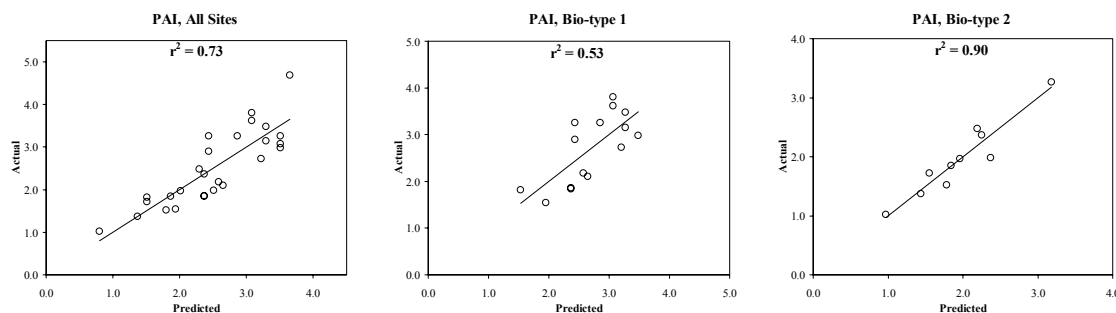


**Figure 10.** Regressions of EAARL CRR-predicted PAI against the field-collected values. From left to right: All sites (n=27), bio-type 1 (n=15), and bio-types 2 (n=10).

STI is a consistent positive factor in biomass growth. Soil textural proportions will likely not change in a monitoring time-frame, and they are more interwoven with longer term development than is the much more plastic DWT. However, STI plays a major role in characterizing water availability through its interaction with water table levels (see Chapter 3). The measure may be a key to understanding how individual stands are going to need to adapt to changing water tables or face decline.

SCA and maxage performed the best out of the common structural variables in DWT tests, but these are resolvable only by ground measures at this time. Average plot SCA is  $85\text{m}^2$  (standard deviation,  $s=104$ , coefficient of variation,  $\text{CV}=123\%$ ) in bio-type 1, and  $145\text{m}^2$  ( $s=81$ ,  $\text{CV}=56\%$ ) in bio-type 2. SCA is a broad vegetation type indicator, albeit very dependent on water table position, and may not change at the temporal scale needed for monitoring changes due to sea level rise. PAI requires more investigation and sampling to generate reliable models, but the results thus far indicate PAI adequacy in integrating leaf area change (the general trends per Fig. 9), and its fair correspondence with DWT. While stand-level stem-only measures are predicted more accurately (Fig. 8)

by EAARL than is PAI, these also will not change at the scales necessary for near-term monitoring schedules. Direct derivation of a subcanopy energy peak (not shown) entailed a 1.3m MAE (mean absolute error) or an average 48% of total stratum height, and is thus unacceptable for moisture status inference. The factors leading to subcanopy information loss are discussed below.

#### **4.4.5. Alternative method of canopy information comparisons: principal components analysis**

In the canopy PCA, all crown presence frequencies from the field and all EAARL backscatter counts were entered separately into a PCA for vertical one meter increments (downward from maximum) over the five environmental site types (1a, 1b, 2, 3, 4). Site type 5, comprising two field plots, was excluded as it skewed the distribution (this site type is located in the structurally well-developed “Green Run” portion of Assateague). This reduced the total number of PC’s from 30 to 23 and the sample size to n=24.

The first two PC’s of field canopy account for 76% of total variation, and are loaded by the 16m and 2.5m heights, respectively. In the EAARL canopy PCA, 62% of total variation is represented in the first two PC’s (loaded by the 13.5m and 18m heights, respectively), and 75% in the first three. Table 3 lists the principal component statistics; PC locations are shown superimposed across all mean plot height profiles in Figure 11; and the arrangements of the five site types in EAARL and field PC space are mapped in Figure 12. Note that canopy weighting measures are included in Figure 11 for reference: MMH-tree is graphed in the field chart, and HOME in the EAARL chart. Approximate

minimum foliage heights (terminating crown lengths) are also located on the field chart of Figure 11 for reference.

Canopy PCA Statistics				
	PC1 % Total Variation	PC2 % Total Variation	PC1 Loading	PC2 Loading
Field	43.3	32.5	16m	2.5m
EAARL	37.8	24.2	13.5m	18m

**Table 3.** Numerical results of the PCA on canopy returns.

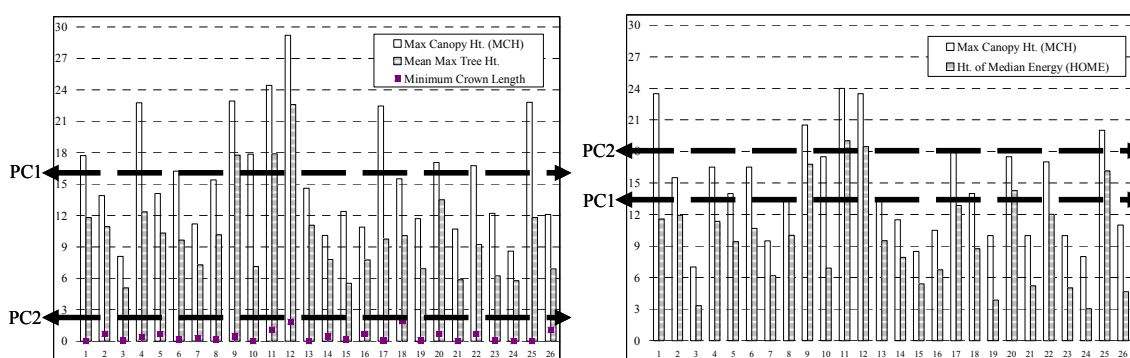


**Figure 11.** The PC loading locations in the canopy across all plots in the field measures of maximum foliage presence frequency (left) and the EAARL returns of backscatter energy (right). Mean maximum tree height is paired with maximum height in the field chart, and minimum crown length is indicated. Height of median energy (HOME) is coupled with maximum height in the EAARL chart.

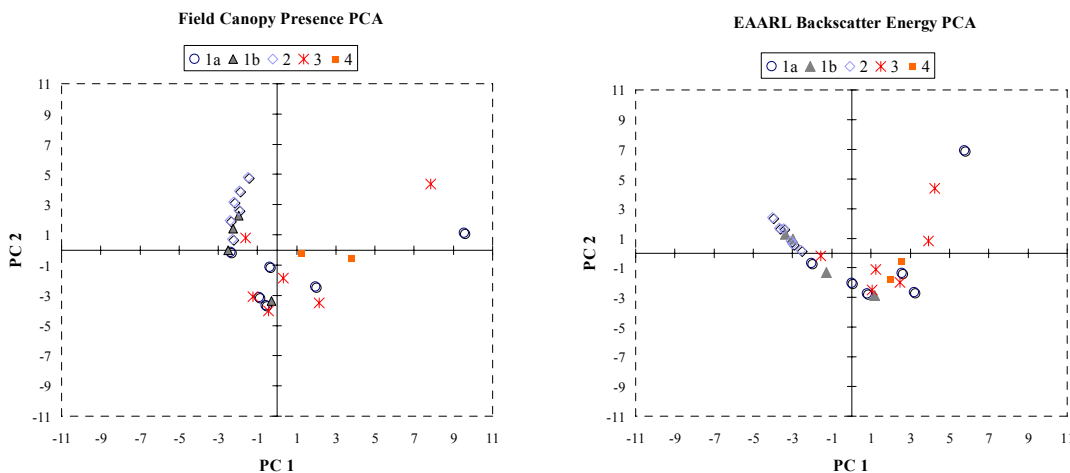


**Figure 12.** Site type groups plotted in canopy density PCA space (PC1 X PC2) for field and EAARL according to their respective scores.

Variation is limited to the upper canopy in the EAARL data (Fig. 11) because of occlusion of the EAARL laser, illustrating the inconsequence of not measuring shrub crown lengths in the field (using tree information only). Inclusion of some modification of the relative shrub canopy area measure in the tree canopy results would therefore be unlikely to change the agreement between PC sets. More experimentation to find a reliable subcanopy representation in EAARL should be a priority (see “Ecohydrological relationships and monitoring” in the Discussion below).

As HPCD is in better agreement between the data sets (Fig. 7) than the maximum heights, the same PCA exercise is run on the canopy information with HPCD as the upper bound to test if the loss of canopy tops can be overcome in comparing variation. The first two principal components are at a more comparable distribution in the two canopy representations (Fig. 13), though cumulative variation in PC1 and PC2 is now only 55% in EAARL and 56% in field.

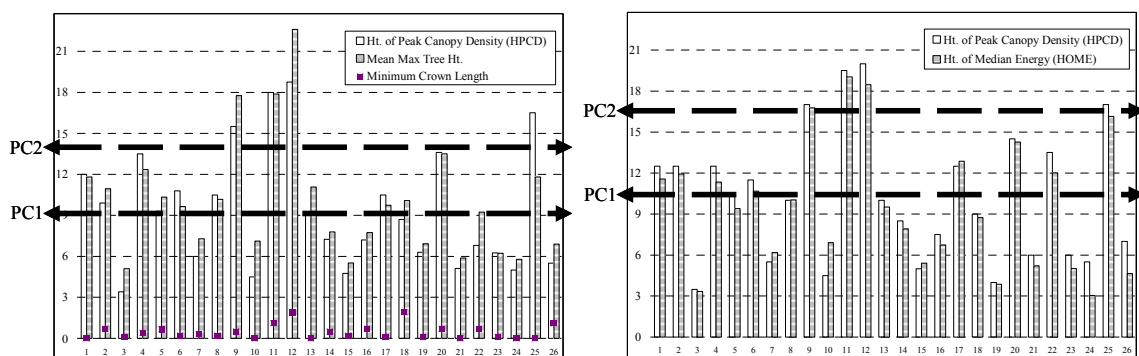


**Figure 13.** New PC loading locations with the heights to canopy peak density (HPCD) as upper bounds in the field measures of maximum foliage presence frequency (left) and the EAARL returns of backscatter energy (right). Mean maximum tree height is included for reference in the field chart, and minimum crown lengths are indicated. Height of median energy (HOME) is coupled with HPCD in the EAARL chart.

Ungrouping data and testing blind association by cluster analysis (by average distance) for both PCA designs tentatively shows that this canopy peak PCA is more effective at drawing out matching groups (by visual inspection of cluster dendrograms, not shown) by removal of canopy top outliers, and the new geometry in the field PC space (Fig. 14) resulting from the PC2 shift from sub to upper-canopy.

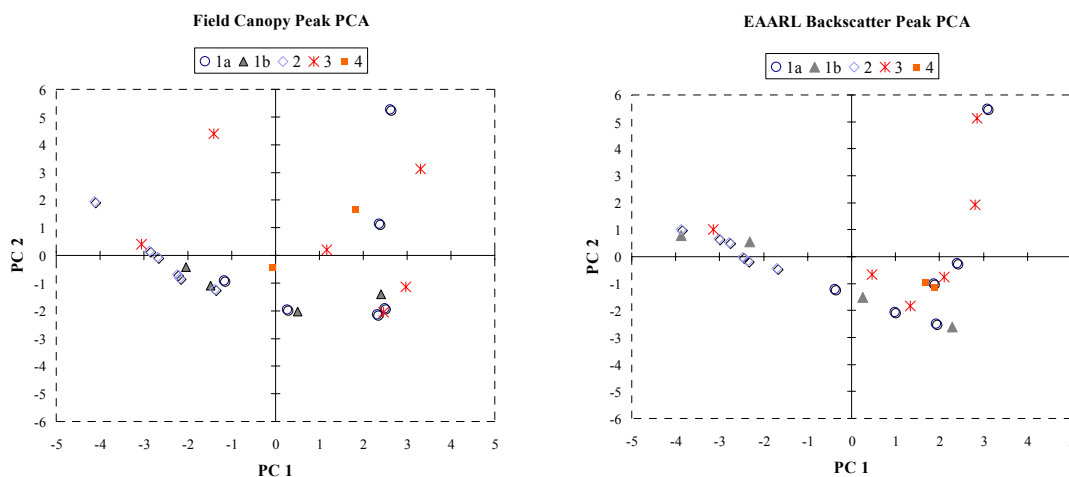


**Figure 14.** Site type groups plotted in the new HPCD-based canopy density principal component space (PC1 X PC2) for field and EAARL according to their respective scores.

## 4.5. Discussion

### 4.5.1. Direct comparisons

Direct comparisons show the EAARL accuracy to be comparable to other lidar instruments and better in many cases (Lim *et al.* 2003b has a review). Previous EAARL work (Nayegandhi *et al.*, 2006) based on a small (n=6) subset of the data at AINS found an RMSE of 0.8 in MCH regression analysis compared to the 2.4 RMSE in the present study. With the increase in sample size, however,  $r^2$  has increased to 0.80 from 0.73 (Fig. 7). There are 5 outliers, all with relatively high maximum field heights, and in all but one

the field value exceeds the EAARL estimate. Outlier plots except for one also have relatively low stem density. As noted earlier, canopy top exclusion is common in lidar surveys. This fact coupled with the greater range possible for error in tall, open stands may have produced the error. Two outliers have a large BEE range and averaging this for the EAARL BEE value would necessarily skew the plot-level MCH (LFPW synthesis begins with the isolation of BEE from the total backscatter “cloud”). In the short term, finer resolution LFPW’s may result in better BEE agreement with the field. Later, higher EAARL sampling density along with better georectification (the tallest trees may not be included in the LFPW boundary) would likely increase accuracy substantially for BEE and MCH (see Table 1 for error magnitudes).

The dramatic decrease in MCH prediction success ( $r^2=0.01$ , RMSE=2.9, not shown) at PIVCR is expected because of the extremely low foliar density and low stem density (Fig. 6), as well as the very small sample population ( $n=5$ ). Laser posting density requirements for better MCH prediction would be prohibitively high in greatly impacted canopies. At plot PIVCR 65 (Fig. 6), a significant difference in canopy material presence could have resulted from the time lag of field measures after the EAARL survey (about 1 year) as canopy decline continued. A close inspection of the stem profile chart (Fig. 6) for PIVCR 12 may explain the discrepancy of 6.7m in MCH as there are only 7 dominant stems with some foliage remaining. One may assume from this that the majority of damage was done by the time of the EAARL survey at PIVCR 12, and decline was slower and continuous at PIVCR 65. This is supported by the CRR values at the time: 0.99 for PIVCR 65, and 0.49 for PIVCR 12. Notably, maximum CRR at the intact AINS area was 0.94.

In direct comparisons between field and EAARL metrics, HPCD is a readily-contrasted attribute. HPCD positions are visible in the full waveform and crown presence frequency spectrums of Figure 6 and Appendix A. Prediction for HPCD by EAARL is better than MCH prediction (Fig. 7) while field HPCD correlates better than field MCH with the other structural variables: vol, SCA (negatively), BA and maxage (Fig. 15); MCH is better correlated with PAI.

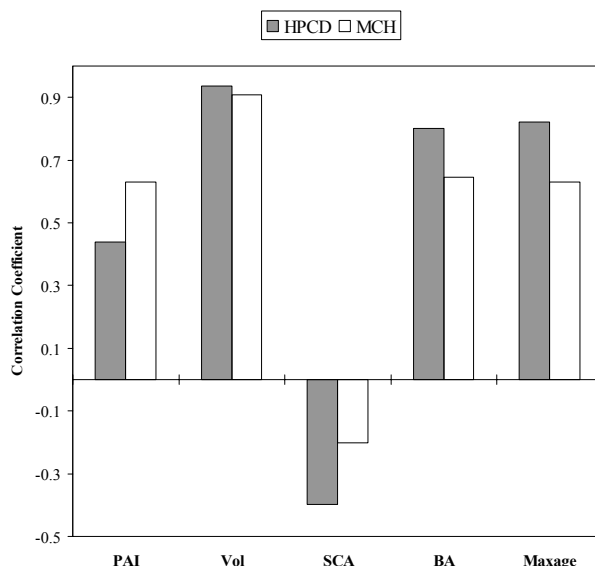


**Figure 15.** Correlations of height of peak canopy density (HPCD) and maximum canopy height (MCH) with the other major structural parameters plant area index (PAI), parabolic volume (Vol), shrub canopy dripline area (SCA), basal area (BA), and maximum age of trees in field plots (maxage). PAI, vol and SCA were log transformed to normal for Pearson r correlation, and BA and maximum age are Spearman rank  $r_s$  correlated (non-normally distributed). All are significant at  $p \leq 0.05$  except SCA.

HPCD is a plausible surrogate for MCH in lidar studies. Researchers and managers can begin compensating for the loss of canopy top and subcanopy information in EAARL and other lidar returns by the simple collection of the crown length measure in field surveys. EAARL has yet to be tested in conical-shaped tree stands, but this would

likely decrease maximum height accuracy and mandate the use of HPCD to a greater extent. While MCH is a good overall indicator of site quality for a specified area, HPCD may better represent change in stocking density and, therefore, developmental stage.

EAARL HPCD, however, is eliminated in the stepwise regressions to predict field stand-level metrics (Fig. 8) while MCH and HOME are retained as these two remote measurements are more sensitive to within-plot vertical variability. Work is continuing on utilizing the total field crown presence and EAARL crown energy return information maximally and efficiently. The respective frequency data are to be characterized and compared with distributional statistics in Kolmogorov-Smirnov tests (pers. comm. G. Okin) based on the empirical distribution function (Gibbons and Chakraborti 1992).

Another one-dimensional lidar metric, HOME, is likely indicative of weighting in a leaf area index profile as originally employed by Aber (1979) as the foliage height profile and later modified for lidar by Lefsky *et al.* (1999b) as the canopy height profile (CHP). These result from a more labor-intensive process of vertically stratified cover estimates and their conversion to leaf area using fine allometric equations. While the method comprehensively truths waveform returns, it is more suited to large footprint lidars because relativity of the energy profile is self-contained within the plot-sized (about 10m diameter) pulses.

#### **4.5.2. Canopy profiles**

Collection of detailed woody vegetation structure data including crown lengths enables the development of theories of field/remote disagreement on a plot-by-plot basis. Those plots with fairly continuous upper canopies as seen in the stem profiles of crown

and bole lengths (see Figure 6 and Appendix A), and those of relatively tall stature are generally subject to some occlusion and loss of subcanopy information. To detail some of the important points of discrepancy, a few of the plots serve as examples. Inspecting the EAARL waveform for plot 29802 (Appendix A) illustrates the complications imposed by occlusion of incident energy in a canopy's upper portions. A strongly bimodal canopy in the field crown frequency histogram, the subcanopy is substantially reduced in the EAARL return. A few issues may be at work, including: simple height-wise and canopy material occluding by numerous tall trees; and the subcanopy preponderance of *Ilex opaca* (American holly), a smooth and shiny-leaved species that may reflect incident laser radiation specularly, away from the sensing telescope. *I. opaca* is not common in the AINS plot network.

Another significant challenge in the processing of lidar data is the accurate depiction of an average bare earth topography. In plot 29202 (Fig. 6) there is a large bare earth elevation (BEE) range (2.3m) that leads to a disagreement of 1.2 meters in average BEE. The rate of change over the plot is too high to be precisely depicted at the present resolution (0.08ha). Ground surfaces will necessarily be registered as vegetation. As there is a 4.5m MCH underestimation here, readings below areal-density thresholds have been eliminated by the IRCF process (waveform processing was not done in the "interactive" mode that allows manual override in tolerances). This condition can also be compounded by the canopy top undersampling mentioned previously.

Georectification imprecision is of concern as may be seen in a number of under-matched profiles. EAARL oversampling of ground or canopy area in relation to what is measured in the field plot could lead to errors in all directly compared measures (one-

dimensional metrics). While generally being less sensitive to a few meters misalignment, integrative measures like CRR may disagree significantly with field correlates like PAI from one vegetation type to another (see Fig. 10 for illustration of the bio-type prediction inconsistency).

#### 4.5.3. Multiple regression models

Lefsky *et al.* (1999a) employed multiple stepwise regression (MSR) to assess SLICER (Scanning Lidar Imager of Canopies by Echo Recovery) large footprint waveform lidar in Northwest USA conifer forests. They isolated about 11 variables from lidar data to run MSR in predictions of embedded stand variables like mean dbh and the number of stems greater than 100cm dbh, and integrative measures like LAI. The same instrument was tested this way by Means *et al.* (1999); they found that two measures of stand height (weighted and maximum) and a canopy reflection sum, predicted total above-ground biomass at an  $r^2$  of 0.96 with MSR, among other significant results.

MCH, CRR, HOME, and HPCD are made available in the MSR models of AINS stand-level variables MMH-tree, MMH-all, vol, and BA (Fig. 8). HPCD is not retained at the cutoff  $p=0.15$  significance level perhaps because it is related more to foliage concentration than the others, and is more randomly affected by occlusion. The field stand descriptors MMH-tree ( $r^2=0.86$ ), MMH-all ( $r^2=0.84$ ), and vol ( $r^2=0.95$ ) are modeled by the type-sensitive CRR and precisely weighted HOME. BA ( $r^2=0.72$ ), an embedded feature, is interdependent on maximum height and stocking levels, and is best modeled with the terminal MCH and density-dependent HOME.

EAARL can be put to immediate use in forest mensuration projects as seen in the results above. AINS forests are unique, but because of NPS protections, can not be harvested to provide site-specific biophysical allometric relationships. In more well-studied areas, accurate field biomass and LAI values can likely be readily produced for remote modeling by EAARL metrics.

#### **4.5.4. Canopy principal components analysis**

The canopy profile comparison with stem profile (Fig. 6 and App. A) is a limited visualization method to make qualitative assessments and guide specific interpretations. The PCA set forth by Caylor *et al.* (2004) holds great potential in comparing multi-dimensional structure data among remote and field data sets, including material density in laser backscatter counts and crown presence frequency. To our knowledge, PCA has not previously been applied to lidar studies in this manner. Spectral PCA is regularly employed in passive optical remote sensing analyses, and others have used PCA in spatial pattern characterization of discrete return lidar in one and two dimensions (Ollier *et al.* 2003 and Frazer *et al.* 2005, respectively).

Caylor *et al.* (2004) looked at groupings of sites according to average leaf area distribution by regular vertical increment. In the present study, the PCA results between the field and remote representations of canopy density distribution are qualitatively examined and assessed for the routine's potential for quantitative analyses. Widlowski *et al.* (2004), in a discussion focused on examples and current deficiencies in the derivation of canopy structure from remote sensing, state "the availability of quantitative information on the structure and spatial distribution of terrestrial surface types across the

globe (preferably at regular intervals) would...improve the biome-specific parameterization of biophysical processes...”.

The canopy principal components are assessed for structural group signification by the five environmental types. These are summarized by major structural parameters in Figure 16; recall that the outlier site type 5 is excluded from the PCA. Site types 1b and 2 vary mainly along the PC2 axis which is dominated by variation in the 2-3 meter vertical segment range (Fig. 12, Table 3); note this is just above the upper limit (1.9m) of lowest crown lengths. These are generally multi-aged, small-stature, variably-stocked stands with substrates of low water holding and nutritive capacities. Site types 1a and 3 are average to tall stands with more variation along the 15-17meter-loaded PC1 axis; note the average maximum MCH for the network is 15.9m. The environment in these plots is generally moderate, with average elevations and average to good soil productivity. Site type 4 encompasses the deep soil, high biomass, even-aged stands that also vary along PC1.

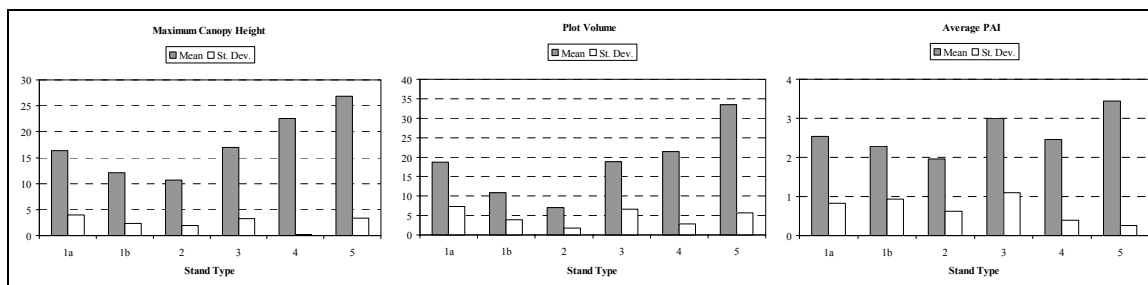


**Figure 16.** Major biophysical parameters in the six environmental site types used to stratify PCA and other analyses.

Clearly, PC1 and PC2 interactions are fairly analogous between the field and remote data sets, with similar site clustering – yet rotations of the functional sets are

unequal (Figure 12). The axis of variation is tilted from a predominant PC2 in the field to a more varied PC1 in EAARL.

PC loadings are not automatically correspondent between the two data sets. The EAARL PC1 loading (13.5m) is not comparable to the average MCH of 14.7m in the remote data nor is it close to the average MMH-all of 9.09m in the field (Table 4).

EAARL PC1 could be explained however, by the random combinations at plot level of canopy top misreading and the pulse-return decay downward from this artificial canopy top. Rotation of the PC space appears to be due to EAARL PC2 residing in the upper edge of these canopies, where as stated, random effects of survey posting space and real canopy topography interact in returns. Note also that the lower canopy is neglected in PCA due to occlusion and its equalization effect on information below the dominant canopy.

Mean Maximum Height (MMH) - All Stems	
Maximum MMH-all	17.20
Minimum MMH-all	4.69
Mean	9.09
St. Dev. Plot Height	3.23
CV	36%

**Table 4.** Field plot mean maximum height (m) of all stems (trees and shrubs) for the entire plot network (n=26). EAARL principal component loadings do not automatically correspond with these standard variables and appear to be subject to the unpredictable nature of laser incidence and penetration. CV is the coefficient of variation.

The inclusion of the lowest terminating crown presence in the field data – at times well removed down the bole from the bulk of the continuous crown (see Appendix B) – may be overstating the canopy density to the point of creating false variation at the lower

levels (PC2 here). Ends of *continuous* crown should be recorded and used to bound crown divisions in the future.

With continued calibration of the PCA method, the alternate use of the HPCD heights as upper physical bound on available variation in PCA should be further investigated in studies where tree tops are underrepresented. Lower total variation in the first two PC's here (Fig. 13) is due to the new compressed nature of the profiles, and the result of more equitable weighting (Nichols 1977) among the levels of canopy. This is not an optimal case for typing as it may lead to non-resolvable (Nichols 1977) canopy material distributions at our scale. It is initially apparent, however, that the groupings and rotations are better matched between field and lidar data sets (Fig. 14 compared to Fig. 12). Also, comparison of PC-loading locations (Fig. 13) show the HPCD-bounded sets are off by a distance (1-2 meters) and direction (EAARL variation is shifted upward from field variation) attributable to the physics of laser occlusion.

The fact that the principal components are not immediately transferable between data sets suspends meaningful conclusions. However, the potential utility of PCA is readily evident for vegetation-classification procedures, environmental site type prediction, and habitat characterization with canopy return information in the near term. Better agreement between field and remote variation may be a simple matter of increasing the arbitrary resolution of the current one-meter canopy segmentation units.

Agencies like the NPS are very interested in the creation of precise and accurate vegetation maps for management purposes. Lidar canopy PCA could outperform related methods of imagery interpretation and provide for more detailed vegetation maps. The subsampling of large-scale data tiles in GIS environments for canopy waveform quanta

would be a straightforward implementation of the PCA method. Widlowski *et al.* (2004) state that such standardized structural variation description in remote sensing data can “allow for better assessment of the effectiveness of specific management practices for carbon sequestration and conservation...”. With increased analysis time and more data (especially allometric relationships for biomass) precise production models based on structural type (E.g., Shugart 2000, Caylor *et al.* 2004) could be developed and made dynamic enough to model change expected over time.

#### 4.5.5. Occlusion

It can not be taken for granted that occlusion occurs because some layers are diminished or absent from the subcanopy returns. In an attempt to isolate causation of reduced variation below the HPCD of EAARL waveforms it is necessary to look at individual plot species distribution in the subcanopy as there may be inherent foliar properties leading to variation of “the diffuse component of the backscattered radiation” (Kalshoven *et al.* 1995). There may also be some disproportional effects of “*range walk*...due to backscatter strength variations” (Jensen 2000). Studies determining backscatter intensity differences between species appear limited. In one example, Holmgren and Persson (2004) find very good predictability between pine and spruce using empirical reflection frequency and intensity data derivatives related to the relative infiltration of pulses through each species to the forest floor and the “standard deviation of the intensity of the returned pulses.”

Kaasalainen *et al.* (1995) attempt to isolate specific surface properties and their effects on laser return intensity for calibration purposes. They find that surface

characteristics other than surface brightness (the nominal reflectance at a specific wavelength) “dominate ... the optical properties in backscatter.” Foliage internal elements are generally transparent to green visible light (Kalshoven *et al.* 1995), so surface roughness will play a larger role in green (532nm – the EAARL laser wavelength) than in NIR (1064nm) laser reflectivity physics. Kalshoven and Dabney (1993) show that depolarization (the increase of diffuse scattering) signatures are unique within vegetative divisions (conifer and broadleaf) as tested, and green light reflection depolarization is generally greater in the tested conifers (perhaps due to increased surface area and leaf angles) than in the broadleaf species. They do not test *P. taeda*, and if their result is extended to AINS and PIVCR, *I. opaca* and *M. cerifera* returns should be detected from under *P. taeda*.

Referring to the respective Appendix A figures for this discussion, note that in plot 21903 there is *I. opaca* (with shiny, smooth, thick, lustrous evergreen leaves), *V. corymbosum* (highbush blueberry; with pale green, thin leaves, matte surface), and *M. cerifera* (bayberry; with shiny, dimpled, lustrous leaves). The fairly prominent EAARL subcanopy peak is centered at 2.50m above ground and this is approximately equivalent to a concentration of *V. corymbosum*. *V. corymbosum* gives way to a mix with the other two subcanopy species at about 3.5m above ground. MMH-tree at this plot is 9.65m. Alternately, the field survey at plot 28506 shows there is clearly a dual layer canopy with large, tall trees and a *M. cerifera* layer that covers 45% of the plot area. This is not reflected in the unimodal EAARL waveform.

It would seem from these cases that the shiny leaves are reflecting in a specular nature (i.e., away from the lidar telescope) while the matte leaves are more directionally

diffuse (Grant *et al.* 1993) allowing for telescope capture. Again, the dominant canopy layer is very large in the *M. cerifera* plot and average to small in the *V. corymbosum* plot. But as to what is most limiting to EAARL canopy proportional reflection and 3-D coverage – species in the subcanopy or tree heights and biomass – will need more study. Perhaps until mechanisms are identified, exercises like the PCA above will need to be stratified by dominant species and sizes.

#### **4.5.6. Ecohydrological relationships and monitoring**

Lidar is becoming a common tool in geomorphic and land cover descriptions, but regular interval vegetation monitoring applications have thus far been generally restricted to stand-level growth (Omasa *et al.* 2007). There are publications of potential and recommended directions in biophysical system monitoring (E.g., lacunarity analysis with PCA in Frazer *et al.*, 2005), while detailed schemes of description and monitoring of environmental stress effect with lidar waveform products and field verification do not appear to be represented in the literature.

A remote sensing monitoring relationship can now be developed (Figure 18 is a conceptual model for the plan) that utilizes changes in above-ground vegetation structure and linked changes in water tables and soil moisture. Implementation of these broad guidelines will allow for the prediction of ecosystem-wide water relations disruption as may be expected of forcing by sea level rise. The barrier island systems in this study are ideal test sites for such a program owing to their generally simplified physical structure.

The foundation of the scheme is the modeling of PAI with the EAARL waveform metric CRR (conclusions are limited to *P. taeda* stands as it is likely that the PAI-CRR

correspondence will change in stands of conically-shaped trees and broadleaf trees). CRR successfully predicts PAI at AINS ( $r^2=0.73$ ,  $p<0.0001$ ; Fig 10). The mechanism of interest reflected in change of these values is near-term alteration of moisture availability and concomitant adjustment in fine forest structure (see Chapter 3). Ground-truthing can be minimally labor and time-intensive, a significant advantage as the time frame is accelerated by anthropogenic influence on atmospheric greenhouse gas content. Collection of PAI with the Li-Cor LAI-2000 requires strict adherence to instructions, and while it would be labor-intensive to derive the true physiologically-active all-sided LAI, the raw PAI value is found to incorporate LAI to an adequate degree at AINS. General leaf and fine shoot biomass change was detected in serial PAI readings over the seasonal “green-up” and abscission periods (Fig. 9).

It is difficult to divide the PAI courses into absolute gain and loss of true leaf area because of the shifting sample time periods and the omission of intensive analysis of living tissue (E.g., specific leaf areas (SLA), from which a surface area estimate of the litter could be made, are unknown for this habitat). An exercise to relate PAI change as seen in Figure 9 with changes in litterfall, and derive a functional correlation was inconclusive with an  $r_s$  of -0.40 in large stature stands, and +0.62 (more significant at  $p=0.10$ ) in small stature stands (Chapter 3). Correlation in the smaller stands was likely positive as a result of green-up and the attendant shedding of old foliage. The divergence of the two stand types in correlation and significance in this test could be a result of a variety of conditions including: variable water relations and soil moistures; foliar/woody material proportions and arrangement; and inherent limitations of the LAI-2000. See also

that CRR predicts PAI with variable reliability among types (Fig. 10), with the smaller bio-type 2 more confidently modeled.

For these reasons, a dynamic causal relationship of PAI/LAI course with changes in plot water levels (DWT) is not attained at this time. It is possible, however, to draw general conclusions from average DWT and average PAI values (Chapter 3) during common periods. Though the correlation of DWT and PAI is best when readings are grouped across all sites ( $r_s=0.46$  and  $p=0.133$ , Chapter 3) than in the separate stand groups, the difference in direction ( $r_s=0.46$ ,  $p=0.179$  in bio-type 1;  $r_s= -0.37$ ,  $p=0.239$  in bio-type 2) resulting between the groups may be due to differing water uptake strategies by developmental control and/or rooting zone constraints (Chapter 3).

Utilizing a site soil's STI profile in tandem with the fluctuating DWT enhances the general description of moisture status as this incorporates a water-holding element. As seen in Chapter 3, STI had better individual correlations than DWT with the canopy tree-based coarse structural measures and PAI. Figure 17 is a basic model of the STI, DWT and water availability interactions. If STI is greater at a more shallow DWT in the soil column, water table rise may increase water availability at the average DWT, and conversely, at a lower STI, water availability may decrease. In the majority of soil column profiles at AINS, STI increases with depth from surface; forests at these sites could be expected to adjust foliage levels downward and hence, overall growth through time, as more of the rooting system is forced to reside in the low matric potential coarse sand.

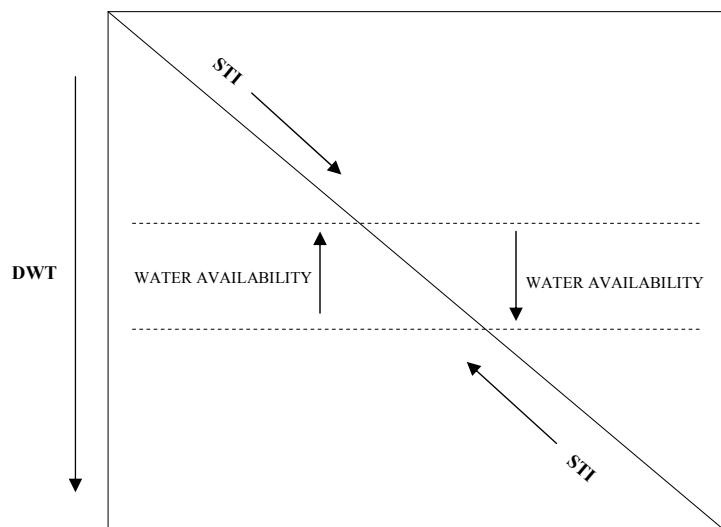


**Figure 17.** Diagram of water availability scale in an idealized Assateague Island soil column. Arrows indicate direction of increase. In the top right half, STI increases downward through the profile, and water table rise will result in lower water availability. In the bottom left half, STI is increases upward through the profile so that water table rise will lead to greater water availability.

The sensitivity of the LAI-2000 to leaf biomass change as demonstrated qualitatively here and quantitatively in other studies (see Holst *et al.* 2004, and Chason *et al.* 1991), and the expectation that the maximum supportable foliage and fine shoot biomass will adjust with available site moisture over short to long terms – especially in *P. taeda*, a well-studied species in moisture-dependence – support the continued study for a material equivalency in the PAI-LAI and moisture status feedback circuit.

Chapter 3 of this volume is concerned with the connectivity of the AINS upland water tables and sea levels. While more complicated than a 1:1 influence by the sea surface, it is reasonable to assume that continued fine temporal scale measurements of freshwater tables and sea level will allow for forcing functions on a site-by-site basis. Continued PAI collections over expanded areas and times and more detailed moisture measures will help resolve the interactions further to better model effects of rising water

tables on fine scale vegetation structure. It is likely that, as covered in the dendrochronological analyses (Chapters 2 and 3), and the litterfall study (Chapter 2), description of the previous year's climate and depths to water tables will better predict current-year foliage levels. This would very much improve the probability to create accurate productivity models based on water availability.

The field PAI and remote CRR relationship may be tightened further with application of a variant of the Lefsky *et al.* (1999a) cover correction method in which they applied an empirical 2:1 ratio to the reflectance in the 1064nm wavelength of ground to canopy material. This effectively weighted all canopy cover estimates and allowed them to build incremental canopy height profiles (cover by vertical increment). A spectrometer could be acquired and green 532nm wavelength reflectance measured from representative canopy species and sands at AINS sites. This operation could make CRR more accurate, and perhaps correct the within-canopy differentiation of layers.

In the interim, it is quite useful that CRR is retained in the significant multiple regression predictions (Figure 8) of vol ( $R^2=0.95$ ), MMH of trees ( $R^2=0.86$ ), and MMH of all woody stems ( $R^2=0.84$ ). These integrative parameters are all field-verified and may be more sensitive to moisture status than the one-dimensional plot MCH that is less confidently predicted by EAARL. A correlation test, not shown, does indeed result in stronger and more significant positive correlations for the integrative metrics with STI. Other uses of the data and new inferential methods should be explored such as applicability to variously-scaled transpiration and production models. Figure 18 is the conceptual model for the monitoring of changing above ground structure for detection and prediction of effects of rising water tables in AINS uplands.

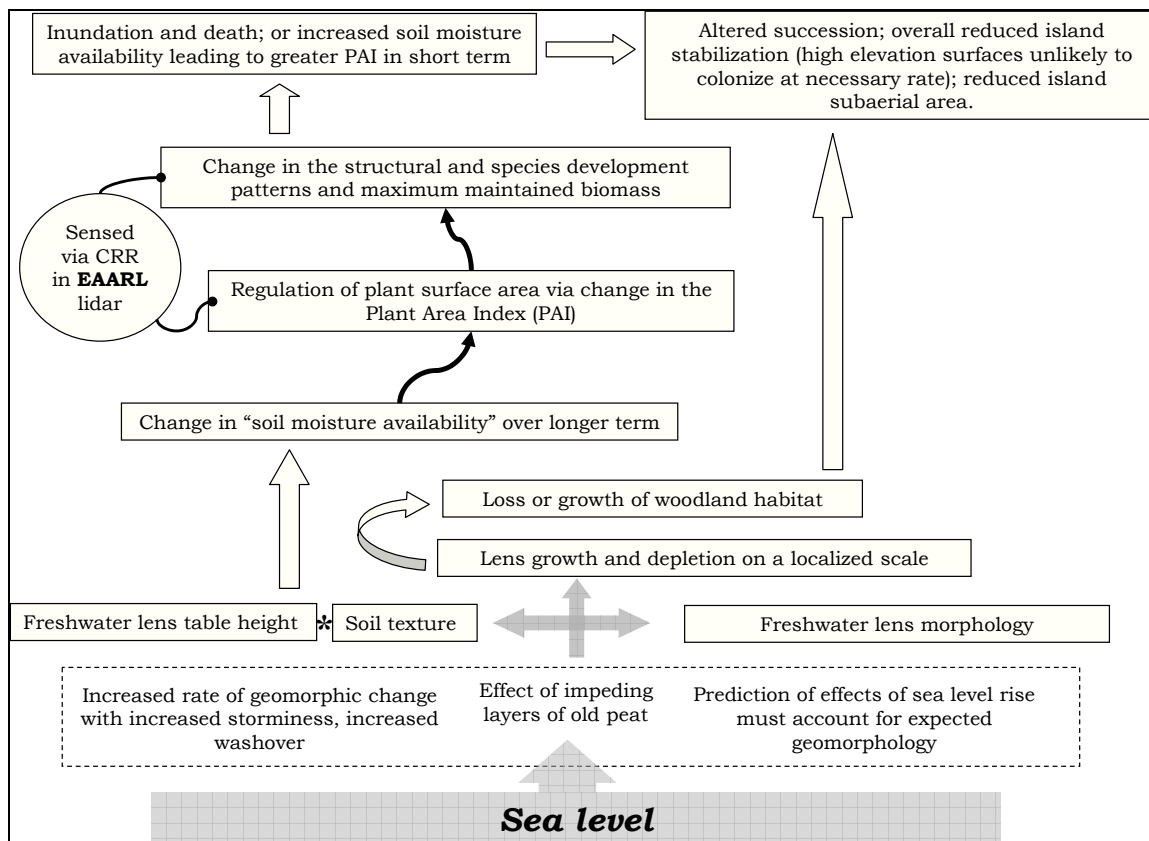


**Figure 18.** Conceptual model of the Mid-Atlantic barrier island sea-level and above-ground forest structure relationship. EAARL lidar would be employed at regular intervals to provide fine resolution CRR changes with quantified water level changes and ground-verified structural changes. Ground verification could be suspended after regression relationships of the structure-moisture interaction reach significant levels. Further remote monitoring would provide predictions of decline thresholds due to sea level rise. The figure is developed based on recommendations in Fancy *et al.* (2009) “Monitoring the Condition of Natural Resources in US National Parks.”

#### **4.6. Conclusions**

Results outlined in this study demonstrate the capabilities of the small-footprint full-waveform lidar system, EAARL, in capturing fine-scale (0.08ha plots) structural variation across environmental gradients. EAARL data offer a significant advancement in the temporal analysis of system-wide biophysical change with ecohydrological and ecophysiological change associated with sea level rise. With continued work, it is clear

that EAARL will allow for powerful modeling and validation exercises for many areas of management and research.

The use of lidar-specific ground measures such as height of peak canopy density (HPCD) may be critical in continuing applications as there is at the moment no efficient way to correct for loss of canopy top information. EAARL HPCD predicts the field HPCD parameter better than EAARL maximum canopy height (MCH) predicts field MCH; however, MCH is still a more reliable site quality indicator (see Chapter 3). These results advocate for standardizing the field collection of crown length in lidar validations. HPCD is derived from plot-integrated crown lengths, which in turn allow for generalized plot-level vertical density frequency spectrums. These spectrums become raw input for an experimental principal components analysis (PCA). Canopy density PCA is a promising new direction for many if not most lidars in comparisons with ground structure, *a posteriori* structural grouping, and in survey reproducibility among various lidars. Study-specific adjustment of the arbitrary segmentation of canopy information (presence frequency in the field, backscatter returns in the lidar data), currently at 1m, may lead to better overall agreement.

Occlusion of the lidar signal will require greater attention in future applications. Unquantified reduction of incident and backscattered energy in the subcanopy surfaces leads to greater overall error rate and unpredictability. Some layers are underrepresented and the structure-dependent HPCD is, on average, in error by about 14% at a standard deviation (s) rate of 19%. This may also indicate the limitations of the field collection method here and a need for more detailed field measures of canopy distribution.

Collection of crown widths in addition to length would likely enhance reliability of metrics to site factors and may help parameterize an occlusion factor.

In addition to standard reproduction of ground structure, a major intent of this study is to demonstrate EAARL utility in the reproduction of physiologically significant biotic factors indicative of general ecohydrological conditions. Plant area index (PAI), the finest scale resolved in structure here, trends with leaf area changes related to season and, likely, water availability (at various temporal lags). The repeated ground measurement with a standard instrument (Li-Cor Biosciences Plant Canopy Analyzer, LAI-2000) can be reliably modeled with EAARL waveform information in the canopy reflection ratio (CRR).

Depth to water table (DWT) alone does not appear to be adequate in characterizing a water availability gradient influencing structural parameters. In combination with the soil texture index (STI), however, a new basic function for prediction and modeling is described that requires minimal ground truthing. STI, as a surrogate for more intensive soil moisture characteristics, is essential to the understanding of results thus far, and to predictions of effects to barrier island forests of changing water tables (see Chapter 3). Good correlation of the STI•DWT product (DWST) with PAI (up to  $r_s=0.54$ ,  $p=0.004$ ) and a simple model of changing water availability with intersection gradients of water table and texture is recommended as a monitoring framework.

Water availability to *P. taeda*-dominated forests will change depending on the direction of the STI gradient (assuming a unidirectional rise in water tables with sea level). With water table rise, EAARL CRR (and PAI) can be expected to trend upward in those areas where STI increases upward through soil, and CRR will likely trend

downward in those areas where STI decreases upward through the soil profile (the majority of sites). An STI profile may be the only plot environmental parameter needed to interpret CRR changes if reliable sea level forcing functions are developed for AINS and/or appropriate island-wide error is assumed for a uniform forcing.

As seen in Chapter 3, the shrub component represented by SCA is significantly dependant on water table levels. Analyses should proceed to correct canopy occlusion and derive a suitable measure of shrub presence from EAARL waveforms. It appears this would greatly increase the inferential power of the lidar data in monitoring vegetation change due to sea level rise.

Basic monitoring of fine-scale ecophysiological indicators like PAI/CRR, the use of new techniques like the principal components analysis (PCA) drafted here, and detailed modeling and testing to further refine the structure-hydrological change relationship should continue at these barrier islands in assessment of threats from sea-level rise. Another field season collection to include tree-level physiological measurement like sap-flow may allow for the allocation of causal activity to plant/leaf area change performed here in a correlative fashion. At a minimum, water tables should be recorded throughout an initial year, and these correlated to total leaf areas of the following year as these have been shown to be directly related (Hennessey *et al.* 1992).

#### **4.7. References**

- Aber, J. D. 1979. Method for Estimating Foliage-Height Profiles in Broad-Leaved Forests. *Journal of Ecology* **67**:35-40.
- Caylor, K. K., P. R. Dowty, H. H. Shugart, and S. Ringrose. 2004. Relationship between small-scale structural variability and simulated vegetation productivity across a regional moisture gradient in southern Africa. *Global Change Biology* **10**:374-382.
- Chason, J. W., D. D. Baldocchi, and M. A. Huston. 1991. A Comparison of Direct and Indirect Methods for Estimating Forest Canopy Leaf-Area. *Agricultural and Forest Meteorology* **57**:107-128.
- Drake, J. B., R. G. Knox, R. O. Dubayah, D. B. Clark, R. Condit, J. B. Blair, and M. Hofton. 2003. Above-ground biomass estimation in closed canopy Neotropical forests using lidar remote sensing: factors affecting the generality of relationships. *Global Ecology and Biogeography* **12**:147-159.
- Fancy, S. G., J. E. Gross, and S. L. Carter. 2009. Monitoring the condition of natural resources in US national parks. *Environmental Monitoring and Assessment* **151**:161-174.
- Frazer, G. W., M. A. Wulder, and K. O. Niemann. 2005. Simulation and quantification of the fine-scale spatial pattern and heterogeneity of forest canopy structure: A lacunarity-based method designed for analysis of continuous canopy heights. *Forest Ecology and Management* **214**:65-90.

- Gaveau, D. L. A. and R. A. Hill. 2003. Quantifying canopy height underestimation by laser pulse penetration in small-footprint airborne laser scanning data. *Canadian Journal of Remote Sensing* **29**:650-657.
- Gibbons, J. D. and S. Chakraborti. 1992. *Nonparametric statistical inference*. 3rd edition. M. Dekker, New York.
- Gilman, E. F., and D. G. Watson. 2006. *Pinus taeda: Loblolly Pine*. Document ENH-637, One of a Series of the Environmental Horticulture Department, Florida Cooperative Extension Service, Institute of Food and Agricultural Sciences, University of Florida.
- Grant, L., C. S. T. Daughtry, and V. C. Vanderbilt. 1993. Polarized and Specular Reflectance Variation with Leaf Surface-Features. *Physiologia Plantarum* **88**:1-9.
- Grier, C. C. and S. W. Running. 1977. Leaf Area of Mature Northwestern Coniferous Forests - Relation to Site Water-Balance. *Ecology* **58**:893-899.
- Hayden, B. P., M. C. F. V. Santos, G. F. Shao, and R. C. Kochel. 1995. Geomorphological Controls on Coastal Vegetation at the Virginia-Coast-Reserve. *Geomorphology* **13**:283-300.
- Holmgren, J. and A. Persson. 2004. Identifying species of individual trees using airborne laser scanner. *Remote Sensing of Environment* **90**:415-423.
- Holst, T., S. Hauser, A. Kirchgassner, A. Matzarakis, H. Mayer, and D. Schindler. 2004. Measuring and modelling plant area index in beech stands. *International Journal of Biometeorology* **48**:192-201.
- Jensen, J. R. 2000. *Remote sensing of the environment : an earth resource perspective*. Prentice Hall, Upper Saddle River, N.J.

- Kaasalainen, S., E. Ahokas, J. Hyyppa, and J. Suomalainen. 2005. Study of surface brightness from backscattered laser intensity: Calibration of laser data. *Ieee Geoscience and Remote Sensing Letters* **2**:255-259.
- Kalshoven, J. E. and P. W. Dabney. 1993. Remote-Sensing of the Earths Surface with an Airborne Polarized Laser. *Ieee Transactions on Geoscience and Remote Sensing* **31**:438-446.
- Kalshoven, J. E., M. R. Tierney, C. S. T. Daughtry, and J. E. McMurtrey. 1995. Remote-Sensing of Crop Parameters with a Polarized, Frequency-Doubled Nd-Yag Laser. *Applied Optics* **34**:2745-2749.
- Lefsky, M. A., W. B. Cohen, S. A. Acker, G. G. Parker, T. A. Spies, and D. Harding. 1999. Lidar remote sensing of the canopy structure and biophysical properties of Douglas-fir western hemlock forests. *Remote Sensing of Environment* **70**:339-361.
- Lefsky, M. A., D. Harding, W. B. Cohen, G. Parker, and H. H. Shugart. 1999. Surface lidar remote sensing of basal area and biomass in deciduous forests of eastern Maryland, USA. *Remote Sensing of Environment* **67**:83-98.
- Lim, K., P. Treitz, K. Baldwin, I. Morrison, and J. Green. 2003. Lidar remote sensing of biophysical properties of tolerant northern hardwood forests. *Canadian Journal of Remote Sensing* **29**:658-678.
- Lim, K., P. Treitz, M. Wulder, B. St-Onge, and M. Flood. 2003. LiDAR remote sensing of forest structure. *Progress in Physical Geography* **27**:88-106.

- Means, J. E., S. A. Acker, D. J. Harding, J. B. Blair, M. A. Lefsky, W. B. Cohen, M. E. Harmon, and W. A. McKee. 1999. Use of large-footprint scanning airborne lidar to estimate forest stand characteristics in the Western Cascades of Oregon. *Remote Sensing of Environment* **67**:298-308.
- Naesset, E. 2002. Predicting forest stand characteristics with airborne scanning laser using a practical two-stage procedure and field data. *Remote Sensing of Environment* **80**:88-99.
- Nagel, L. M. and K. L. O'Hara. 2001. The influence of stand structure on ecophysiological leaf characteristics of *Pinus ponderosa* in western Montana. *Canadian Journal of Forest Research-Revue Canadienne De Recherche Forestiere* **31**:2173-2182.
- Nayegandhi, A., J. C. Brock, C. W. Wright, and M. J. O'Connell. 2006. Evaluating a small footprint, waveform-resolving lidar over coastal vegetation communities. *Photogrammetric Engineering and Remote Sensing* **72**:1407-1417.
- Nichols, S. 1977. Interpretation of Principal Components-Analysis in Ecological Contexts. *Vegetatio* **34**:191-197.
- Nilsson, M. 1996. Estimation of tree weights and stand volume using an airborne lidar system. *Remote Sensing of Environment* **56**:1-7.
- Ollier, S., D. Chessel, P. Coueron, R. Pelissier, and J. Thioulouse. 2003. Comparing and classifying one-dimensional spatial patterns: an application to laser altimeter profiles. *Remote Sensing of Environment* **85**:453-462.

- Omasa, K., F. Hosoi, and A. Konishi. 2007. 3D lidar imaging for detecting and understanding plant responses and canopy structure. *Journal of Experimental Botany* **58**:881-898.
- SAS Institute Inc. 2002-2003. Statistical Analytical Software Version 9.1 for Windows. Cary, NC.
- Shugart, H. H. 2000. Importance of structure in the longer-term dynamics of landscapes. *Journal of Geophysical Research-Atmospheres* **105**:20065-20075.
- Spurr, S. H. and B. V. Barnes. 1980. *Forest ecology*. 3d edition. Wiley, New York.
- Todd, K. W., F. Csillag, and P. M. Atkinson. 2003. Three-dimensional mapping of light transmittance and foliage distribution using lidar. *Canadian Journal of Remote Sensing* **29**:544-555.
- Vose, J. M. and H. L. Allen. 1991. Quantity and Timing of Needlefall in N and P Fertilized Loblolly-Pine Stands. *Forest Ecology and Management* **41**:205-219.
- Whittaker, R. H., F. H. Bormann, G. E. Likens, and T. G. Siccama. 1974. Hubbard Brook Ecosystem Study - Forest Biomass and Production. *Ecological Monographs* **44**:233-252.
- Widlowski, J. L., B. Pinty, N. Gobron, M. M. Verstraete, D. J. Diner, and A. B. Davis. 2004. Canopy structure parameters derived from multi-angular remote sensing data for terrestrial carbon studies. *Climatic Change* **67**:403-415.

## V. Summary

The ecohydrological evidence presented in this dissertation supports the paradigm of depth to water table and the associated rooting zone dynamics as an overarching vegetation structuring agent on the sandy barrier islands of the Mid-Atlantic coast. Study of the current spatial gradients in biophysical structure and site water has formed the basis of forest development theories within a sea level rise scenario.

With common forest structure and site mensuration, and small circular plots of the design, the 26 plot study area of AINS appears to yield robust biophysical and environmental classifications. For example, the simplified soil matric potential description in STI introduces a widely applicable index that delineates sites by growth potential. STI is key to describing simple field water availability in combination with average water table depth. The new DWST variable holds significant potential in structuring a monitoring regime of sea level rise effects on barrier island upland forest structure.

Plant areal change over the season and across sites can reflect gradients in water availability. This, and the other supporting information developed throughout this volume, informs the generalized predictions that, with short term sea level rise: supportable leaf area (and hence, growth) can be expected to trend upward in those areas where STI increases upward through soil, and trend downward in those areas where STI decreases upward through the soil profile (the majority of sites). Shrub canopy area (SCA) is the most reliable structural variable in determining site hydrology. Increases in the shrub component relative to trees, and decreased forested area, can be expected with rising water tables.

Results from an uncommon dendroecological technique show that radial growth increment trends are significantly different among forest types, and these can be extrapolated to predict future growth under environmental change. By developing individual site type radial growth and climate correlations, it is evident that on the limited spatial scale of a barrier, site can determine the effects of common climate signals on yearly growth.

The importance of collecting crown length data with tree heights in studies of ecohydrology and remote sensing has been clearly demonstrated with the successful applications here of the new HPCD (height of peak canopy density) variable. Derived from crown length measures integrated at the plot level, HPCD is useful as an alternative to maximum canopy height, a parameter often underestimated by lidar. HPCD also may better indicate average site moisture availability.

EAARL lidar is shown to hold significant potential in monitoring structural changes related to the hydrology of sites on a large scale. The relationship of PAI to field moisture is evolving as seen throughout this work, but it is clear that EAARL CRR captures PAI variation to a predictive degree. PCA of metered canopy presence frequency in plot aerial space appears sensitive to structural gradients related to site moisture; PCA of this type may also allow for a new standard method of structural comparison between field and remote data sets.

The synthesized results and interpretations of this study are designed to be of immediate reference to managers of natural areas, like the National Park Service, that are tasked with determining “vital signs” of ecosystem health and monitoring systems for change expression of these signs. Lidar surveys that are performed regularly to monitor

coastline geomorphology (Stevens *et al.* 2005) could be expanded to track vegetation. As suggested in this dissertation, disruptions to water relations of coastal vegetation with forcing by higher sea levels and increased or intensifying storm surges, may be detected in incremental and community-level structural changes. As relationships between important variables like PAI and DWST are tightened, there is also significant potential to create precise, fine-scale models of growth with average water levels.

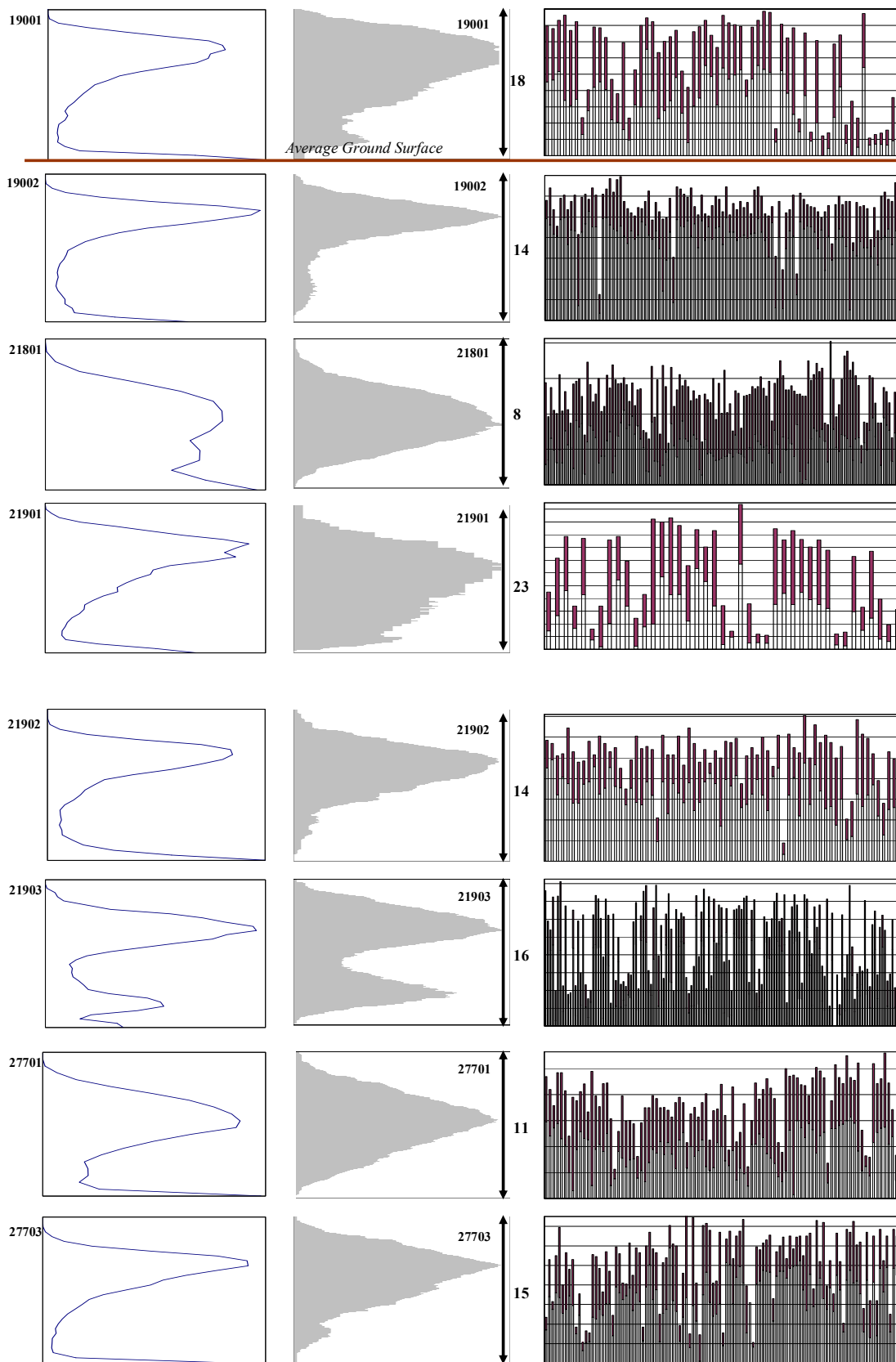
### **5.1. References**

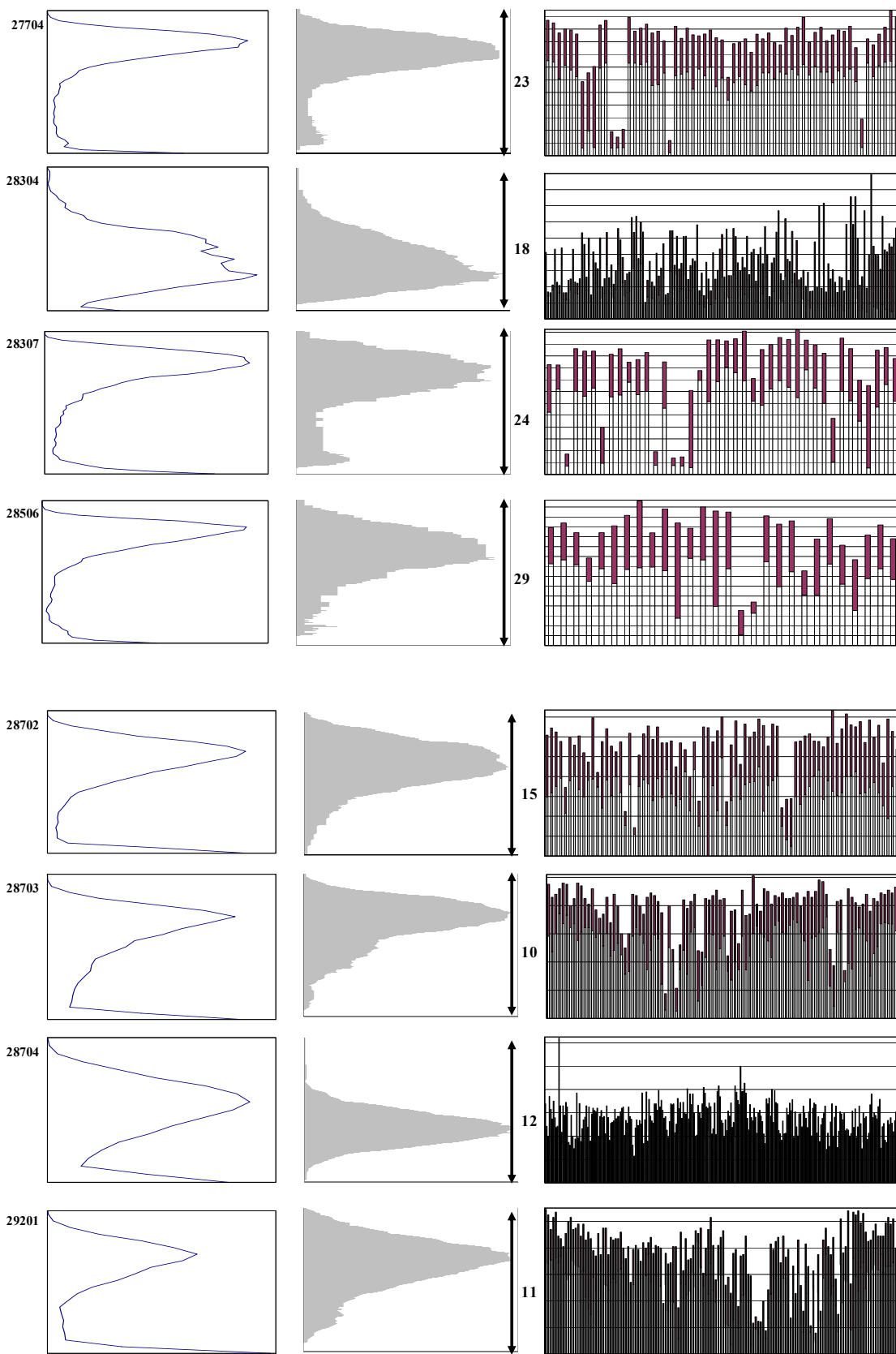
Stevens, S., B. Milstead, M. Albert, and G. Entsminger. September 2005. Northeast Coastal and Barrier Network Vital Signs Monitoring Plan. Technical Report NPS/NER/NRTR--2005/025. National Park Service. Boston, Massachusetts.

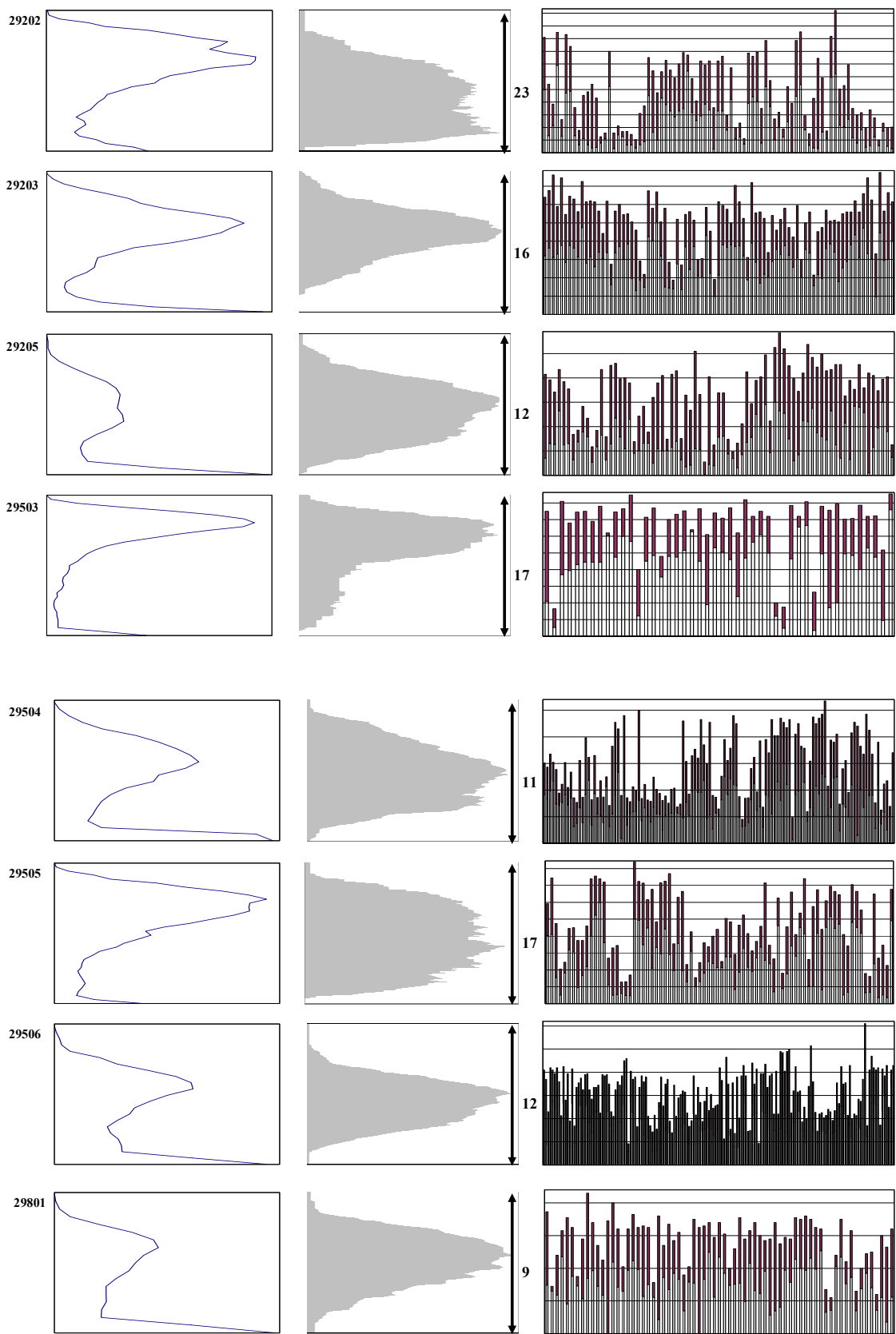
### Appendix A. Canopy profiles

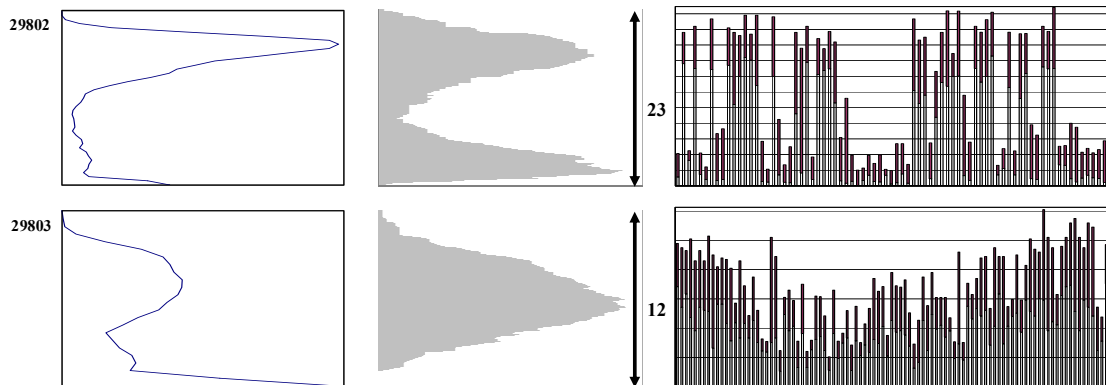
The figures here include (from left): the EAARL waveform diagrams, the canopy presence frequency by height increment histograms, and the stem profiles. The waveform is a graph of return energy (backscatter count) by 50 cm height increment. The plot crown presence frequency estimates foliage density by counting individual presence in the crown length range at 10 cm increments. Stem profiles represent individual presence data graphically with the shaded portion of each column.. Crown ratios are derived from these stem profile data directly as:

$$\text{crown ratio} = \frac{\text{crown length}}{\text{total tree height}}$$

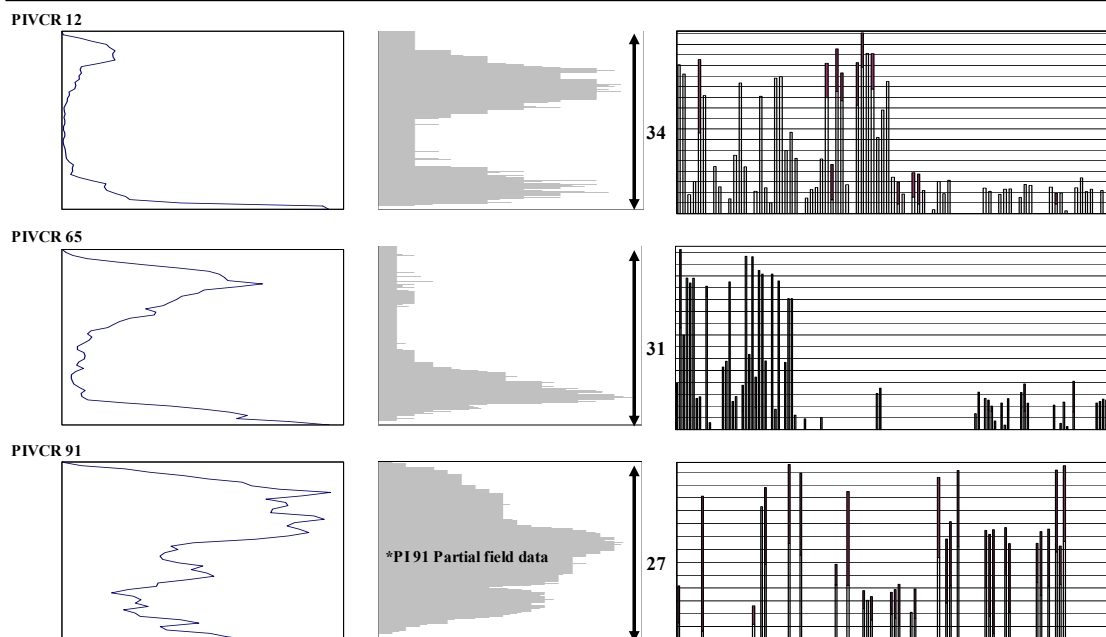








**Parramore Island Plots**



## Appendix B. Crown lengths

### **Crown length measurement issue**

I am unsure of the degree to which crown lengths may be overestimated in some plots. There is a chance that prior to about mid-August 2005 in data collections, secondary crown lengths (isolated foliated branches removed down the bole from the main crown) were accepted erroneously as ends of continuous crown. This would have the effect of overestimating the crown presence frequencies in the canopy segments concerned. Of the 14 plots possibly affected by the omission, 29202 and 29504 (relatively low density stands of uneven age structure) are most likely to be significantly affected.

Plot 21901 (Fig. 1) serves as an example of a “worst-case-scenario”: of 41 total stems, crown lengths of 11 (27% of stock) were noted in the original field data as ‘secondary’. In other plots where the discrepancy has been identified, affected stock percentage is in the single digits. This plot is of rather high relief (1.7m range) and high average elevation (1.4m), with an open habit, and several very large trees.

Frequencies along the length from 3.5m above ground level (AGL) to 12.7m AGL are changed by reducing crown presence by one-third from previous lengths of affected individuals. This reduction level is a best guess from memory. The result of about a 13.5m height of peak canopy density (HPCD) is unchanged. The recalculation does affect subcanopy representation, or that portion of canopy below the tallest point of unfoliated bole.

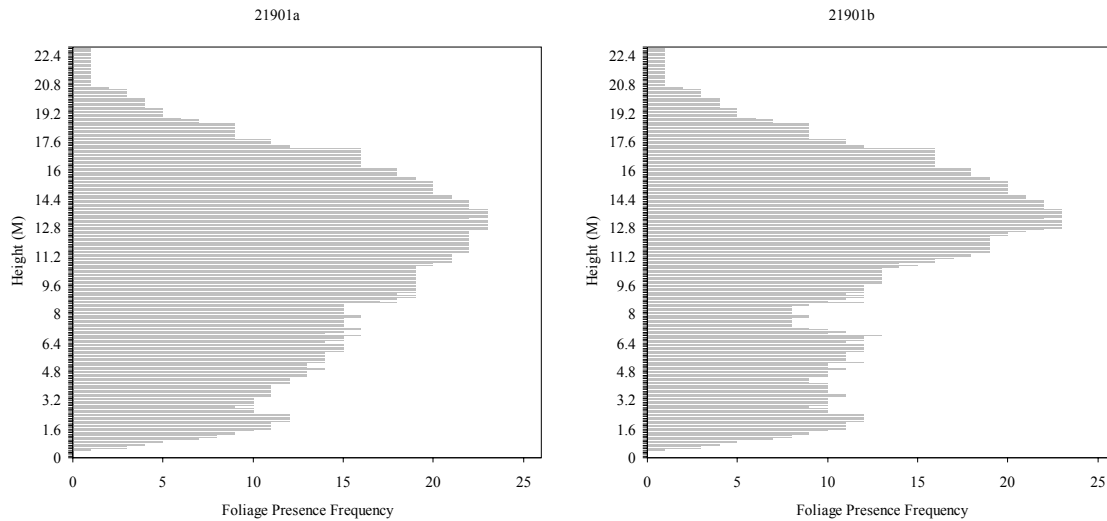


**Figure 1.** A comparison of the two results from separate crown length data sets for AINS plot 21901. 21901a graphs the current, uncorrected crown lengths, incorporating the length fractions from ends of main crowns to ‘secondary’ ends of crown. Upwardly adjusting the terminating crown length by a hypothetical 33% for the flagged individuals (11 trees) results in the histogram of 21901b.

It is also important to note that each methodology is an approximation of true crown presence in aerial space. The high relief of the area reduces accuracy because tree bases are not measured for elevation.

### **Bimodality test**

I experimented with producing the ‘bimodality coefficient’ (SAS Institute, Inc. 2002-2003) based on skewness and kurtosis of the tree canopy frequency distributions. This variable did correlate significantly with most of the base structural metrics, yet not to as high a degree as HPCD. It seems likely that inclusion of shrub crown lengths (not measured) in the computations here would improve results because of the interdependence of the tree and shrub growth in, for example, evapotranspirational function (see Chapter 3).

### **Appendix C. PAI “fluctuation”**

As an estimate of relative leaf area index (LAI), the LAI2000 (Li-Cor, Lincoln, NE) PAI metric does not differentiate woody and leaf area. It seems that one could verify and roughly depict a material loss of foliage by measuring PAI throughout the growing season. The fluctuation variable (the ratio of PAI range to average PAI) may be an acceptable index to assess approximate foliar change with certain environmental cues – especially groundwater levels – in appropriate time periods.

#### **PAI distribution**

Figure 1 shows the 2005 PAI distribution for bio-types based on the range as a proportion of average PAI. This statistic of annual fluctuation is approximately twice the coefficient of variation (CV) and may approximate the areal contribution by an annual cohort of foliage. As this statistic recedes from 50%, the proportion of woody area to leaf area increases. The bio-type averages accompanying the information in Figure 1 are listed in Table 1. Stand biophysical metrics are included to illustrate directions of correlation of leaf area to stand stature and biomass levels.

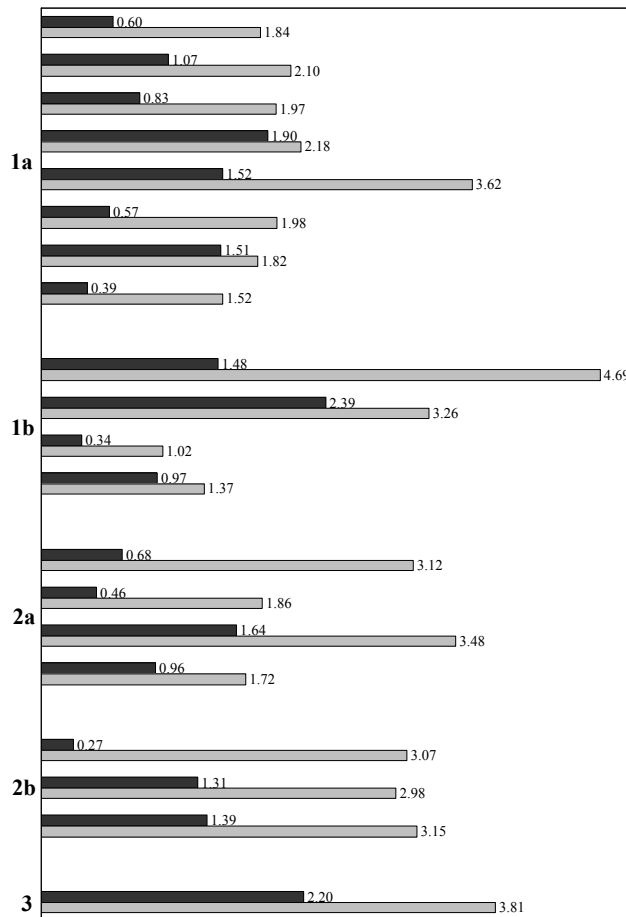


**Figure 1.** The 2005 average PAI (■) and the range in PAI (▨) of 2005 for the bio-types 1a-3, where 3 is the outlier group.

	Bio-type			
	1a	1b	2a	2b
2005 Annual PAI fluctuation (%)	49.07	52.30	37.40	32.32
Standard Deviation (s)	23.74	23.01	16.73	20.37
n	8	4	4	3
Maximum Canopy Ht.	16.65	23.37	9.78	11.83
Basal Area	34.68	37.99	20.30	26.86

**Table 1.** Total PAI fluctuation (PAI range:average PAI) in the 2005 field collections for the bio-types (less outlier type 3) varies directly with stand stature (represented by height and basal area here) in type 1, and varies negatively in type 2.

Litterfall rate is often found directly correlated to measures of stand stature (see Gresham 1982, Hennessey et al. 1992). This occurs in our large stature bio-type 1 only, not bio-type 2. Crown ratio is anomalously higher in type 2a perhaps explaining the inverse relationship of PAI change to stand magnitude found between types 2a and 2b. Environmental variability could dominate the PAI changes in these small stature, lower quality sites. Low site index (SI), a general site quality assessment usually based on vertical growth potential (Spurr and Barnes 1980) is associated with greater variability in growth than in high site index (Johnson and Young 1992) as seen in the dendrochronology results.

A correlation test of fluctuation with informal litter totals for 6 littertrap-equipped plots shows no immediate relationship. The variation in the fluctuation statistic across bio-types is only significant across the 2 major bio-types (1 and 2) and derives no variation from site types.

It appears that finer temporal representation of PAI may be required. A Spring to Winter field season of intensive measurement at a few sites on AINS should aid in deriving a reliable fractional PAI related to true leaf area change.

### C.1. References

- Gresham, C. A. 1982. Litterfall Patterns in Mature Loblolly and Longleaf Pine Stands in Coastal South-Carolina. *Forest Science* **28**:223-231.
- Hennessey, T. C., P. M. Dougherty, B. M. Cregg, and R. F. Wittwer. 1992. Annual Variation in Needle Fall of a Loblolly-Pine Stand in Relation to Climate and Stand Density. *Forest Ecology and Management* **51**:329-338.
- Johnson, S. R. and D. R. Young. 1992. Variation in Tree-Ring Width in Relation to Storm Activity for Mid-Atlantic Barrier-Island Populations of *Pinus-Taeda*. *Journal of Coastal Research* **8**:99-104.
- Spurr, S. H. and B. V. Barnes. 1980. *Forest ecology*. 3d edition. Wiley, New York.